UNIVERSITÉ DU QUÉBEC

THÈSE PRÉSENTÉE À
L'UNIVERSITÉ DU QUÉBEC À TROIS-RIVIÈRES

COMME EXIGENCE PARTIELLE
DU DOCTORAT EN BIOPHYSIQUE

PAR
LEI SHAO

SURFACE CHEMISTRY AND STRUCTURAL STUDIES OF PHOTOSYSTEM II USING UV-VIS AND FLUORESCENCE SPECTROSCOPIES AND ATOMIC FORCE MICROSCOPY

AOÛT 1998

Université du Québec à Trois-Rivières

Service de la bibliothèque

RÉSUMÉ

Le photosystème II (PS II) est un complexe supramoléculaire pigment-protéine intégré dans la membrane thylacoïdale des plantes supérieures, des cyanobactéries, des algues vertes et rouges. Ce complexe joue un rôle vital dans le processus photosynthétique en utilisant l'énergie electromagnétique solaire pour décomposer l'eau, ce qui génère la formation d'oxygène moléculaire et un gradient de proton transmembranaire nécessaire à la synthèse d' ATP. La fonction biologique du complexe PS II est liée à sa structure en trois dimensions et à l'interaction entre ses diverses sous-unités. A pour objectif l'examen de la morphologie du PS II et de ses sous-unités dans des conditions experimentales bien définies en employant les méthodes des films monomoléculaires, de spectroscopies et de microscopie à force atomique (AFM). La membrane du PS II et du "core complex" du PS II sont, en premier lieu, extraits de la plante supérieure en prenant soin de maintenir leur activité biologique. Ces complexes lipo-protéiques sont ensuite examinés à l'interface air-eau pour s'assurer de leur stabilité dans des couches monomoléculaires. Nous avons déterminé les propriétés interfaciales de la membrane et du "core complex" par l'entremise des mesures des isothermes de pression et de potentiel de surface, ce qui a permis d'obtenir la dimension moyenne de ces particules supramoléculaires.

Nous avons aussi déterminé les propriétés interfaciales du mélange "core complex" du PS II et du lipide monogalactosyldiacyglycerole (MGDG). L'interprétation de ces propriétés indique que le MGDG augmente la stabilité de la monocouche du complexe ainsi que son intégrité structurale. Les données spectroscopiques telles que l'absorption et la fluorescence directement à l'interface air-eau montrent que la membrane du PS II maintient son intégrité structurale lorsqu'elle se trouve en couche monomoléculaire. La topographie de la couche monomoléculaire de la membrane du PS II a été étudiée en employant la microscopie à force atomique (AFM) en mode oscillant. Les images AFM révèlent que les particules de PS II sont distribuées au hasard à travers la membrane. Nos données AFM indiquent aussi l'existence d'une cavité intramoléculaire près du centre de chaque particule, ce qui confirme les mesures publiées récemment en microscopie electronique à balayage sur des échantillons marqués. Nous avons finalement étudié la hauteur apparente des particules et les dimensions de la cavité en fonction de la force appliquée sur le levier de la pointe AFM. Cette étude nous fournit une information unique sur les propriétés microélastiques d'une seule particule de PS II.

ABSTRACT

Photosystem II (PS II) is a pigment-protein complex integrated into the thylakoid membrane of higher plants, cyanobacteria, red and green algae. It plays a major role in photosynthesis process by using solar energy to decompose water, generate molecular oxygen and transmembrane proton gradient that drives the synthesis of ATP. Much of biological functionality of PS II system arises from its three-dimensional structure and interaction among its various subunits. This work combines the Langmuir surface preparation technique with surface spectroscopy and atomic force microscopy (ATM) to study the structure of PS II and its subcomponents under well defined conditions. The PS II membranes and PS II core complex are first extracted from green plants while maintaining their biological activities. These isolated protein complexes are then tested for their film-forming ability by using Langmuir technique. The optimum conditions of constructing stable monolayer structures at the air-water interface are established. The monolayer systems of PS II membranes and PS II core complex represent a controlled experimental environment which mimic the natural biomembrane. The surface pressure and surface potential properties of these proteins yield information about their average particle sizes through

surface pressure-area isotherm analysis. The surface studies of the mixture of PS II core complex and lipid (MGDG) indicate that the lipid enhances the ability of protein to form stable monolayer structures and also protect protein structural integrity in the thin films. The comparison of surface spectroscopic information of PS II systems with that of bioactive suspensions indicates that the PS II membrane systems maintain their structural integrity in the monolayer. However, the spectroscopic shifts of PS II core complex at the air-water interface suggest that the artificial monolayer structure modifies the protein conformation of PS II core complex. The well characterized PS II membrane monolayer systems are further studied by using tapping mode atomic force microscopy (AFM). The tapping mode AFM provides a direct observation of individual protein particles. AFM images reveal that the PS II particles distribute randomly across the membrane. Our AFM data also reveals the existence of an intramolecular cavity near the center of each particle which confirms the previous electron microscopy data of stained samples. A study of the particle's apparent height and cavity size as a function of applied forces through AFM tip provides unique information about the microelastic properties of single PS II particles.

ACKNOWLEDGMENTS

I deeply appreciate my graduate study advisor, Professor Roger M. Leblanc for the opportunity, knowledge, guidance, encouragement and the financial support. I would also like to thank Prof. Robert Carpentier, Prof. François Boucher, Prof. Christian Salesse and Prof. Claude Gicquaud for their help on the correction of my dissertation and as my dissertation committee members.

Thanks to Prof. Nong-jiang Tao for his cooperation in taking all AFM measurements. I also would like to thank Dr. Konka for his useful discussion on the sample preparation. Thanks to Shaopeng Wang for his computer skill help through this research work.

Thanks also to the Department of Chemistry at University of Miami for their teaching assistantship to complete my graduate program.

Special thanks to my husband, Xin Luo, for all of his support, encouragement and sharing.

Finally, taking this opportunity, I would also express the most sincere appreciation to my parents and my older sister. They always support and encourage me with love.

TABLE OF CONTENTS

LIST OF ABBREVIATIONS:

AFM	atomic force microscopy
BChl	bacteriochlorophyll
Bis-Tris	2-[bis(2-hydroxyethyl)amino]-2-hydroxymethylpropane-1,3-diol
CF_0-CF_1	ATP-synthase
Chl	chlorophyll
CP47/43	antenna chlorophyll-binding proteins of photosytem II
cyt	cytochrome
D1/D2	reaction center-binding proteins of photosytem II
DGDG	digalactosyldiglyceride
LDS	lithium dodecyl sulphate
LHC II	light-harvesting chlorophyll a/b-binding protein complex II
MES	2-(N-morpholino)ethanesulfonic acid
MGDG	monogalactosyldiacylglycerol
MW	molecular weight
NADPH	reduced nicotinamide adenine dinucleotide phosphate

P680	primary electron donor of photosystem II
PAGE	polyacrylamide gel electrophoresis
PG	phosphatidylglycerol
Phe	pheophytin
PMSF	phenylmethylsulphonyl fluoride
PS I	photosystem I
PS II	photosystem II
Q_A / Q_B	plastoquinone bound to PS II reaction center
RC	reaction center
SDS	sodium dodecyl sulphate
SQDG	sulphoquinovosyldiacylglyceride
Tris	2-amino-2-hydroxyethylpropane-1,3-diol

LIST OF TABLES

LIST OF FIGURES

FIGURE

CHAPTER I

INTRODUCTION

Photosynthesis is a natural process by which plants convert solar energy into chemical energy. On a global basis, annually this process fixes about 10 billion tons of carbon in the biosphere as carbohydrate, which equals to about 8 times mankind's energy consumption in 1990, and releases about 30 billion tons of oxygen to the atmosphere. The photosynthetic apparatus used by plants to perform this process is both complex and highly efficient (Barber, 1993a; Fleming and van Grondelle, 1994). Those photosynthetic apparatus are called photosystems. The photosystem has been an intensive studying project in recent years due to its high quantum and energetic efficiency.

The overall photosynthetic reaction is

$$H_2O + CO_2 \xrightarrow{h\nu} O_2 + (CH_2O)$$
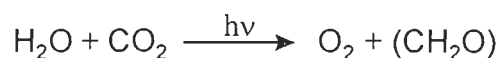
where (CH_2O) represents carbohydrate, mainly in the form of sucrose and starch. Photosynthesis converts about 70% of the absorbed light energy into chemical energy, and about 3% to fluorescence emission and the rest into heat.

Primary events of photosynthesis take place in thylakoid membranes of chloroplast. The process requires many small molecules and protein complexes and involves several physical and chemical mechanisms.

There are five functionally distinct protein complexes within the thylakoid membrane: light-harvesting chlorophyll a/b (LHC-2), photosystem II (PS II), photosystem I (PS I), cytochrome b_6f complex (cyt b_6f), and ATP-synthase (CF_1-CF_0) (Simpson and Wettstein, 1989). These supramolecular complexes interact together to promote the conversion of light energy into chemical energy. The process is initiated when light is absorbed by antenna molecules, chlorophylls, in light harvesting proteins. The resulting electronic excitation energy is transferred to reaction centers (PS I and PS II) where the energy is converted into a separation of charges. In essence, light is used to create reducing potential. Two distinctive photoreactions take place at . two different reaction centers, i. e. photosystem I and photosystem II. Photosystem I utilizes the reducing potential to produce NADPH (reduced nicotinamide adenine dinucleotide phosphate). Photosystem II, however, transfers the electrons of water to a quinone and produces molecular oxygen concomitantly. Electron flow within each photosystem as well as between them, assisted by the cytochrome b_6f complex, generates a proton gradient across the thylakoid membrane which drives the

synthesis of ATP using the ATP-synthase protein. The energetic molecules of ATP and NADPH form in the light reactions of photosynthesis are used to convert CO_2 into glucose and other organic compounds in a series of "dark reactions" called Calvin cycle.

In addition to those functional protein complexes, the lipids constitute about 25-30% of the total thylakoid mass. The neutral galactolipids, monogalactosyldiglyceride (MGDG) and digalactosyldiglyceride (DGDG) make up the major fraction (75%), while the remaining fraction consists of the negatively charged lipids phosphatidylglycerol (PG) (10%) and sulphoquinovosyldiacylglyceride (SQDG) (10%) and a small amount of other phospholipids (5%). Although these lipids do not contribute directly to the photosynthetic reactions, they form the backbone of membrane structures that not only supports various functional proteins but also maintain electrical potential that drives many important cellular activities such as transport and energy conversion. The thylakoid membranes are asymmetric in their content. The two faces of these membranes are different from each other and have distinctively different bio-functionality. The lipid distribution in thylakoid membranes is also most likely asymmetric laterally, as it supports different protein complexes (Murphy, 1986; Gounairs et al., 1986; Anderson, 1987; Hansson and Wydrzynski, 1990).

Photosystem II

As stated above, photosynthesis in green plants is mediated by two photosystems, photosystem I and photosystem II. The functionality of photosystem II is of particular interest because it harvests solar energy and utilizes it to 'split' water molecules. Investigation of this process will not only facilitate our understanding of photosynthesis in natural green plants, but it may also reveal valuable clues that could allow us to harvest solar energy efficiently in the form of artificially designed catalytic systems. Much can be learned from mother nature considering the astonishing efficiency of the photosynthesis processes!

Photosystem II (PS II) is a pigment-protein complex which can be found in the thylakoid membranes of plants, algae and cyanobacteria. The schematic model of PS II in the thylakoid membrane is shown in Figure 1.1 (Andersson and Styring, 1991). More than 20 polypeptides have been suggested to be associated with PS II (Masojidek et al., 1987). Extensive studies have been conducted to identify the primary functions of these polypeptides (Green and Camm, 1982; Green, 1988; Greene et al., 1988; Thornber et al.,1988; Erickson and Rochaix, 1992; Jansson, 1994). These results are summerized in Table 1. PS II complex consists in several main parts with distinctive functionality— 1) light -harvesting chlorophyll a/b proteins (LHC II), the main functions are absorption of the light, transfer of the excitation energy to PS II reaction center, contribution to the stacking of
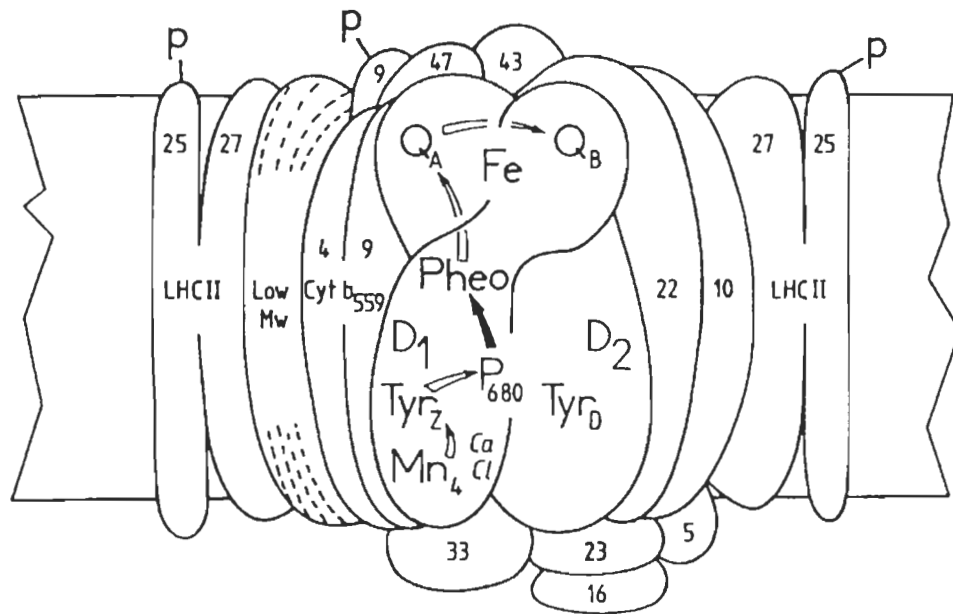
Figure 1.1 Schematic model of PS II in the thylakoid membrane. (Andersson and Styring, 1991)

the thylakoids (Staehelin, 1986) and partitioning of absorbed energy between

PS I and PS II (Williams and Allen,1987; Veeranjaneyulu and Leblanc, 1994);

2) the internal antenna proteins CP 47 and CP 43 which function to couple

energy transfer from LHC II to the reaction center (van Grondelle, 1985;

Pearlstein, 1987); 3) PS II reaction center in which the excitation energy

leads to the charge separation. The charge separation drives the abstraction

of electrons from water molecule by the positive charge which results in

evolution of molecular oxygen, and the reduction of plastoquinone by the

negative charge which results in the generation of a proton gradient across

the membrane; 4) extrinsic proteins 33, 23, and 17 kDa which are usually

assigned functions in regulating the ionic requirements for oxygen evolution

(Andersson and Akerlund, 1987). The overall function of PS II is driving light-

induced electron transfer from water to plastoquinone and reducing water to

molecular oxygen.

Light-harvesting chlorophyll a/b binding pigment-protein complex (LHC II):

The most abundant photosynthetic pigment-protein complex in higher

plants is the light-harvesting complex II (LHC II), which functions as an

antenna to enhance the efficiency of photosynthesis. LHC II contains several

polypeptides with molecular masses in the range of 25 to 30 kDa (Green and

Camm, 1982; Green, 1988; Greene et al., 1988; Thornber et al., 1988). It can

be resolved into 4 pigment-protein components termed as LHC IIa, b, c and d of which LHC IIb is the major component. The LHC IIb functions as an antenna; but LHC IIb and/or one or more of the other LHC II components also contribute to the stacking of the thylakoids (Staehelin, 1986), and partitioning of absorbed energy between PS I and PS II (Williams and Allen, 1987; Veeranjaneyulu and Leblanc, 1994). LHC IIa, c and d may be closely coupled to LHC IIb and the core complex and may serve in anchoring the LHC IIb to the core complex (Thornber, 1986; Thornber et al., 1988). LHC II exists in a trimeric form and consists mainly of a mixture of the highly homologous forms, LHCb1 and LHCb2. Besides several xanthophylls, each monomeric unit contains approximately 8 Chl a and 6 Chl b molecules (Jansson, 1994). Little is known on the nature of the association of pigments with proteins and the assembly of these pigment-protein complexes into a functional unit.

CP47 and CP43 polypeptides:

The two Chl a complexes CP 43 and CP47 must be considered as part of the PS II light-harvesting system. Several types of evidence suggest that these two CPs are in direct contact with the PS II reaction center, which is now clearly identified in the PS II fraction containing the two proteins D1 and D2 plus cyt b559. CP43 and CP47 are therefore to be regarded as internal Chl a antennae (Bricker, 1990). Although little is known about the actual physiological role of CP43 and CP47, some evidences have accumulated,

indicating that both of them are necessary to form a stable PS II unit (Bennoun et al., 1986).

PS II reaction center:

It is now generally accepted that the PS II reaction center is arranged as a protein heterodimer. The two involved proteins were designed as D1 and D2 which carry all the redox components—P680, Phe, Chls, Q_A and Q_B which are required for the primary photochemical reactions (Babcock et al., 1989; Rutherford, 1989) and may also host the manganese cluster catalyzing the photosynthetic water oxidation (Virgin et al., 1988; Svensson et al., 1990). The actual pigment composition of the D1-D2-cyt b559 reaction center has been found to vary with different preparation methods between 4 (Braun et al., 1990) and 6 (Kobayashi et al., 1990) of Chls . The detailed structure of the PS II reaction center is not known, but it is widely assumed that the arrangement of the cofactors is similar to that of the bacterial reaction center and that it contains two "extra" Chls which are more loosely coupled to the core and function as kind of "antenna Chls". At present, there also occurs an intense debate about the nature of P680, the primary electron donor in the PS II reaction center. It most likely involves two Chls which are arranged to form a special pair (Renger, 1992; Barber, 1993a,b). In bacterial system, the primary electron donor consists of a pair of exciton-coupled bacteriochlorophyll molecules. In higher plant PS II, van Kan et al. (van Kan et al., 1990) proposed a dimeric arrangement of chlorophyll with exciton

bands at 679.5 and 683.5 nm and with an angle of about 60° between the Q_y transitions of the monomers. The Q_y transitions of the two chlorophyll constituents of P680 are solely responsible for the observed absorption peak at 680-682 nm. The accessory chlorophylls absorb around 670 nm (van Kan et al., 1990).

Extrinsic proteins 33, 23, and 17 kDa:

PS II contains a set of hydrophilic proteins that have apparent molecular masses of about 33, 23 and 17 kDa, which are defined as Regulatory Cap. These components are designated as EP33, EP23 and EP17, where EP stands for "extrinsic protein". Those Regulatory Cap proteins are extrinsically bound to the lumenal surface of the membrane (Andersson and Âkerlund, 1987) and are usually assigned functions in regulating the chloride and calcium requirements for oxygen evolution or in controlling the exchange of reactants with the manganese center. Based on cross-linking (Bowlby and Frasch, 1986; Machold,1986; Millner et al., 1987; Enami et al., 1989), proteolytic (Isoagai et al., 1985) and immunological studies (Ljungberg et al., 1984; Ivey and Berg, 1985; Aoki et al., 1986; Camm et al., 1987), the EP33 can link directly with the reaction center and internal antenna components, whereas the two smaller proteins EP23 and EP17 appear to link to the LHC II complex.

Table 1

Summary of polypeptides of PSII core complex (Green and Camm, 1982;

Green, 1988; Greene et al., 1988; Thornber et al.,1988; Erickson and

Rochaix, 1992; Jansson, 1994).

Protein name	Protein size (kDa)	Description
D1	32	Reaction center (RC) core, binds Q_B, pheophytin, Mn?, chlorophyll special pair
CP47	47-51	chlorophyll-a binding, inner antenna, RC core complex
CP43	43-47	chlorophyll-a binding, inner antenna, RC core complex
D2	34	RC core, binds Q_A, pheophytin, Mn?, chlorophyll special pair
Cyt b559	9	RC core
Cyt b559	4	RC core
10-kDa phosphoprotein	7.6	PSII particle, affects D1/D2 dimer conformation
I polypeptide	4.2	RC core
?	< 5	?
K polypeptide	4.3	present in PSII complex, absent in purified O_2-evolving preparations
L polypeptide	4.3	PSII oxygen-evolving particles
M polypeptide	3.8	PSII oxygen-evolving core
N polypeptide	4.7	PSII oxygen-evolving core
OEE 1	33	O_2-evolving core, Mn-stabilizing OEC component
OEE 2	23	OEC component (absent in cyanobacteria)
OEE 3	16	OEC component (absent in cyanobacteria)
10-kDa nuclear	10	regulatory OEC component
LHC IIa	29	anchoring LHC IIb to PS II core
LHC IIb	28	major antenna
LHC IIc	27	anchoring LHC IIb to PS II core
LHC IId	25	anchoring LHC IIb to PS II core

Previous studies of PS II

Considering the sheer volume of works done on the subject, a comprehensive review of past work is obviously out of scope of this dissertation. However, a brief discussion of experimental techniques that have been used to study the function and structure of PS II complexes will provides a guideline for the work done in this thesis. Table 2 lists some of these techniques reviewed in this thesis.

Much of our current understanding of PS II system has resulted from biochemical separation and isolation methods. These techniques employ various detergents to break a complex biomembrane system into smaller subunits, while maintaining their distinctive biofunctions. The electrophoretic methods such as SDS-PAGE and LDS-PAGE have normally been used to identify each individual component. Application of these biochemical techniques to the studies of PS II system enable us to isolate a variety of PS II complexes with different integrity or activity and provide wealthy samples and subjects for structure-function relationship studies of PS II complex.

Thylakoid membranes of plants are differentiated into stacked (appressed) and unstacked (nonappressed) regions. PS I and the ATP synthase (CF_1-CF_0) are located almost exclusively in the nonappressed stromal regions and in the nonappressed regions of the grana stacks. They are laterally segregated from PS II and LHC II, which have their main location in the appressed regions (Andersson and Adderson, 1988). Berthold and coworkers exploited this fact and successfully separated fully functional PS II

membrane from the rest of the thylakoid membrane (Berthold et al., 1981; Dunahay et al., 1984). The PS II membrane can then be further reduced into PS II core complex retaining O_2 evolution activity (Ghanotakis et al., 1987; Haag et al., 1990) or into a PS II reaction center having D1, D2, and cyt b559 polypeptides (Nanba and Satoh, 1987). These studies have contributed to our current understanding of PS II by deducing the structure and function of the PS II complex. Although these biochemical preparation methods provide an enormous amount of information about identifying functional subunits within the PS II complex, they can not tell the structural details of each individual subunit neither they can provide the association and interaction among different subunits.

Spectroscopic methods have also been widely used in studying functions of PS II complexes. In higher plants, each Chl a, Chl b and carotenoid molecules is complexed with, but not covalently linked to, one of several specific membrane-associated proteins (Andersson and Styring, 1991). Both Chls and carotenoids are essential for proper folding of the proteins which bind them (Paulsen, 1995). These pigment molecules also play central roles in harvesting solar radiation and transferring and redistributing charges within and among various components of PS II complexes. The existence of the pigment molecules in PS II complexes offers a spectroscopic 'window" that allows us using various spectroscopic tools to study the function and structure of PS II systems at molecular level. Time-resolved spectroscopy, as a prime example, has revealed the dynamics

and time scales of charge separation and electron transfer processes (Zinth and Kaiser, 1993). The information obtained from dynamic studies provides important insights into possible reaction schemes and mechanism of electron transfer processes. Spectral hole burning experiments can also provide us wealthy information on excited state electronic structure, heterogeneity, electron-phonon coupling, and transport dynamics of photosynthetic units (Jankowiak and Small, 1993). The absorption and emission spectra of chromophores such as chlorophylls are sensitive to their environment which is determined by the dynamic structures of associated proteins. Therefore, by monitoring spectroscopic information such as absorption and emission intensity and band position of these chromophores at different preparation states, one can infer the structural changes of their associated protein complexes.

X-ray crystallography, which reveals the precise three-dimensional positions of most of the atoms in a protein molecule, can greatly enhance our understanding of protein structure and function. However, the application of this technique to the study of PS II system is hindered by the difficulties of forming PS II single crystal. Nevertheless, X-ray crystallography has been successfully employed to probe the structure of bacterial reaction center (Michel, 1982; Deisenhofer et al., 1984). The structural analysis of three-dimensional crystals of membrane protein complexes from *Rhodopseudomonas viridis* indicated that the reaction center contains four different protein subunits of H (heavy), M (medium), L (light), and cytochrome

c (Michel, 1982). Two BChls attached to L and M subunits form a closely associated and noncovalently linked dimer (special pair) (Deisenhofer et al., 1984) as primary electron donor. Among major functional constituents of PS II protein complex, D1 and D2 exhibit remarkable sequence analogies with the subunits L and M of bacterial reaction center (Michel and Deisenhofer, 1988). Through extensive work by use of biochemical and biophysical techniques, it is currently believed that D1 and D2 proteins form a heterodimer, which binds the chromophores for photochemistry and the electron transfer components. Nevertheless, the detailed structure of the D1/D2 heterodimer of PS II complex remains unresolved.

Electron microscopy (EM) (Hagg et al., 1990; Holzenburg et al., 1993; Santini et al., 1994; Boekema et al., 1995; Holzenburg et al., 1996; Nakazato et al., 1996; Tsiotis et al., 1996) offered another powerful tool for probing PS II structures. This technique traditionally requires that the protein sample to be stained or metal coated. Interpretation of these results, however, remains difficult because negative staining visualizes the stain-exclusive density but not the true protein density. Recent progress in cryo-electron microscopy has opened a way to solve the structure of membrane proteins at high resolution (Kühlbrandt et al., 1994). However, such high-resolution electron microscopy is possible only with unstained, large, well-ordered 2D crystals. Only recently, this technique has been applied to the studies of PS II (Nakazato et al., 1996; Marr et al., 1996).

Electron microscopy and image analysis of two-dimensional crystals of PS II complex (Bassi et al., 1989; Boekema et al., 1990) have shown that the mass of the complex is around 600-700 kDa. Since the sum of the molecular weights of the component polypeptides is about 250 kDa, this result strongly suggests that the core complex is present as a dimer in PS II. The clearest electron microscopy picture comes from negatively stained cyanobacterial PS II particles and spinach PS II core complex, subjected to sophisticated image analysis (Boekema et al., 1995). These particles clearly have an axis of twofold symmetry across their largest dimension. Molecular weight estimates and the presence of two separate 33 kDa polypeptides per particle support the idea that they are dimeric. On the other hand, images of ordered arrays of particles in PS II membranes containing the full complement of Chl a/b proteins have been interpreted as having a monomeric PS II core. The core particle internal or lumenal face is characterized by four strong central domains surrounding a cavity (Holzenburg et al., 1993; Holzenburg et al., 1996).

Electron microscopy results also implied that the organization of PS II may differ for cyanobacteria and higher plants. A dimeric form of PS II is suggested for cyanobacteria. In contrary, dimers of PS II core complex from spinach attached at their membrane-exposed sides were scarcely seen on electron micrographs (Haag et al.,1990).

By stepwise removal of the components of PS II complex, the conventional transmission electron microscopy results showed that the

removal of CP 47 induces monomerization of PS II, which indicates the importance of this subunit for maintaining the PS II dimeric structure (Santini et al., 1994).

Scanning tunneling microscopy (STM), which has advantages of directly applicable to samples in air or solutions, had also been applied to the structural studies of PS II (Amrein and Marti, 1993). However, since electrons cannot directly tunnel through large insulating molecules such as PS II, interpretation of these earlier results is difficult and rather ambiguous. In recent studies, platinum replicates or metal coated PS II membranes were therefore used instead of native protein particles (Facci et al., 1994; Seibert, 1995). Requirement of metal coating of protein surface introduces additional sample preparation steps and more importantly, exposes protein particles to harsh conditions that may affect their structural conformation. These adverse effects undermined usefulness of STM technique in biological systems. Like EM and STM, atomic force microscopy (AFM) can provide us with topographical information of a two dimensional surface. However, AFM can be directly applied to both conductive and non-conductive samples and therefore it requires no additional metal coating samples. In addition, since AFM technique senses atomic forces between probe tip and sample surface, this method may allow us, at least in principle, to probe the interaction among various protein sub-units at their boundaries. These characteristics of AFM make it well suited for imaging biological systems where minimum intrusion during sample preparation is required (Yang and Shao, 1995).

Table 2

Techniques for probing photosystem II structure.

Techniques	Author	Year
Biochemistry	Andersson and Adderson	1980
	Andersson and Akerlund	1987
	Green	1988
	Shinozaki et al.	1989
	Peter and Thornber	1991
	Vermaas	1993
	Green and Durnford	1996
Spectroscopy	van Kan et al.	1990
	Zinth and Kaiser	1993
	Jankowiak and Small	1993
X-ray Diffraction	Michel	1982
	Deisenhofer et al.,	1984
Electron Microscopy(EM)	Haag et al.,	1990
	Holzenburg et al.,	1993
	Santini et al.,	1994
	Boekema et al.,	1995
	Holzenburg et al.,	1996
	Nakazato et al.,	1996
	Marr et al.	1996
Scanning Tunneling Microscopy (STM)	Facci et al.,	1994
	Seibert	1995
Atomic Force microscopy (AFM)	Lyon et al.,	1993
	Yamada et al.,	1994
	Shao et al.,	1997

Research objectives

The photosynthetic proteins have an unusually large number of pigment molecules associated with a single protein. A detailed biochemical, biophysical, and structural description of each pigment-protein complex is essential to fully understand how light energy is trapped and converted into chemical energy. To achieve this objective, this study works on obtaining information on structure and function of photosystem II, which is responsible for water oxidation and electron transfer upon absorption of light. The main goal of this work is to obtain structural information of PS II complexes and try to correlate this information to their function in Langmuir-Blodgett (L-B) films using atomic force microscopy. The specific goals are the following: 1) to study the spectroscopic properties of PS II in Langmuir films at the air-water interface and in Langmuir-Blodgett (L-B) films on a solid substrate; 2) to record the topographical images of PS II preparations differing in polypeptide composition in L-B films using tapping mode atomic force microscopy.

Organization of the thesis

In the present thesis, the PS II membranes and PS II core complex are first extracted from green plant while maintaining their biological activities. These isolated protein complexes are tested for their film-forming ability by using the Langmuir technique. The optimum conditions for constructing stable monolayer structures at the air-water interface are established. Then the monolayer systems of PS II membranes, PS II core complex and the

mixture of PS II core complex with lipid MGDG are produced under a controlled experimental environment to mimic the natural biomembrane. The comparison of surface spectroscopic information of PS II systems with that of bioactive solutions are made to monitor if these protein supramolecular assemblies maintain their structural integrity in the monolayer. The well-characterized PS II membrane monolayer systems are further studied by using tapping mode atomic force microscopy (AFM). The tapping mode AFM provides a direct observation of individual protein particles. A study of the micro-elastic properties of protein particles is also performed.

Chapter 2 of the thesis discusses the experimental techniques used in this study (L-B technique, Spectroscopic methods, and AFM method). Chapter 3 discusses sample preparation and studies of film forming ability of PS II particles. Chapter 4 presents spectroscopic data of PS II particles in solution and at the air-water interface. Chapter 5 describes the structural information and the micro-elastic properties of PS II particles using the tapping mode AFM technique. Finally, chapter 6 summarizes the dissertation and offers some suggestions for further studies. Appendix describes the design and implementation of a home-built surface spectroscopic instrument.

CHAPTER II

EXPERIMENTAL TECHNIQUES

<u>Langmuir technique</u>

The surface of a liquid always has excess free energy; this is due to the difference in environment between the surface molecules and those in the bulk. The surface tension (γ) of a plane interface is given by the partial differential:

$$\gamma = (\partial G / \partial S)_{T, P, n_i} \qquad (2.1)$$

where G is the Gibbs free energy of the system, S is the surface area, and the temperature T, pressure P, and compositions n_i are held constant.

Wherever a gas or a liquid is in contact with another liquid or a solid surface, there is a layer of molecules at the interface and often this layer is oriented. In this work we need to compress an oriented and uniform layer of protein molecules at the air-water interface for further spectroscopic and structural studies.

<u>Surface pressure-area isotherm (π-A)</u>

A classical monolayer- forming material such as stearic acid has two distinct parts in the molecule: a hydrophilic headgroup, which is easily soluble in water, and a long alkyl chain, which provides a hydrophobic tail. When a solution of stearic acid in a water- immiscible solvent is placed onto a water surface, the solution spreads rapidly to cover the available area. As the solvent evaporates, a monolayer is formed: the headgroup immersed in the water surface and the tail group remains outside.

When the distance between stearic acid molecules is large, their interaction is small, and they can be regarded as a two- dimensional gas, as shown in Figure 2.1. Under these conditions, the surface monolayer has relatively little effect on the water surface tension. When one reduces the area of surface available to the monolayer, the molecules exert a repulsive effect on each other. This two- dimensional analog of a pressure is called surface pressure (π):

$$\pi = \gamma - \gamma_0 \qquad\qquad (2.2)$$

where γ is the surface tension in the absence of a monolayer and γ_0 is the value with the monolayer present.

The single most important indicator of the monolayer properties of a material is given by a plot of surface pressure as a function of the area of
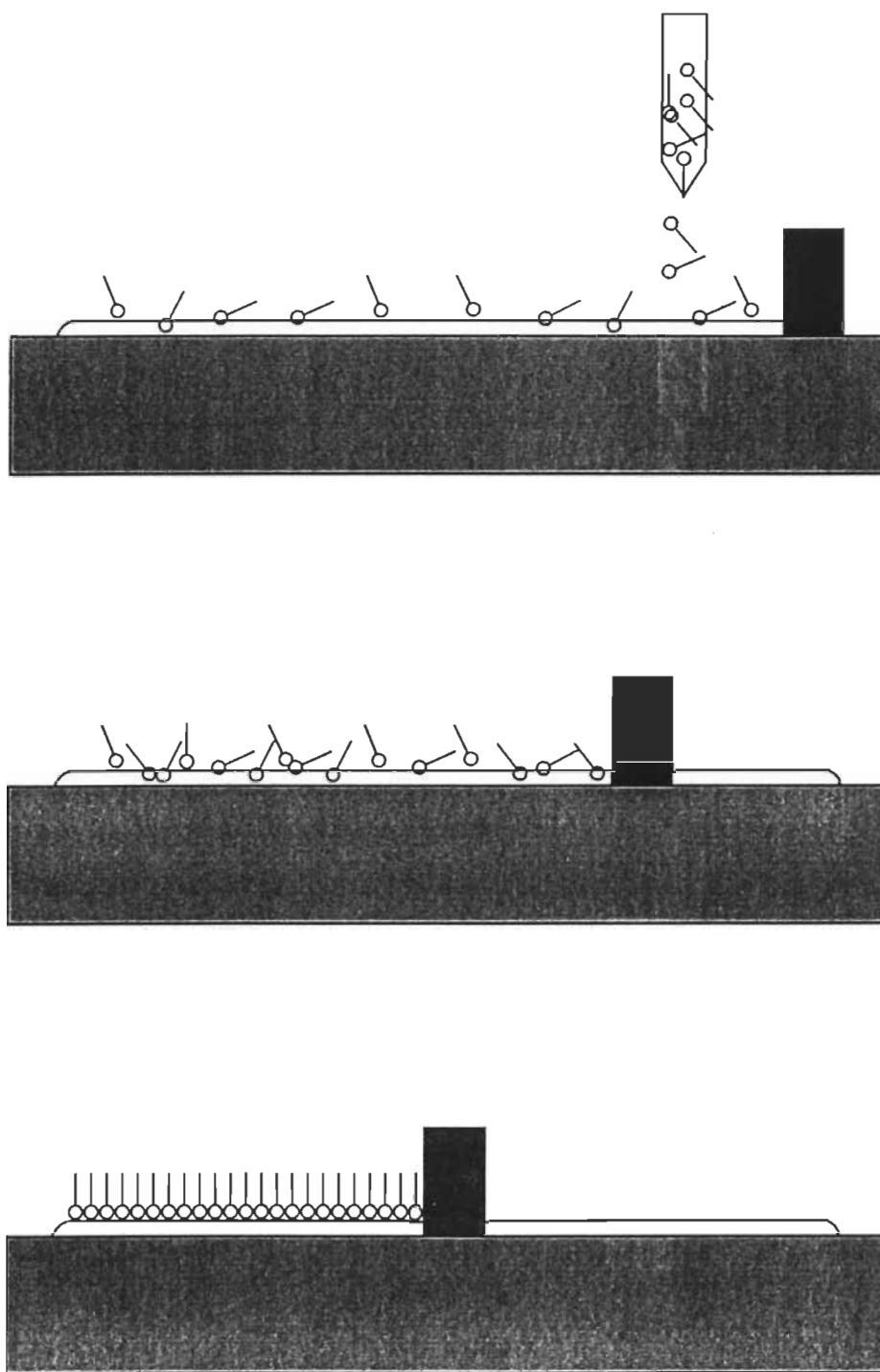
Figure 2.1   A scheme of monolayer at the air-water interface.

water surface available to each molecule. This is carried out at constant temperature and is know as a surface pressure- area isotherm (Langmuir, 1917). Equilibrium values can be measured on a point- to- point basis, but it is more common to record a pseudo-equilibrium isotherm by compressing the monolayer at a constant rate while continuously monitoring the surface pressure. Since we know the total number of molecules and the total area that the monolayer occupies, we can calculate the area per molecule ($Å^2$) and construct a π -A isotherm that describes the surface pressure as a function of the area per molecule. Figure 2.2 presents a schematic isotherm of stearic acid on 0.01 M HCl (Gaines, 1966; Ulman, 1990).

The isotherm was divided into three main parts: the gas-, liquid-, and solid- like phases. There is a consensus that the low - density limit is similar to a two- dimensional gas, where molecules are separated, although aggregation may occur, and that the highest- density limit is a two- dimensional solid. Between these extremes, there may be a variety of phases, such as orientationally disordered (liquid expanded, LE), orientationally ordered (liquid condensed, LC), and striped.

The compressibility of a monolayer is defined by the equation:

$$C = - (1/ A) \cdot (\partial A / \partial \pi)_{T, P, n_i}$$ (2.3)
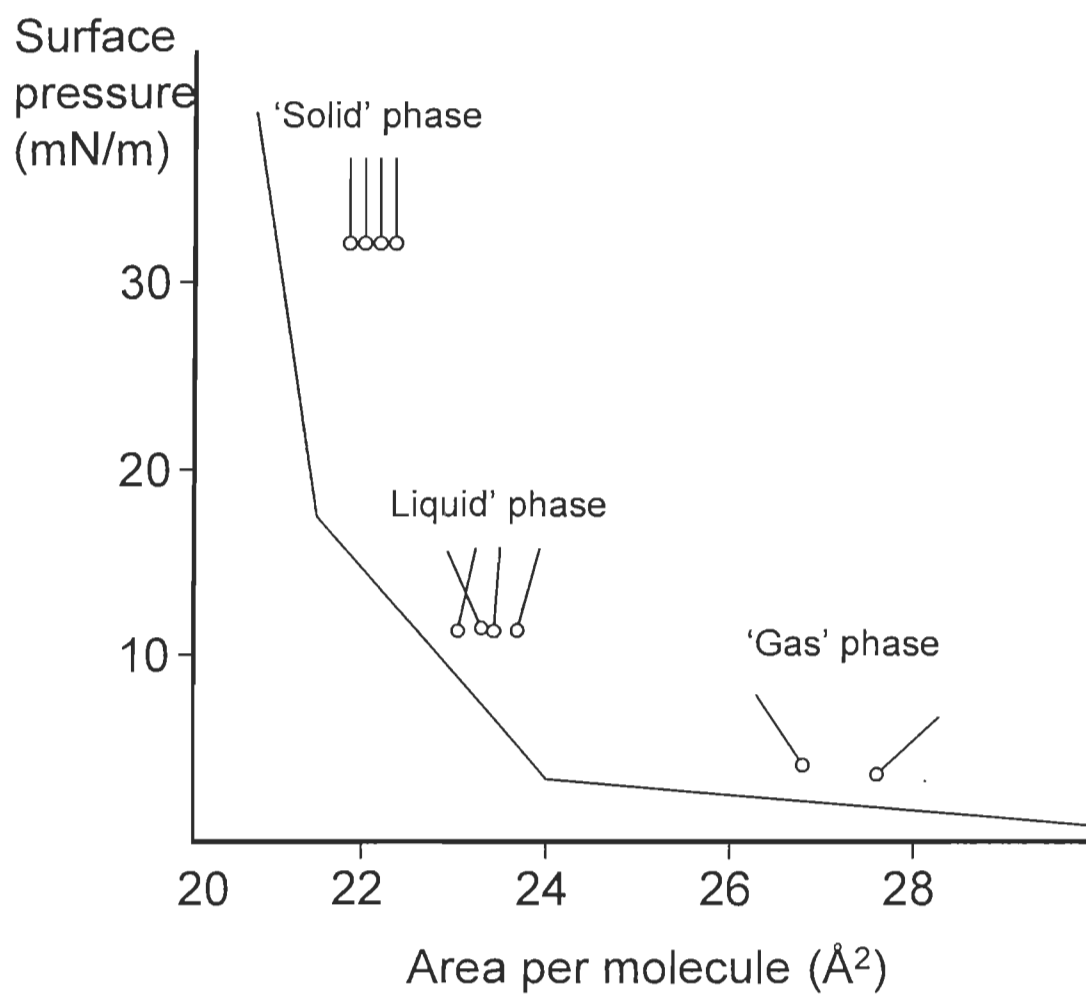
Figure 2.2   A scheme of surface pressure (π) vs area per molecule (A) for stearic acid on 0.01 M HCl.

When the compressibility of a monolayer approaches infinity, the phenomenon of collapse occurs at small surface area. The onset of collapse depends greatly on such factors as the past history of the monolayer and the rate at which the monolayer is being compressed. In this type of collapse, it is believed that molecular layers are riding on top of each other and disordered multilayers are being formed (Gabrielli et al., 1976).

The shape of the surface pressure- area isotherm of a monolayer depends greatly on temperature and a number of different phase transitions can be observed if the temperature is varied.

Surface potential-area isotherm (ΔV-A)

The Volta potential change that occurs when an insoluble monolayer is spread at a liquid-gas or liquid-liquid interface is commonly called the surface potential, ΔV, of the monolayer.

The surface potential method is an important tool for analysis of the electrical structure of surfaces, i. e. the distribution of polar vs. nonpolar groups. At the air- water interface, we measure the Volta potential between the surface of a liquid and that of a metal probe immersed in the liquid. Figure 2.3 presents one available procedure to measure surface potential. The pressure of the monolayer on the water surface influences this potential. Thus, the practice usually is to measure the difference between the potential of the clean surface and that of a monolayer-covered subphase (ΔV), rather than to try to determine a single- surface potential.

Surface potential values usually are expressed alternately in terms of surface dipole moments, $\mu_{\perp}$, calculated from the equation

$$\mu_{\perp} = (1 / 4\pi)(\Delta V / n) \qquad (2.4)$$

where n is the number of molecules per cm^2 in the monolayer. If we write A, the molecular area, in $Å^2$ /molecule, and ΔV in millivolts, this becomes

$$\mu_\perp = A \; \Delta V / \; 12 \; \pi \qquad\qquad\qquad (2.5)$$

where the surface dipole moment $\mu_\perp$ is obtained in millidebye units (mD).
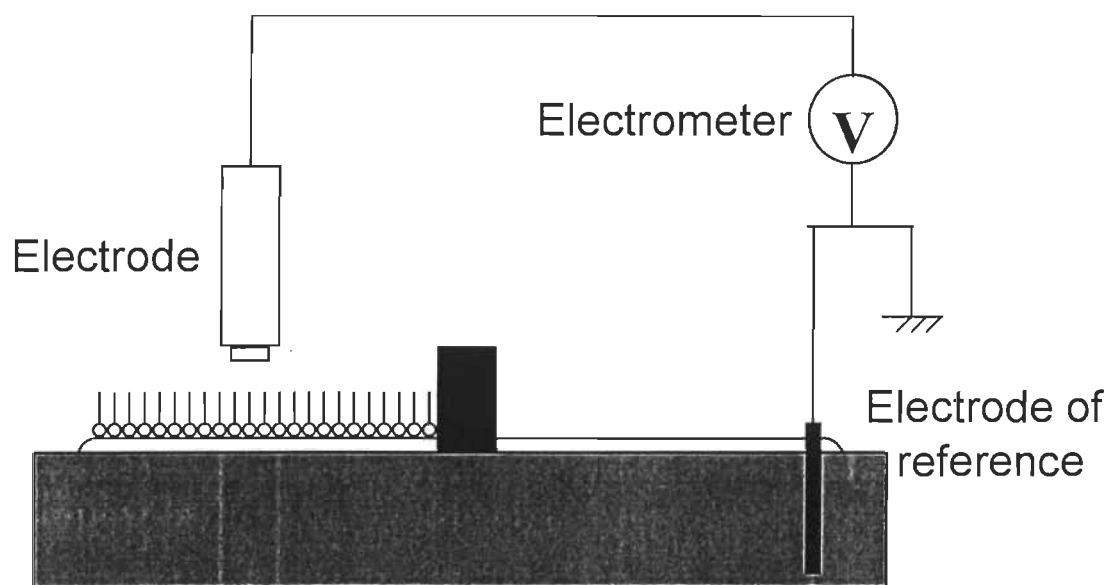
Figure 2.3   The principle scheme of surface potential measurement.

UV-VIS absorption and fluorescence spectroscopes

Historically, the term spectroscopy referred to a branch of science in which light (that is, visible radiation) was resolved into its component wavelengths to produce spectra. With the passage of time, the meaning of spectroscopy has become broadened to include studies not only with light but also with other types of electromagnetic radiation, such as X-ray, ultraviolet, infrared, microwave and radio-frequency radiation. Nowadays, spectroscopy has proved to be a powerful tool for qualitative and quantitative analysis.

In this work, we focus on absorption and fluorescence spectroscopy (Skoog et al., 1988).

General principle

Absorption of radiation

In spectroscopic nomenclature, absorption is a process in which a chemical species in a transparent medium selectively attenuates certain frequencies of electromagnetic radiation. According to quantum theory, every elementary particle (atom, ion or molecule) has a unique set of energy states, the lowest of which is the ground state; at room temperature, most elementary particles exist in their ground state. When a photon of radiation passes near an elementary particle, absorption becomes probable only if the energy of the photon matches exactly the energy difference between the ground state and one of the higher energy states of the particle. Under these circumstances, the photon energy is transferred to the particle, converting it

to the higher energy state, which is termed an excited state. Excitation of a species M to its excited state M* can be depicted by the equation

$$M + h\nu \longrightarrow M^* \tag{2.6}$$

After a brief period (10^{-6} to 10^{-9} sec), the excited species relax to its original ground state, transferring its excess energy to other atoms or molecules in the medium. This process, which causes a small rise in temperature of the surrounding, is described by the equation

$$M^* \longrightarrow M + heat \tag{2.7}$$

Relaxation also occurs by photochemical decomposition of M* to form new species or by the fluorescent or phosphorescent emission of radiation. The lifetime of M* is very short so that its concentration at any instant is ordinarily negligible.

The absorbing characteristics of a species is conveniently described by means of an absorption spectrum, which is a plot of some function of the attenuation of a beam of radiation versus wavelength, frequency, or wavenumber.

Figure 2.4 is a partial energy-level diagram that depicts some of the processes that occur when a molecule absorbs infrared, visible, and
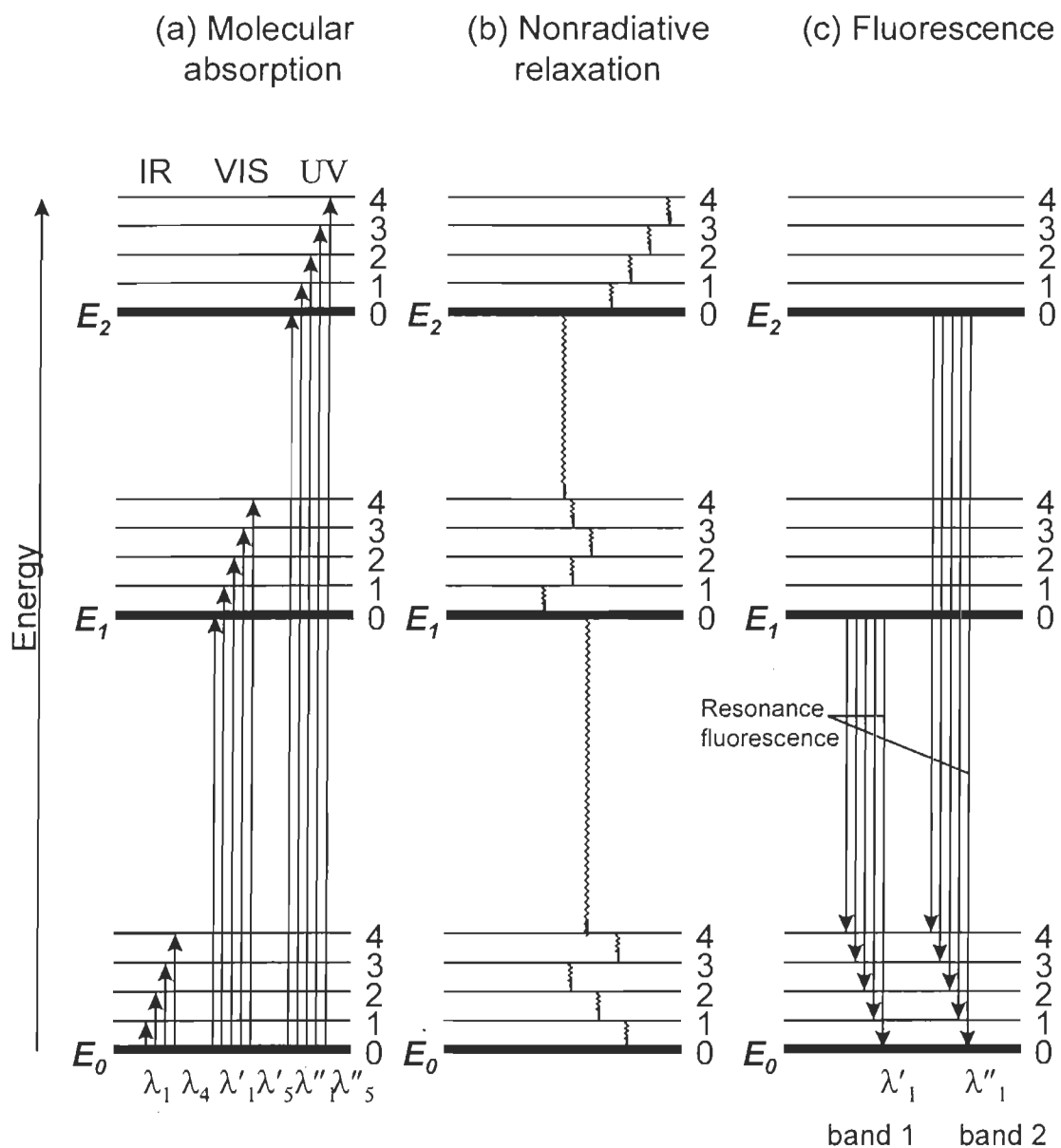
Figure 2.4   Energy-level diagram showing some of the energy changes that occur during absorption, nonradiative relaxation, and fluorescence by a molecular specie.

ultraviolet radiation. The energies E_1 and E_2, two of the excited states of a molecule, are shown relative to the energy of its ground state E_0. In addition, the relative energies of a few of the many vibrational states associate with each electronic state are indicated. As shown in Figure 2.4, molecular absorption in the ultraviolet and visible regions consists of absorption bands made up of closely spaced lines.

<u>Relaxation processes</u>

An excited species can give up its excess energy and relax to its ground state. Two of the most important of these relaxation processes are nonradiative relaxation and fluorescence/phosphorescence relaxation.

(A). Nonradiative relaxation

Two types of nonradiative relaxation are shown in Figure 2.4b. Vibrational relaxation depicted by the short wavy arrows between vibrational energy levels, takes place during collisions between excited molecules and solvent molecules. During the collisions, the excess vibrational energy transferred to solvent molecules in a series of steps as indicated in the figure. The gain in vibrational energy of the solvent is reflected in an increase in the temperature of the medium. Vibrational relaxation is such an efficient process that the average lifetime of an excited vibrational state is only about 10^{-12} s.

Nonradiative relaxation between the lowest vibrational level of an excited electronic state and the upper vibrational level of another electronic state, depicted by the two long wavy arrows in Figure 2.4b, is much less

efficient than vibrational relaxation so that its average lifetime is between 10^{-6} and 10^{-9} s.

The mechanisms of this type of relaxation are not fully understood, but the net effect is still a rise in the temperature of the medium.

(B). Fluorescence relaxation

Fluorescence/phosphorescence are analytically important emission processes. Fluorescence takes place much more rapidly than phosphorescence and is generally complete in about 10^{-5} s or less from the time of excitation. Phosphorescence emission may extend for minutes or even hours after irradiation has ceased.

As shown in Figure 2.4c, bands of fluorescence radiation are produced when molecules are excited by the absorption of a beam of electromagnetic radiation and then relax. Like molecular absorption bands, molecular fluorescence bands are made up of a multitude of closely spaced lines that are often difficult to resolve. Note that the lines that terminate the fluorescence bands on the high-energy, side (λ'_1 and λ''_1) are resonance lines. That is, molecular fluorescence bands consist largely of lines that are longer in wavelength than the band of absorbed radiation responsible for their excitation. This shift in wavelength is sometimes called the Stokes shift.

When a molecule is irradiated by a single wavelength λ''_5, absorption of this radiation promoted an electron into vibrational level 4 of the second excited electronic state E_2. In 10^{-15} s or less, relaxation to the zero vibrational

level of E_1 occurs. At this point, further relaxation can follow either the nonradiative route or radiative route. If the latter is followed, relaxation to any of the several vibrational levels of the ground state can take place, giving a band of emitted wavelengths. All those lines are lower in energy, or longer in wavelength, than the excitation line λ''_5.

Absorption and fluorescence spectra of chlorophyll

Two porphrin derivatives, chlorophyll a and b are found in photosystems of higher plants. Chl a is by far the most common pigment, forming part of light-harvesting protein complexes in higher plants, algae, prochlorophytes, and cyanobacteria, and functioning in the reaction centers of PS I and PS II as primary electron donor. In addition, Chl a is found in intrinsic antenna complexes that are closely connected to the reaction centers.

The visible absorption spectra of chlorophyll molecules consist of two distinctive bands in the blue and red spectral regions. The red absorption band corresponds to the transition between ground electronic state and the first singlet excited state (Q_y) while the blue absorption band corresponds to the transition between ground and second singlet excited state. The spectroscopic properties of chlorophyll molecules depend strongly on their environment. It has been observed that aggregation of chlorophyll molecules changes their absorption intensities and spectral positions (Gouterman, 1961; Goedheer, 1966). The chlorophyll dimer and other oligomers exhibit a red
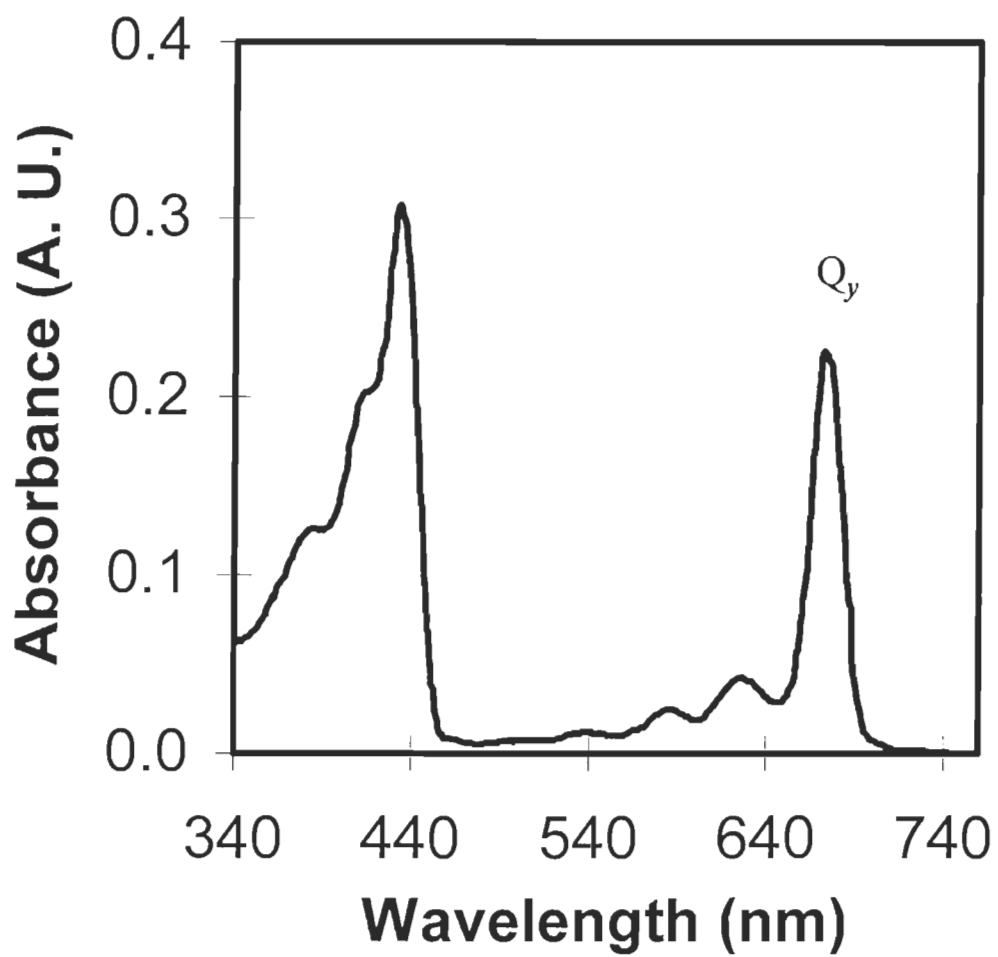
Figure 2.5 The absorption spectrum of fresh extracted Chl a in benzene.

shift in absorption bands, indicating the formation of chlorophyll aggregates which means lower energy gaps between ground and excited electronic states.

The fluorescence spectra of chlorophyll molecules, however, originate only from the lowest singlet excited state. The second singlet excited state resulted from blue absorption does not fluoresce directly and undergo a rapid, radiationless internal conversion to the lowest excited singlet state. As their absorption spectra, the emission spectra of chlorophyll molecules also depends on their degree of aggregation (Livingston et al., 1949; Evstigneev et al., 1950).

As mentioned above, spectroscopy of Chl can be affected by its concentration and surrounding solvents (Goedheer, 1966). These concentration and solvent effects indicate that Chl spectra are sensitive to their aggregation states and dipole interactions with other nearby molecules. In photosystems of higher plants, there are several types of chlorophyll aggregates that are attached to different protein sub-units. These protein sub-units define localized environment for these Chl molecules. Any structural and conformational changes in these protein subunits are likely to perturb the aggregation states of Chl molecules and their dielectric interaction with surrounding protein and solvent molecules. Therefore, analysis of *in vivo* chlorophyll spectra provides us a very powerful probe to study the dynamic structure of these complex systems because of the environmental dependency of chlorophyll spectroscopy (Goedheer, 1966).
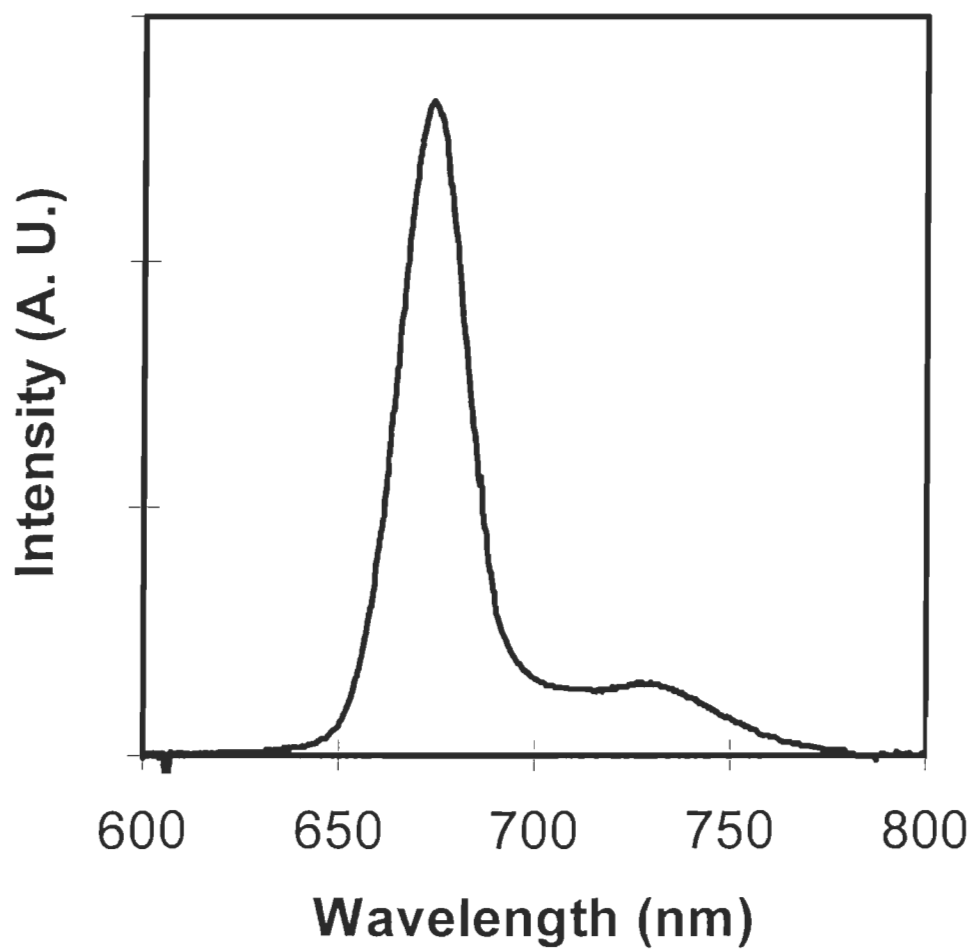
Figure 2.6 The fluorescence spectrum of fresh extracted Chl a in benzene.

Scanning probe microscopy (SPM)

In the over 300 years of optical and 50 years of electron microscopy development, nothing could have prepared us for the incredible imaging power and simplicity of the scanning tunneling microscopy (STM) (Binnig and Rohrer, 1982). The STM can give atomic resolution images of conductive samples in vacuum and atmosphere, even under water and other fluids (Hansma and Tersoff, 1987; Sonnenfeld and Hansma, 1986). The immense importance of these discoveries was confirmed by the fact that Binnig and Rohrer shared the Nobel Prize in Physics in 1986, only four years after the first STM paper was published.

The success of the STM has led to the invention of a host of other scanning probe microscopies, which rely on mechanically scanning a sharp tip over a sample surface. The scanning force microscopy (SFM) or atomic force microscopy (AFM) is the one of the most successful of these new devices (Binnig et al., 1986).

In contrast to the better-known scanning tunneling microscopy (STM), which detects a current of tunneling electrons between a scanning tip and a sample, the scanning force microscopy (SFM) does not require the surface under study to be electronically conductive. Instead, the SFM measures tip-surface interactions due to forces such as van der Waals, electrostatic, frictional, and magnetic forces. Thus, it can be applied to both conductive and insulating samples. The SFM has become an important tool for imaging surfaces (Wickramasinghe, 1989).

Principle of scanning force microscopy (SFM)

The force microscopy, in general, has several modes of operation. In the repulsive- force or contact mode, the force is of the order 10^{-9} - 10^{-8} Newton, and individual atoms can be imaged. In the attractive-force or noncontact mode, the van der Waals force, the electrostatic force or magnetic force is detected. The latter does not provide atomic resolution, but important information about the surface is obtained. These modes comprise different fields in force microscopy, such as electric force microscopy (EFM) and magnetic force microscopy (MFM) (Sarid, 1991). Here, we will be concentrated on scanning force microscopy (SFM).

Whatever the origin of the force, all force microscopies have five essential components :

• A sharp tip mounted on a soft cantilever spring.

• A way of sensing the cantilever's deflection.

• A feedback system to monitor and control the deflection (and, hence, the interaction force).

• A mechanical scanning system (usually piezoelectric) that moves the sample with respect to the tip in a raster pattern.

• A display system that converts the measured data into an image.

The SFM has a number of elements common to STM: the piezoelectric scanner for actuating the raster scan and Z positioning, the

feedback electronics, vibration isolation system, and the computer control system. The major difference is that the tunneling tip is replaced by a mechanical tip, and the detection of the minute tunneling current is replaced by the detection of the minute deflection of the cantilever.

The SFM images surfaces by raster- scanning a sharp tip gently over the surface at forces as small as the forces between atoms in molecules. Raster-scanning is the movement of a tip back and forth across a surface, which produces a topological map of the surface features. The scanning tip is attached to the end of a cantilever, which deflects as the tip scans up and down over features on the surface, as shown in Figure 2.7. The deflection of the cantilever is detected by the displacement sensor.

There are two regimes of force that can be felt by the probing tip. If the tip is scanned extremely close to the surface, the force will be expressed by:

$$F(r) = 12B / r^{13} - 6D / r^{7} \tag{2.8}$$

where B and D are constants which depend upon the material of both the tip and sample (the specific properties of the atoms involved, such as the electron charge distribution) and r is the separation distance between atoms of the tip and sample (Burns, 1985). When scanning at small distance, the first term (the repulsive term) will dominate. Scanning at large separation distances, long-range attractive interaction forces
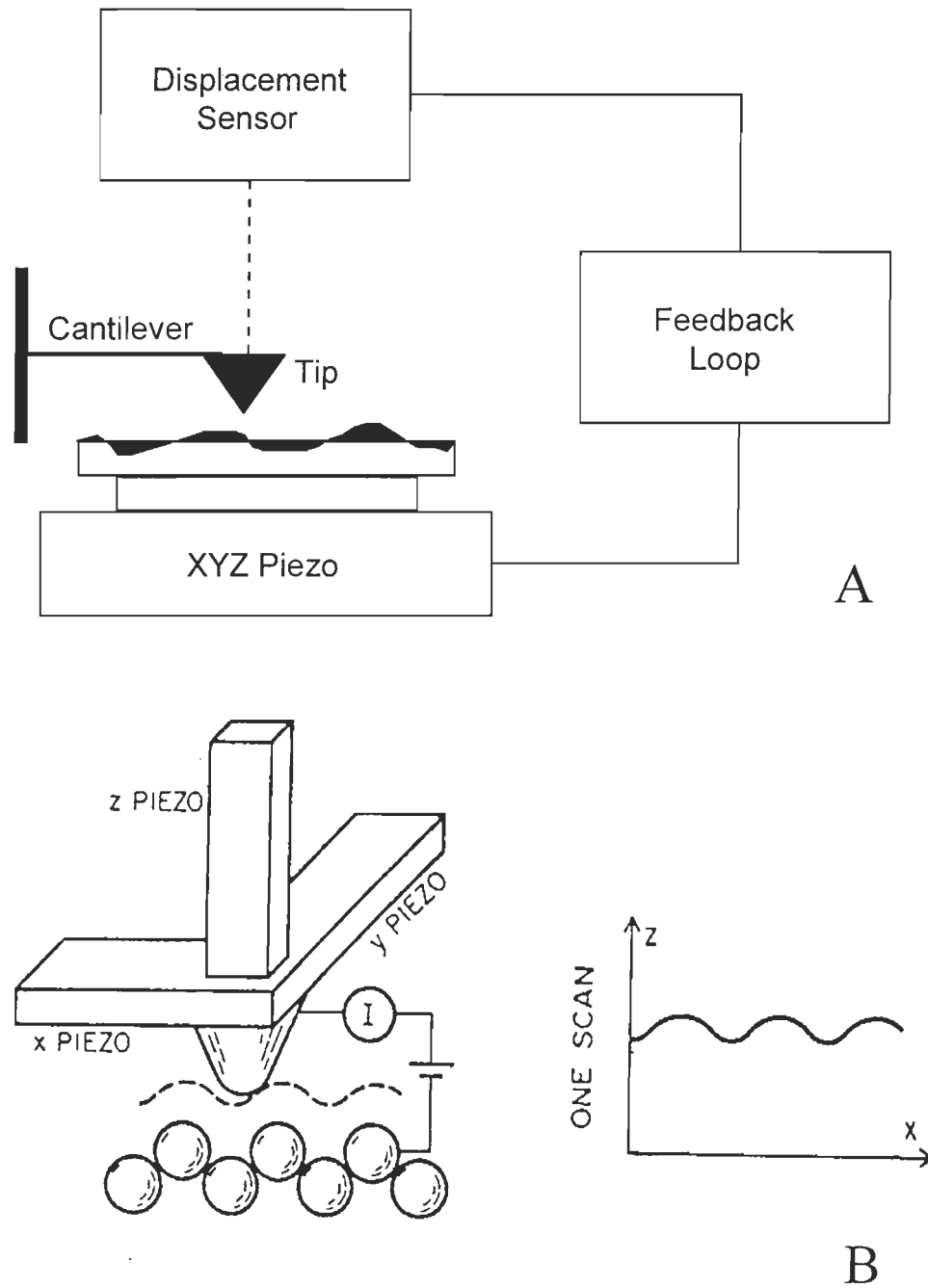
Figure 2.7   (A). A scheme of scanning force microscopy (SFM) (Frommer and Meyer, 1991); (B). Schematic view of interaction between tip and sample surface (Hansma et al., 1988).

between the tip and sample dominates.

With repulsive- force mode, it is important for the scanning tip to maintain a constant low force on the sample surface during imaging. To do this, a feedback loop from the displacement sensor to a piezoelectric translator moves the sample up and down in response to small changes in cantilever deflection. This keeps the cantilever deflection nearly constant, resulting in a nearly constant force between the scanning tip and the sample surface -- constant force mode. To image surfaces as gently and nondestructively as possible, one scans the surface at the smallest force that can be maintained without having the tip lose contact with the surface. The surface is also raster- scanned in the X and Y directions by means of the piezoelectric translator at the same time.

Tip and cantilever

In order to achieve sufficient sensitivity for atomic resolution, the cantilever has to satisfy several requirements (Albrecht et al., 1990). First, the cantilever must be flexible and resilient, with a force constant from 10^{-2} - 10^2 Newton/m. Therefore, a change of force of a small fraction of a nanonewton can be detected.

Second, the resonance frequency of the cantilever must be high enough to follow the contour of the surface. In a typical application, the frequency of the corrugation signal during a scan is up to a few kHz. To

achieve an imaging bandwidth comparable to that obtainable in the STM, the resonant frequency of the AFM cantilever should be greater than 10 kHz.

Third, the cantilever must be very small. The mass of the cantilever must be much smaller than 1 μg. In other words, the dimension of the cantilever must be in the micrometer range.

Fourth, in the vertical and horizontal directions, the stiffness of the cantilever should be very different. When the SFM is operated in the repulsive- force mode, frictional forces can cause appreciable image artifacts. Choosing an appropriate geometry for the shape of the cantilever can yield substantial lateral stiffness, thus minimizing the disturbing artifacts.

Fifth, when optical beam deflection is used to measure cantilever deflection, the sensitivity is inversely proportional to the length of the cantilever.

Finally, a sharp protruding tip must be formed at the end of the cantilever to provide a well- defined interaction with the sample surface, presumably with a single atom at the apex. The slope of the tip should be as steep as possible, and as smooth as possible. During a scan, the geometry of the tip affects the apparent lateral dimension of the molecular image. As shown in Figure 2.8, the apparent lateral dimension of the molecule is given by the following expression:
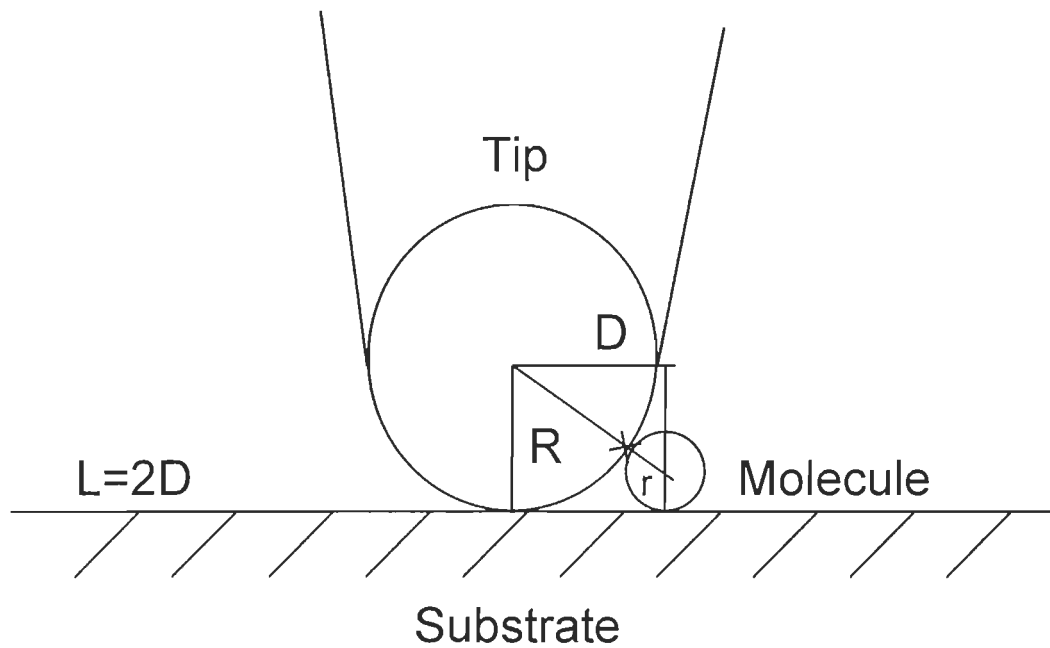
Figure 2.8   A model for tip geometry effect on soft specimen. The apparent

molecular dimension is defined by following expression: $L=4(Rr)^{1/2}$, where R

is the tip radius and r is the molecular radius (Zenhausern et al., 1992).

$$L = 4 (R r)^{1/2} \qquad\qquad (2.9)$$

where L is the image width, R is the tip radius and r is the molecular radius (Zenhausern, 1992).

Displacement sensor

Many different methods have been developed for detecting the minute deflection of the cantilever, the most important two are vacuum tunneling (Binnig et al., 1986) and optical beam deflection (Meyer and Amer, 1988). Here we only describe the optical beam deflection displacement sensor.

As shown in Figure 2.9, a light beam, typically from a solid- state laser, is reflected by the top surface of the cantilever. The back of the cantilever is coated with gold as a mirror, which reflects the laser light beam perfectly. The deflection of the mechanical cantilever deflects the optical beam, thus changing the proportion of the light falling on the two halves of the two- segment photodiode. The difference between the signal from the two halves of the photodiode is detected, and acting as the feedback signal for Z piezoelectric element controlling of the sample.

The force between the tip and sample can be calculated using the equation:

$$F = k \, \Delta z \qquad\qquad\qquad (2.10)$$

where Δz is the distance that the cantilevel bends and k is cantilever's

spring constant.
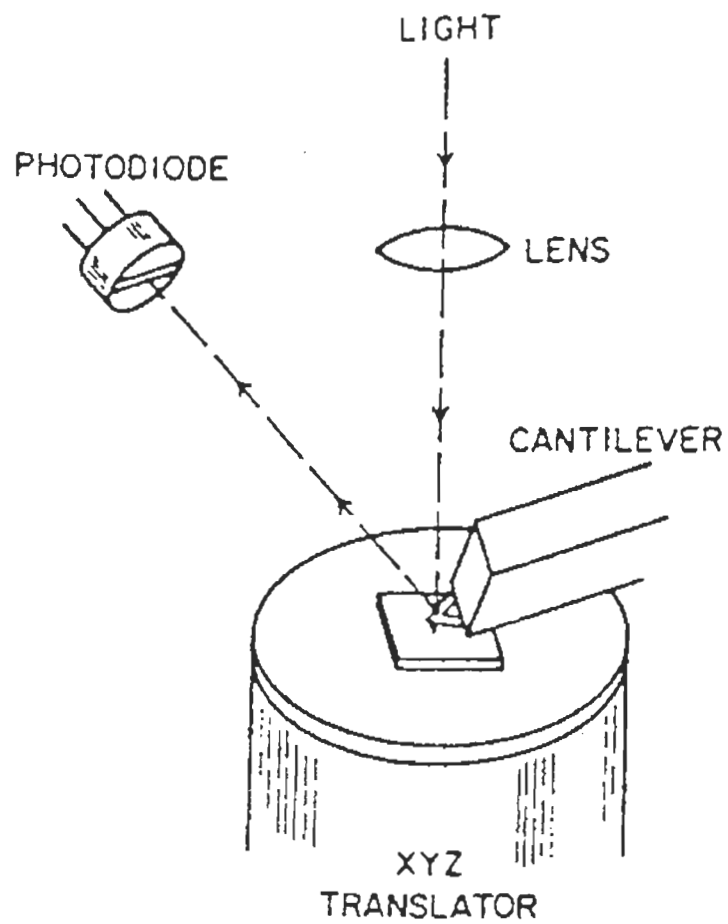
Figure 2.9   A scheme of a SFM with an optical beam deflection detector (Drake et al., 1989).

Atomic force microscopy (AFM) operation modes used for biological research

Conventional scanning mode AFM

The AFM records interatomic forces between the apex of a tip and atoms in a sample as the tip is scanned over the surface of the sample. There are two conventional scanning modes –contact mode and non-contact mode –that have been used for biological research. When the AFM is operated in a mode that senses the repulsive forces between tip and sample, the tip actually touches the sample—contact mode. The AFM can also be operated so that it senses the attractive forces between tip and sample – non-contact mode.

In conventional contact mode AFM, the probe tip is simply dragged across the surface and the resulting image is a topographical map of the surface of the sample. The dragging motion of the probe tip, combined with adhesive force between the tip and the surface, can cause substantial damage to both sample and tip, and create artifacts in image.

Under ambient air conditions, most surfaces are covered by a layer of adsorbed gases (condensed water vapor and other contaminants) which is typically several nanometers thick. When the scanning tip touches this layer, capillary action causes a meniscus formed and surface tension pulls the tip down into the layer. Trapped electrostatic charge on the tip and sample can contribute additional adhesive forces. These downward forces increase the overall force on the sample, when

combined with lateral shear forces caused by the scanning motion, can distort measurement and cause severe damage to the sample, including movement or tearing of surface features.

An attempt to avoid this problem is the non-contact mode AFM in which the probe is held at a small distance above the sample. Attractive van der Waals forces acting between the tip and the sample are detected, and a topographic image is constructed by scanning the tip above the surface. Unfortunately, the attractive van der Waals forces from the sample is substantially weaker than the forces used by contact mode – so weak in fact that the tip must be given a small oscillation so that AC detection method can be used to detect the small forces between tip and sample. Non-contact mode provides substantially lower resolution than either contact or tapping mode AFM.

Tapping mode AFM

In the commonly used contact mode AFM, the tip is in constant touch with the sample during scanning, the tip will therefore exert a lateral force to the sample on the substrate. For those loosely attached molecules, this lateral force is often sufficient to displace these molecules without creating an imaging signal (Hansma et al., 1993a; Lyubchenko et al., 1993).

The recently developed tapping mode AFM (Hansma et al., 1993b; Zhong et al., 1993; Hansma et al., 1994) reduces this problem. Instead of having the tip in contact with the sample all the time, a small a.c. signal is

introduced to drive the z component of the piezo scanner. The tip is only allowed to touch the surface for a short time per cycle, like tapping on the surface. In this approach, the friction effect is much reduced, and a slower scan is needed.

Tapping mode imaging is implemented in ambient air by oscillating the cantilever assembly at or near the cantilever's resonant frequency using a piezoelectric crystal. The piezo motion causes the cantilever to oscillate with a high amplitude (the "free air" amplitude, typically greater than 20 nm) when the tip is not in contact with the surface. The oscillating tip is then moved toward the surface until it begins to lightly tap the surface. During scanning, the vertically oscillating tip alternately contacts the surface and lifts off, generally at a frequency of 50 to 500 kHz. As the oscillating cantilever begins to intermittently touch the surface, the cantilever oscillation is necessarily reduced due to energy loss caused by the tip contacting the surface. The reduction in oscillation amplitude is used to identify and measure surface features, as shown in Figure 2.10.

During tapping mode operation, the cantilevel oscillation is maintained constant by a feedback loop. When the tip passes over a bump in the surface, the cantilevel has less room to oscillate and the amplitude of oscillation decreases. Conversely, when the tip passes over a depression, the cantilevel has more room to oscillate and the amplitude approaches the free air amplitude. The tip oscillation amplitude is measured by the detector. The digital feedback loop then adjusts the tip-

sample separation to maintain a constant amplitude and force on the

sample.

"Free" Amplitude

"Tapping"

Amplitude Reduced
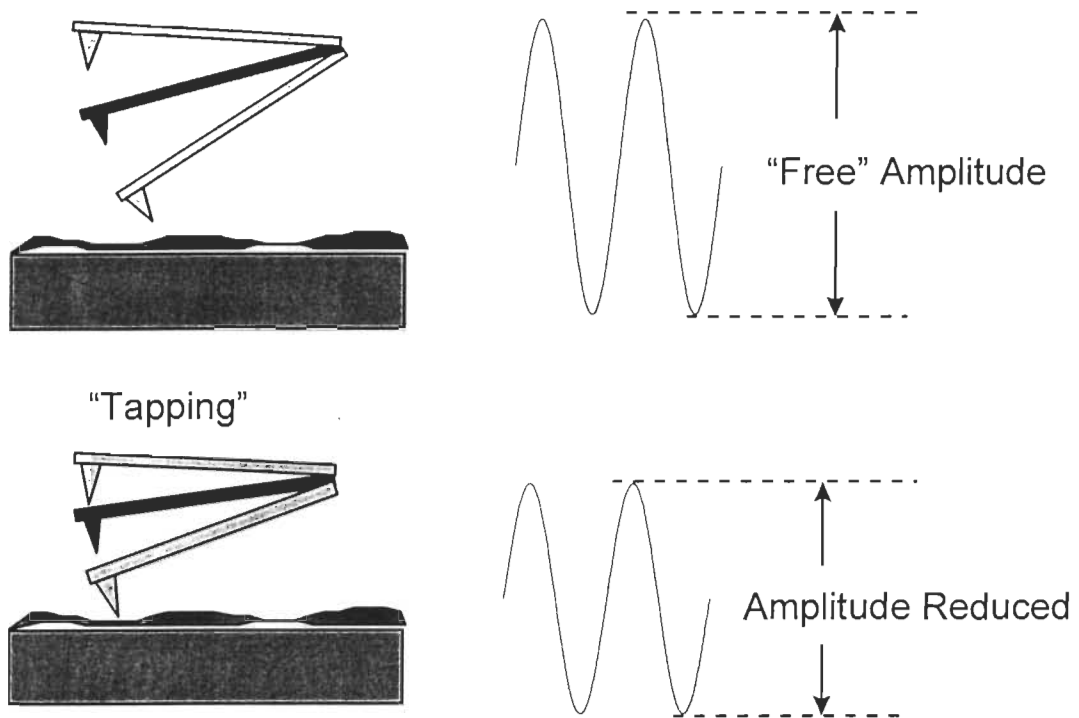
Figure 2.10 The tip and cantilever oscillation scheme of tapping mode AFM.

CHAPTER III

SURFACE CHEMISTRY STUDIES OF PHOTOSYSTEM II

The monolayer studies of photosynthetic membranes and isolated reaction centers have been done in several laboratories in recent years (Alegria and Dutton, 1991; Yasuda et al., 1992). Most of these studies were made on bacteria reaction centers, because of the availability of the X-ray structures for bacterial reaction center (Michel, 1982; Allen et al., 1986). However, less attention was given to the investigation of monolayers of PS II membranes and PS II core complex particles isolated from higher plants.

Thylakoid membranes of higher plants consist of four major protein complexes --PS II, PS I, cytochrome b_6/f, and proton-ATPase complex. Among these protein complexes, PS II performs the function of light absorption, energy transfer, charge separation and evolution of molecular oxygen (Ikeuchi, 1992). PS II complex is a multisubunit protein complex with a total molecular mass of 890 kDa, and is composed of PS II reaction center, chlorophyll a/b binding proteins of CP47 and CP43, extrinsic proteins of 33, 24, and 17 kDa, LHC II, and some smaller protein components (Ikeuchi, 1992; Haag et al., 1990). The minimum PS II complex capable of oxygen-

evolving consists of seven major intrinsic proteins—D1, D2, cyt b559 α and β subunits, CP47, CP43, and one extrinsic protein 33 kDa, with a total molecular mass of about 230- 250 kDa (Ikeuchi and Inoue, 1986; Haag et al., 1990).

Because of its importance in the photosynthetic process, understanding the structure and the functions of PS II complex has been the subject of intense investigations over many years (Haag et al., 1990; Michel, 1982; Roger et al., 1987; Holzenburg et al., 1993; Boekema et al., 1995). Due to the structural complexity of the PS II complex, the morphological basis for biological functions of PS II membranes is difficult to determine. It is desirable methodologically to extract and isolate each functional subunit, and to study them either individually or collectively by reconstructing the membrane in a controlled fashion. The Langmuir technique provides a promising approach in this regard because it allows a fine control of molecular constituents and their relative orientation that are similar to those found in natural membrane. In addition, this technique permits us to study the effects of environmental parameters such as temperature, pH and ionic strength as well as to use those parameters to control the desirable formation of films. One drawback of this technique, however, is that it may cause denaturation of proteins at the interface. Nevertheless, to utilize this technique with confidence, the optimization of the Langmuir technique for PS II and the development of systematic methods for film formation are required.

In this work, we investigated the surface pressure and surface potential properties of PS II membranes and PS II core complex monolayers, as well as the mixed monolayers of PS II core complex particles with a supporting lipid (MGDG) formed at the air-water interface. The optimization of utilizing Langmuir technique to the PS II systems will be essential for further surface spectroscopy and atomic force microscopy studies (Shao et al., 1997).

Experiments

Sample preparation

Extraction of PS II membrane and PS II core complex

Photosystem II enriched membranes were extracted from spinach thylakoids using the method of Berthold et al. (Berthold et al., 1981). The whole preparation procedure was carried out under green light and on ice. The spinach leaves purchased from market were washed with deionized water and dried in the air. 200 g of spinach leaves were blended with 300 ml Buffer A (50 mM Tricine/NaOH, pH 7.6, 10 mM NaCl, 5 mM $MgCl_2$, 400 mM sorbitol, 300 μl of 0.1742 g/ml PMSF in dioxane and 0.1% (w/v) ascorbic acid), and the resulting slurry was filtered through 10 layers of cheese cloth. The filtrate was then centrifuged (Beckman L7-80R ultracentrifuge) at 4000 rpm for 7 min at 4 °C. The pellet was suspended in 80 ml Buffer B (50 mM Tricine/NaOH , pH 7.6, 10 mM NaCl, 5 mM $MgCl_2$ and 0.1% (w/v) ascorbic acid), and centrifuged at 4000 rpm for 7 min at 4 °C. The pellet was

suspended in about 25 ml Buffer C (20 mM MES/NaOH, pH 6.5, 15 mM NaCl, 5 mM $MgCl_2$ and 400 mM sucrose). This suspension was adjusted to [Chl]= 2 mg/ml with the same buffer (Buffer C). A certain amount of Triton X-100 was added to obtain a Triton concentration of 50 mg/ml. The resulting solution was stirred for 30 min on ice, and then centrifuged at 17000 rpm for 20 min at 4 °C. The pellet was suspended in 40 ml Buffer C and centrifuged at 6000 rpm for 10 min at 4 °C. Finally, the PS II membrane fragments were obtained by centrifuging the supernatant at 17000 rpm for 20 min at 4 °C. The PS II membrane sample was suspended in Buffer C. The samples were aliquoted into small volumes, frozen in liquid nitrogen and then kept at -70 °C until use. The chlorophyll a/b ratio (mol/mol) for PS II membrane obtained using above method, measured in 80% acetone, was found to be between 1.2 and 1.5, and the protein/chlorophyll ratio (mol/mol) ranged between 2 and 3 depending on the preparation.

Oxygen-evolving PS II complexes were prepared (Volker et al., 1985; Haag et al., 1990; van Leeuwen et al., 1991) by solubilizing PS II membrane fragments extracted from spinach with detergent n-dodecyl-β-D-maltoside (Sigma). PS II membranes were first diluted in Buffer BTS400 (20 mM Bis-Tris, pH 6.5, 20 mM $MgCl_2$, 5 mM $CaCl_2$, 10 mM $MgSO_4$, 400 mM sucrose and 0.03% (w/v) n-dodecyl-β-D-maltoside) to a concentration of 2 mg chl/ml, and then 1/7 volume of a 10% (w/v) n-dodecyl-β-D-maltoside solution in Buffer BTS400 was added (final concentrations: 1.25% (w/v) detergent and

1.75 mg chl/ml). The suspension was incubated on ice with stirring for 10 min and without stirring for another 10 min. Any non-solubilized material was then removed by short centrifugation at 18000 rpm for 10 min at 4 °C. The supernatant was loaded onto a discontinuous sucrose-density-gradient of 20% - 36% sucrose (5 steps of 20, 24, 28, 32 and 36%) in Buffer BTS (20 mM Bis-Tris, pH 6.5, 20 mM $MgCl_2$, 5 mM $CaCl_2$, 10 mM $MgSO_4$, and 0.03% (w/v) n-dodecyl-β-D-maltoside), and centrifuged at 41000 rpm for 14 h at 4 °C using Beckman rotor 80-Ti in Beckman model L7-80R ultracentrifuge. PS II core complex particles were collected from the lower green band (32% sucrose step) of the two distinct and well separated bands. The upper green band was LHC II that lies in the 24% sucrose step, and was also collected. The samples were aliquoted into small volumes, frozen in liquid nitrogen and stored at -70 °C until use. The chlorophyll a/b ratio (mol/mol) measured in 80% acetone was found to be between 3 and 4, the protein/chlorophyll ratio (mol/mol) ranged between 5 and 7 depending on the preparation.

Chl concentration determination

50 μl of sample was dissolved in 4.95 ml of 80% ice cold acetone at 4 °C under green light to extract total pigments. The solution was sonicated for 1 min to favor pigment release from proteins, and centrifuged for 5 min in a microfuge. Absorbance values are then measured at 663 and 645 nm,

respectively. The chl concentration in the extract can therefore be determined according to Arnon's method with following equations (Arnon, 1949):

$$[Chl\ a] = 12.7 \times A_{663} - 2.69 \times A_{645}\ (mg/l) \qquad (3.1)$$

$$[Chl\ b] = 22.9 \times A_{645} - 4.68 \times A_{663}\ (mg/l) \qquad (3.2)$$

$$[Chl\ ] = 20.2 \times A_{645} + 8.02 \times A_{663}\ (mg/l) \qquad (3.3)$$

The Chl concentration in the sample is determined as following:

$$[Chl]_s = (4.95 + 0.05) \times [Chl] / 0.05\ (mg/l) \qquad (3.4)$$

Protein concentration determination

Sample protein concentration was determined using Bicinchoninic Acid Protein Assay Kit from Sigma (No. TPRO-562). Proteins reduce alkaline Cu(II) to Cu(I) in a concentration dependent manner (Lowry et al., 1951). Bicinchoninic acid is a highly specific chromogenic reagent for Cu(I) forming a purple complex with an absorbance maximum at 562 nm (Mazonski et al., 1963; Tikhonov and Mustafin, 1965). Because of this property, bicinchoninic acid can be used for the determination of protein concentration (Smith et al., 1985), as the resultant absorbance at 562 nm is directly proportional to protein concentration.

A standard curve is prepared by plotting the net absorbance at 562 nm vs the known protein standard. The protein amount as an unknown sample can then be intrapolated from the standard curve.

Electrophoretic analysis

The protein composition was analyzed by using electrophoresis technique (Laemmli, 1970; Chua and Gillham, 1977). The polypeptide composition of PS II membrane and PS II core complex particles were determined by discontinuous LDS/PAGE (3.75% stacking gel, 12.5% resolving gel) with 0.1% LDS (Sigma). Unlike the sodium dodecyl sulphate (SDS) which have tendency of recrystalization at low temperature, LDS allows us to conduct electrophoresis experiments at 4 °C. The samples were first incubated in 1% LDS, 5% 2-mercaptoethanol and 62.5 mM Tris/HCl, pH 6.8, for 1 h at room temperature, before applying to the gel slide. The buffers used for the stacking and resolving gels were 0.125 M Tris/HCl, pH 6.8 and 0.375 M Tris/HCl, pH 8.8, respectively. Electrophoresis buffer contained 0.1% LDS, 25 mM Tris, pH 8.3, and 0.192 M glycine. Electrophoresis was done in the dark at 4 °C with constant voltage 100 V for about 20 h. The gels were Coomassie Brilliant Blue R-250 stained (Oakley et al., 1980).

Figure 3.1 illustrates the composition of PS II membranes and PS II core complex. Our preparation closely resemble those described in previous literature (Haag et al., 1990). PS II membrane contains intrinsic proteins with

apparent molecular masses of 47(CP47), 43(CP43), 34(D1), 32(D2), 26-29(LHC II), 9 and 4.5 kDa(α and β subunits of cyt b559), in addition to the extrinsic 17, 24 and 33 kDa proteins. PS II core complex contains 47(CP47), 43(CP43), 34(D1), 32(D2), 33, 9 and 4.5 kDa(α and β subunits of cyt b559). The electrophoretic analysis results from PS II core complex and LHC II demonstrate that none of the core complex proteins appear in the light-harvesting complex II (LHC II) fraction and practically no LHC II proteins were found in the PS II core complex fraction.

PS II M   PS II CC   LHC II Standard

D1,D2

CP 47

CP 43

D1,D2,
33 kDa

LHC II

17 kDa

cyt b_{559}

Front

84 kDa

55 kDa

36 kDa

29 kDa

20 kDa

14 kDa

6.5 kDa
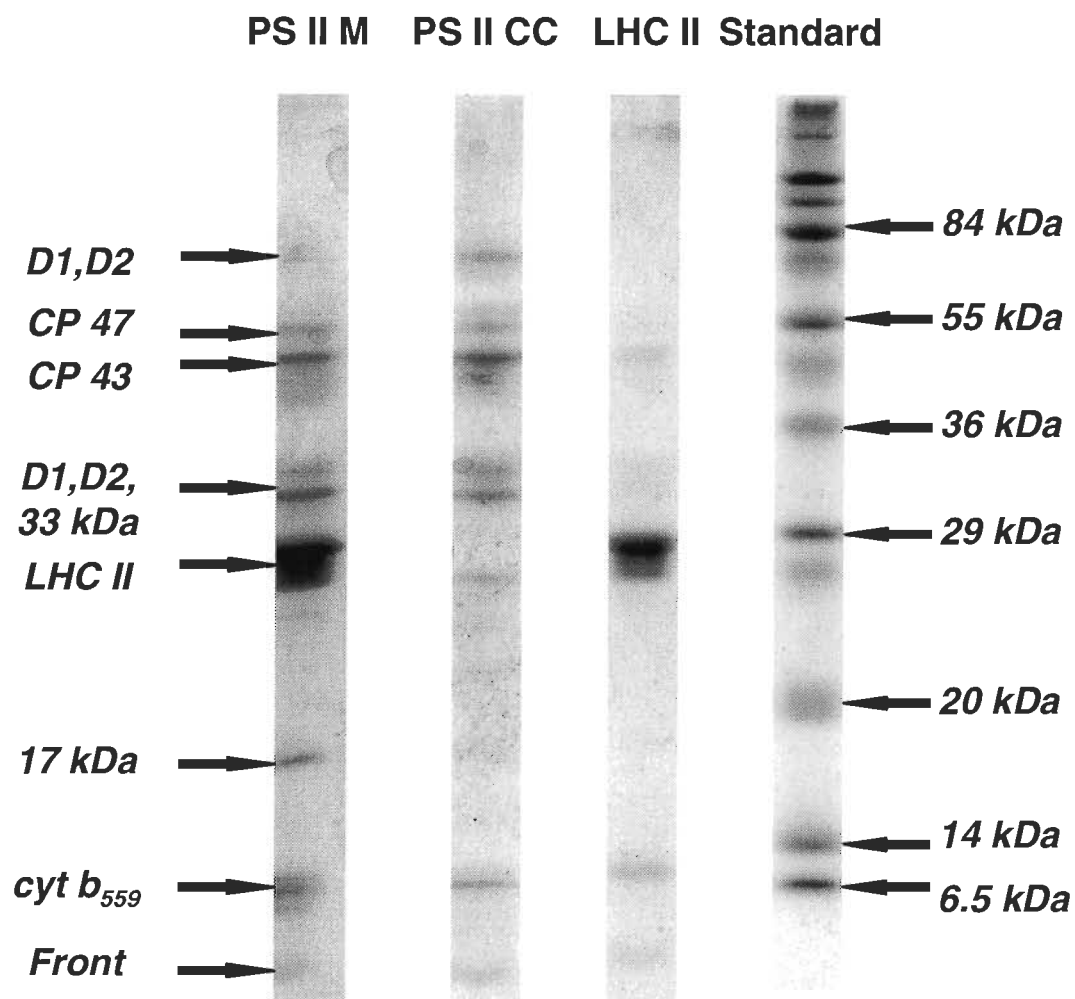
Figure 3.1. LDS-PAGE of PS II membranes, PS II core complex, LHC II and protein standard. The gels were Coomassie blue stained.

Oxygen-Evolution Analysis

In photosynthesis, light energy is absorbed by Chl and used to drive the reduction of carbon dioxide to carbohydrate. If PS II sample is enclosed in a chamber and provided with carbon dioxide from air, and then illuminated, oxygen will be evolved. A Clark-type electrode then detects the oxygen which accumulates as dissolved gas during photosynthesis.

Oxygen evolution was measured with a Clark-type electrode (Hansatech, England) at 20°C. Either PS II membrane or PS II core complex samples were suspended in a buffer solution of 50 mM $CaCl_2$, 10 mM NaCl, and 20 mM MES/NaOH pH 6.5, with 1 mM $K_3[Fe(CN)_6]$ added as electron acceptor, in a water cooled cuvette. Light was provided by a Hansatech Light Source LS 1 with an output of approximately 60 W/m^2 (red light- 660 nm).

The oxygen-evolving rates were about 250 and 600 μmoles O_2/mg chl per hour for PS II membrane and PS II core complex particles, respectively.

Surface Pressure Studies of PS II Systems

Langmuir films

All Langmuir films for surface spectral studies were prepared on a KSV spectral mini- trough (KSV instruments Ltd., Finland) under room temperature (23.0 $\pm$ 0.5 °C) with a humidity of 40 $\pm$ 5%. The trough has an area of 225 cm^2, and is equipped with a Willhelmy balance which has a resolution of 0.02 mN/m. The mini-trough has two barriers which compress the monolayer from

two sides, resulting in improvement of the homogeneity of the monolayer in the central part where the surface pressure was sensed and the surface spectra were measured.

For preparation of films of PS II membranes, the mini-trough contained an aqueous subphase solution of 2 mM $CdCl_2$, 2 mM ascorbate, and 2 mM MES/NaOH, pH 6.5, whereas for films of PS II core complex particles the subphase contained 10 mM Tris-HCl, pH 8.0, 2 mM sodium ascorbate and different concentrations of 100, 200 or 500 mM NaCl. The subphase temperature was maintained at 20 ± 2 °C. The presence of ascorbate in the subphase was needed to provide reducing conditions. The water used for monolayer study was purified by a Modulab 2020 water purification system (Continental Water Systems Corp., San Antonio, TX, USA). The water had a resistance of 18 $M\Omega \cdot cm$ and a surface tension of 72.6 mN/m at 20 °C.

The preparation of protein Langmuir films differs from the standard procedure used to make Langmuir films of amphiphilic fatty acid molecules. Both PS II membrane and PS II core complex particles were spread at the air-water interface using the "glass-rod" method (Trurnit, 1960). This involved placing a 1 mm diameter glass rod at a small angle (< 30°) relative to the trough plane positioned so that it just touched the water surface. Aliquot amounts of sample were spread at the interface via the rod, waiting approximately 5 s between additions.

The films stayed at the interface for 30 min before compression for sample spreading. The barriers were compressed at a speed of 8 nm^2/molecule•min for PS II membrane and 15 nm^2/molecule•min for PS II core complex. Surface pressure-area isotherms of PS II membrane and PS II core complex monolayers on the subphase were then recorded.

Langmuir-Blodgett films

PS II membrane and PS II core complex monolayers were deposited by the Langmuir-Blodgett method (Langmuir, 1917; Blodgett and Langmuir, 1934) at constant surface pressures of 10, 12.5 and 15 mN/m for PS II membranes, on fresh-cleaved mica substrates using a lab-build Langmuir-Blodgett trough.

In order to prepare the L-B films of PS II, the mica slide was cleaved before the deposition. The fresh-cleaved mica slide was mounted on a home-made dipper with its plane at 90° with respect to the air-water interface. The mica slide was inserted into the aqueous subphase and through the Langmuir film prepared as described above and maintained at constant surface pressure. A monolayer was prepared in the upstroke direction. The dipping speed was maintained at 10 mm/min.

Since the slide area was so small (smaller than 1 cm^2) compared with the trough area, the amount of material removed from the air-water interface, i. e. the deposition ratio, could hardly be determined.

Results and discussion

Surface pressure-area studies

The surface pressure as function of molecular area, or π-A isotherm, as the sample at the air-water interface being compressed, is an important indicator of the quality of the monolayer. A sudden change in surface pressure usually means the formation or collapse of a stable layered structure.

Figure 3.2 shows several π-A isotherms using different aliquot of PS II membrane sample. Although quite typical of other proteins (Birdi, 1989; Turko et al., 1992), these isotherms lack some sharp features that are representative for those more rigid and well structured materials such as pure lipids. We have observed that some large pieces of PS II membrane fall into subphase and eventually sink into the bottom of Langmuir trough during initial sample spreading. This observation may explain the inconsistency in PS II membrane isotherms.

PS II membrane extracted from spinach consists of sheet like structure that contains one or several PS II complexes embedded in bilayered lipid membrane. The lumenal and stromal sufaces of PS II membrane sheets are hydrophilic whereas the surrounding edge surfaces are hydrophobic. The relative ratio of hydrophilic and hydrophilic surfaces varies with the particle size. The larger particle has larger hydrophilic/hydrophobic ratio. This size dependency of the hydrophilic/hydrophobic ratio is likely to result in the size

dependency of PS II membrane solubility and thus the ability of forming mono-layer film at air-water interface. Therefore, it entirely plausible that there are not enough hydrophobic surfaces in large PS II membrane particles to support them at the air-water surface. Since it is difficult to control the size distribution of PS II membrane pieces during the sample preparation, fraction of large PS II membrane varies among different aliquots even different sampling of the same aliquot. The inconsistency in PS II membrane π-A isotherms reflects this uncertainty.

In addition to direct observation of large pieces of PS II membranes, furthermore, if we use the total amount of PS II membrane protein to calculate the average particle size from the π-A isotherm, we obtained an area of about 200 nm^2. This value is very small when compared with that of the PS II core complex particles (320 nm^2, as discussed in a subsequent section), which is a smaller subunit compare to the PS II membranes. A PS II membrane fragment contains PS II core complex and several LHC II proteins, and is much larger in size than a PS II core complex particle. Indeed, particle size derived from π-A isotherm, when part of initially spread PS II membrane falls into subphase, does not reflect the true membrane particle size. Since we do not have quantitative measurement of what fraction of PS II membrane falls into subphase, we cannot using the particle area obtained from above mentioned π-A isotherm to deduce the true particle size of PS II membrane.
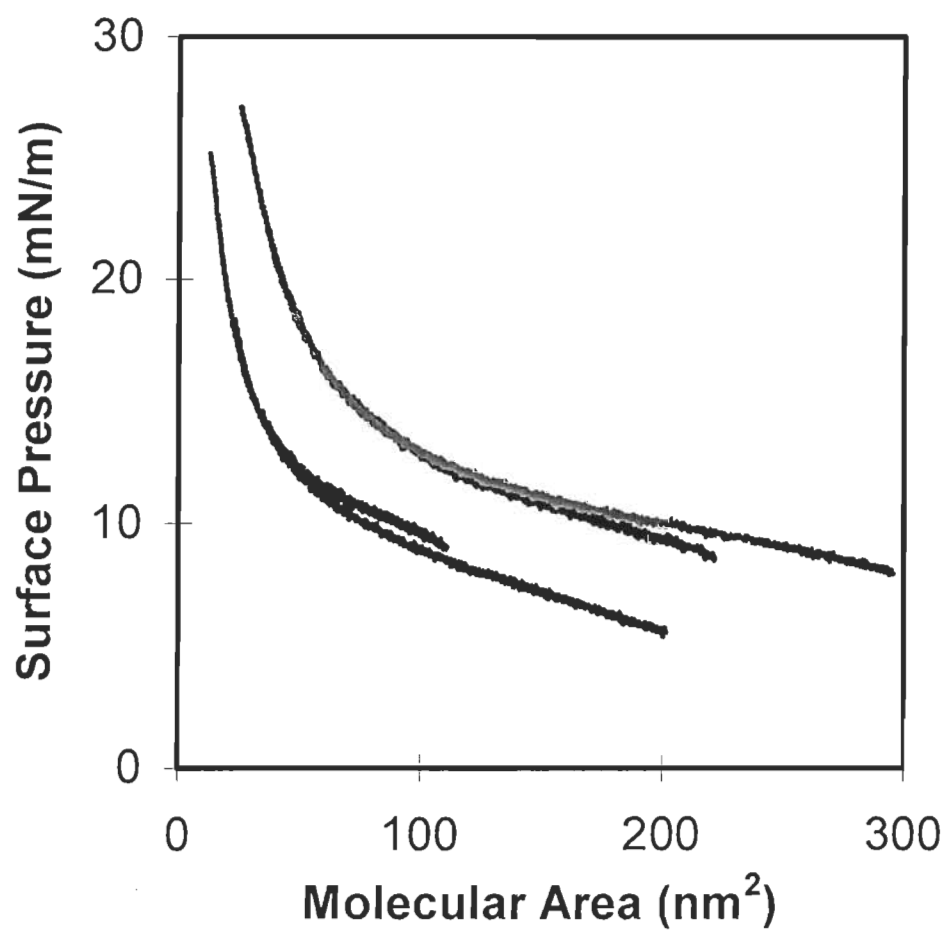
Figure 3.2. The surface pressure-area isotherms (π-A curve) of PS II membranes. Subphase, 2 mM $CdCl_2$, 2 mM ascorbate, and 2 mM MES/NaOH, pH 6.5. Temperature, 23.0 ± 0.5 °C.

π-A isotherms of Figure 3.2 shows limited surface pressure range. This mainly due to the small trough (300 mm X75 mm) experiments. The trough used in this study is the same as used for *in situ* spectroscopic studies where limited space can only accommodate small trough. Surface isotherm studies have also been performed using a larger trough (1200 mm X280 mm). Experiments using small KSV mini trough are present discussed because the exactly same experimental conditions are used as *in situ* surface spectroscopic studies.

π-A isotherm of PS II membranes lacks some sharp turning points that are typical of lipid π-A isotherm and thus it is difficult to determine whether the monolayered structure or multilayered aggregates are formed at certain surface pressure. However, atomic force microscopy images of LB films transferred directly from Langmuir trough suggested that multilayered aggregates are formed when surface pressure is higher than 12.5 mN/m (more detailed results will be discussed in Chapter 6 of the thesis and Shao et al., 1997). Although one can argue that these aggregates may have been formed during transfer of LB films onto mica surface by adsorption of PS II membrane fragments dissolved in the subphase, however, adsorption PS II membranes from subphase will results in multi-layered LB films at any surface pressures not just high pressures. AFM images indicated aggregates increase at increasing surface pressures.

Although our π-A isotherms of PS II membranes can not accurately provide information on the particle size due to some fraction of PS II membrane being lost in the subphase, these curve as well as AFM images of LB films transferred from Langmuir trough clearly indicate that a fraction of PS II membrane fragments stay on the air-water interface and form stable monolayer structure. Our observations further indicates that PS II membranes can only marginally stay at the air-water interface and one must be very careful in choosing the experimental conditions. One possible way of increasing the film forming ability of PS II membranes is to add some salt to the subphase in order to increase the density of subphase. This solution has been applied to the studies of PS II core complex and will be discussed in later paragraphs. However, past studies on membrane protein films have shown that the salt in the subphase can be deposited together with the membranes in the L-B film. The presence of the salt particles results in a very low ordering in the resulting L-B films (Erokhin and Feigin, 1991). Since capabilities of monitoring higher order protein structures *in situ* are not available when this work was done, a more conservative approach, which the salt solutions are added only when it is absolute necessary, was chosen.

In the case of PS II membrane proteins, as discussed above, the hydrophobic and hydrophilic pairs of attached lipids can partially support the protein complex at the air-water interface, despite their large size and density. However, in the case of PS II core complex particles, the detergent strips the

attached lipids and some extrinsic proteins. The remaining protein complex processes hydrophilic surfaces and hydrophobic edge surfaces and is quite appropriate for forming stable mono-layer at water surface. However, the residue detergent surrounding the protein complex made it water soluble. It is very difficult to prepare stable monolayers of water soluble proteins with Langmuir method. Indeed, our attempts to prepare a stable monolayer of PS II core complex directly on the water surface failed completely. One possible solution is to change the density and ionic strength of the subphase by adding salt solutions into the subphase (Erokhin and Feigin, 1991).

Figure 3.3 shows the surface pressure-area isotherms of PS II core complex particles with different concentrations of NaCl into the subphase. Addition of NaCl solution greatly enhances the stability of monolayers of PS II core complex particles at the air-water interface. The π-A isotherms at a subphase concentrations of 100 mM and 200 mM NaCl clearly demonstrated that PS II core complex particles can be compressed to a relatively high surface pressure (40 mN/m), before the monolayer collapses under our experimental conditions. These π-A isotherms are quite reproducible as well. Moreover, the average particle size calculated from π-A isotherms using total amount of protein complexes is about 320 nm^2. This observation agrees well with the particle size directly observed using atomic force microscopy (Shao et al., 1997), and indicates that nearly all the protein complexes stay at the water surface and form a well structured monolayer.
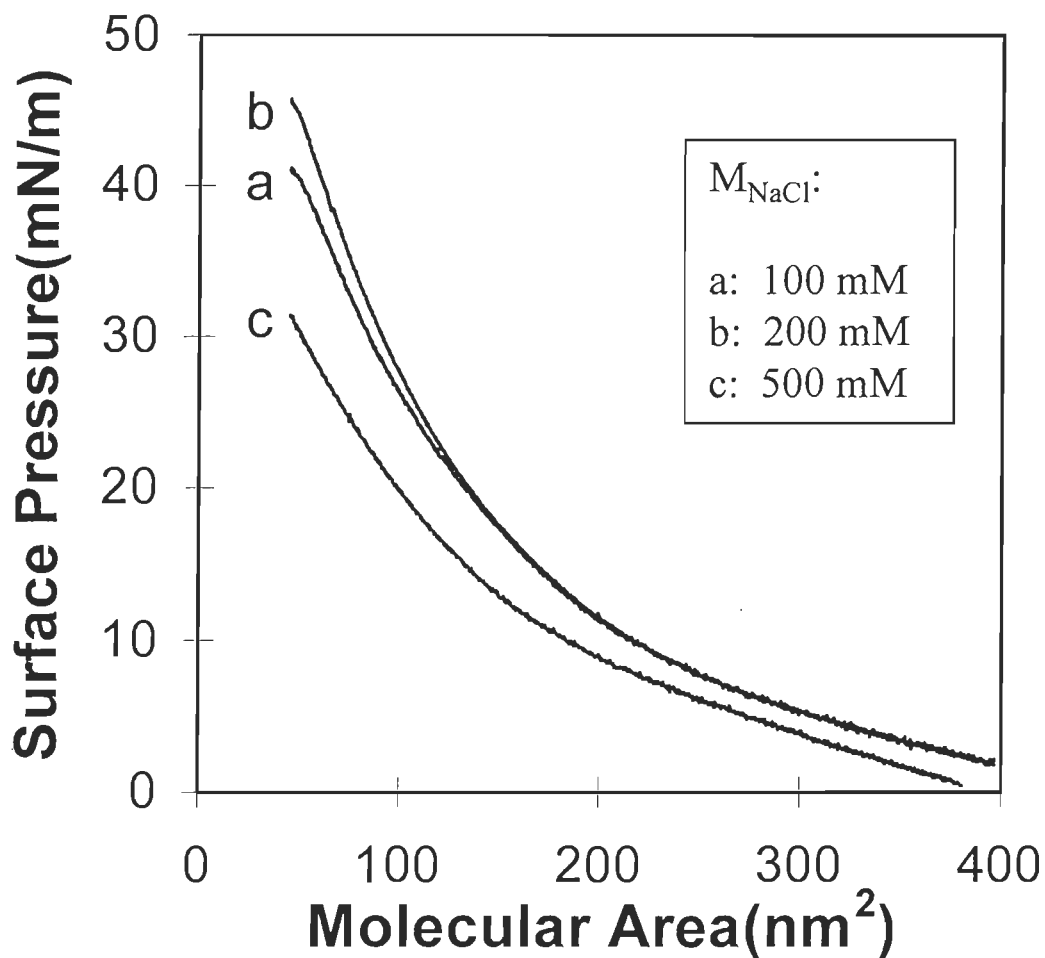
Figure 3.3. The surface pressure-area isotherms (π-A curves) of PS II core complex with different concentrations of salt in the subphase. Subphase: 10 mM Tris-HCl, pH 8.0, 2 mM sodium ascorbate and concentration (M_{NaCl} : molar concentration of NaCl) of 100, 200 or 500 mM NaCl. Temperature, 23.0 ± 0.5 °C.

One must be careful when using the high concentration of salt to increase the density of the water subphase. There are several disadvantages of using a high concentration of salt into the subphase: 1). High concentration of salt solution may cause protein to denature (Tiede, 1985); 2). The salt particles can be deposited together with the protein complex monolayer onto the substrate (e.g. mica) when we prepare L-B films (Erokhin and Feigin, 1991). An optimal condition must be attained in order to use this technique effectively.

From the isotherms of Figure 3.3, we noticed that there are little differences in the π-A isotherms of 100 and 200 mM of NaCl into the subphase. However, for 500 mM of NaCl in the subphase, the average particle size calculated from the π-A isotherm decreases as compared with that of 100 and 200 mM of NaCl in the subphase. This observation is difficult to understand and one possible explanation is that the PS II core complex may have been denatured by the presence of a high concentration of salt solution. We thus chose the 100 mM NaCl concentration in the subphase for our works. We also noticed that the initial surface pressure is not 0 mN/m (2-3 mN/m). This is due to the fact that we used a rather small Langmuir trough and the presence of residual detergent in the sample.

Figure 3.4 illustrates the compression and expansion π-A isotherms of PS II core complex particles. The isotherms are non-reproducible during the compression and expansion. In the sample solution, the hydrophobic regions
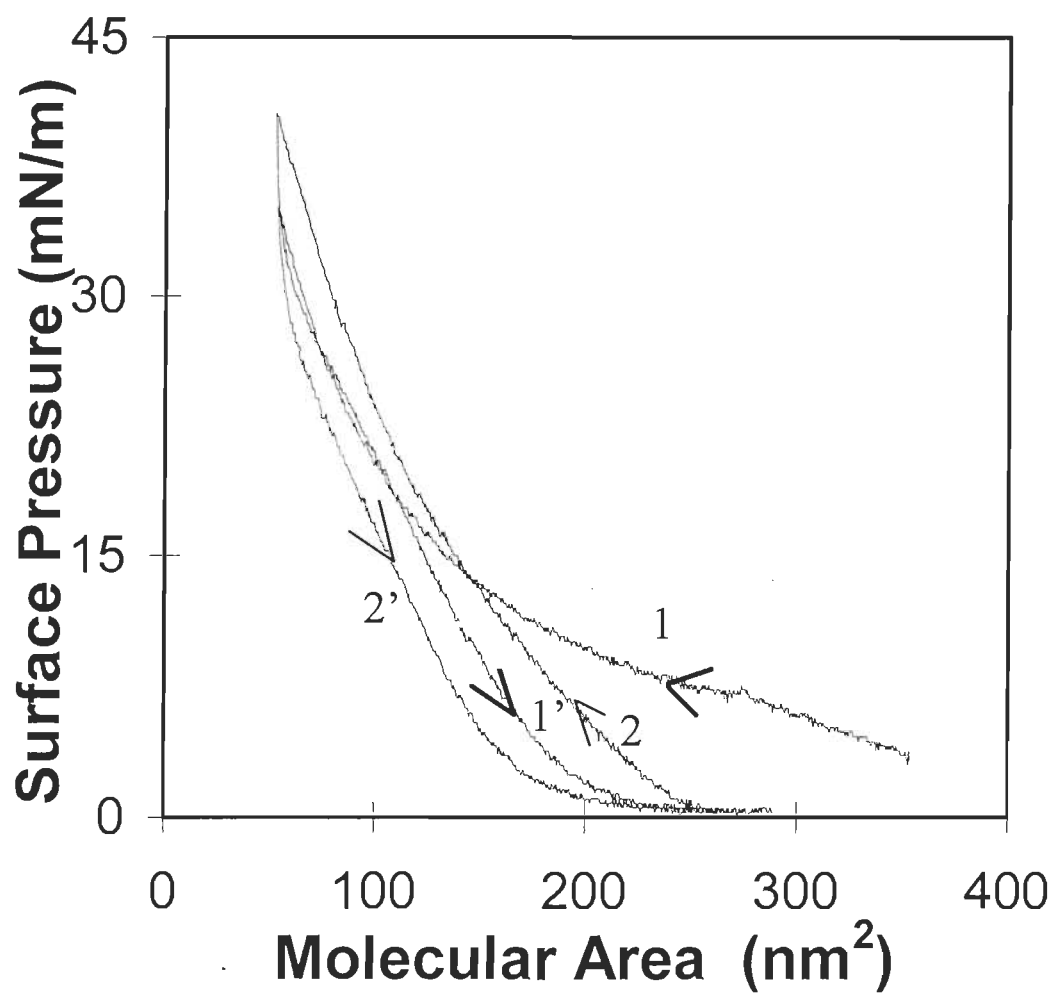
Figure 3.4. The compression (1 and 2) and expansion (1' and 2') π-A

isotherm of PS II core complex particles. The experimental conditions are the

same as Figure 3.3.

of protein subunits are covered by the detergent molecules. Once the PS II samples are spread onto the air-water interface, the excess detergent molecules separate from the protein particles and a mixed monolayer of protein and detergent molecules is formed. However, the detergent molecule has a fairly short hydrophobic chain, which can not form a stable monolayer at the air-water interface. Under the same compression conditions for PS II core complex sample, the detergent monolayer collapse under very low surface pressure (less than 10 mN/m, data not shown). After compression to relatively high surface pressures, detergent molecules are ejected from the monolayer to subphase and the surface concentration of detergent molecules is decreased due to the formation of micelles (Zaitsev et al.,1992; Lvov et al., 1991; Hann, 1990). The presence of detergent molecules resulted in non-identical π-A isotherms during compression and expansion. We also noticed that the molecular area decreases gradually when the surface pressure is held at a certain value. There are several plausible explanations: 1). There may be some leakage of protein molecules from the surface into the subphase at low surface pressures where the detergent molecules have not been completely removed from the interface. 2). Protein denaturalization may be taking place at the air-water interface. 3). The detergent molecules escaped into subphase from the interface.

Thylakoid membranes have a unique set of acyl lipids that form about 25-30% of the total thylakoid mass. The natural galactolipids

monogalactosyldiacylglycerol (MGDG) and digalactosyldiacylglycerol (DGDG)

comprise about 75% of the total acyl lipids (MGDG 50%, DGDG 25%)

(Anderson, 1987). These acyl lipids form the fluid bilayer matrix in which

functional proteins are embeded. During preparation of PS II core complex,

these natural lipids were removed by detergents. Comparing surface

chemistry and spectroscopic properites of 'naked' PS II core complex with

that of embeded in natural membrane may offer us some understanding of

the interaction between the functional protein with the surrounding lipid

matrix. One way of 'mimicing' natural biomembrane systems is to form

monolayer structure of natural membrane lipid component (MGDG) with PS II

core complex embeded.

Figure 3.5 shows the surface pressure-area isotherms of MGDG alone

as well as the mixture of PS II core complex particles and MGDG. In the

mixture, the ratio of PS II core complex to MGDG is 76.7 to 23.3 by weight

(1:99 mol/mol). From the isotherms, the limiting molecular area of MGDG at

the air-water interface is about 120 Å^2 and the average molecular area of the

mixture is about 300 Å^2. The results indicate that we do have both PS II

core complex particles and MGDG in the monolayer. MGDG molecules

diluted the PS II core complex particles concentration in monolayer.

The isotherm for pure MGDG shows the typical features of a good

Langmuir film forming molecule, which includes the zero initial surface

pressure indicative of a gas phase, and sharp surface pressure increments

during compression which correspond to gas-liquid-solid like phase
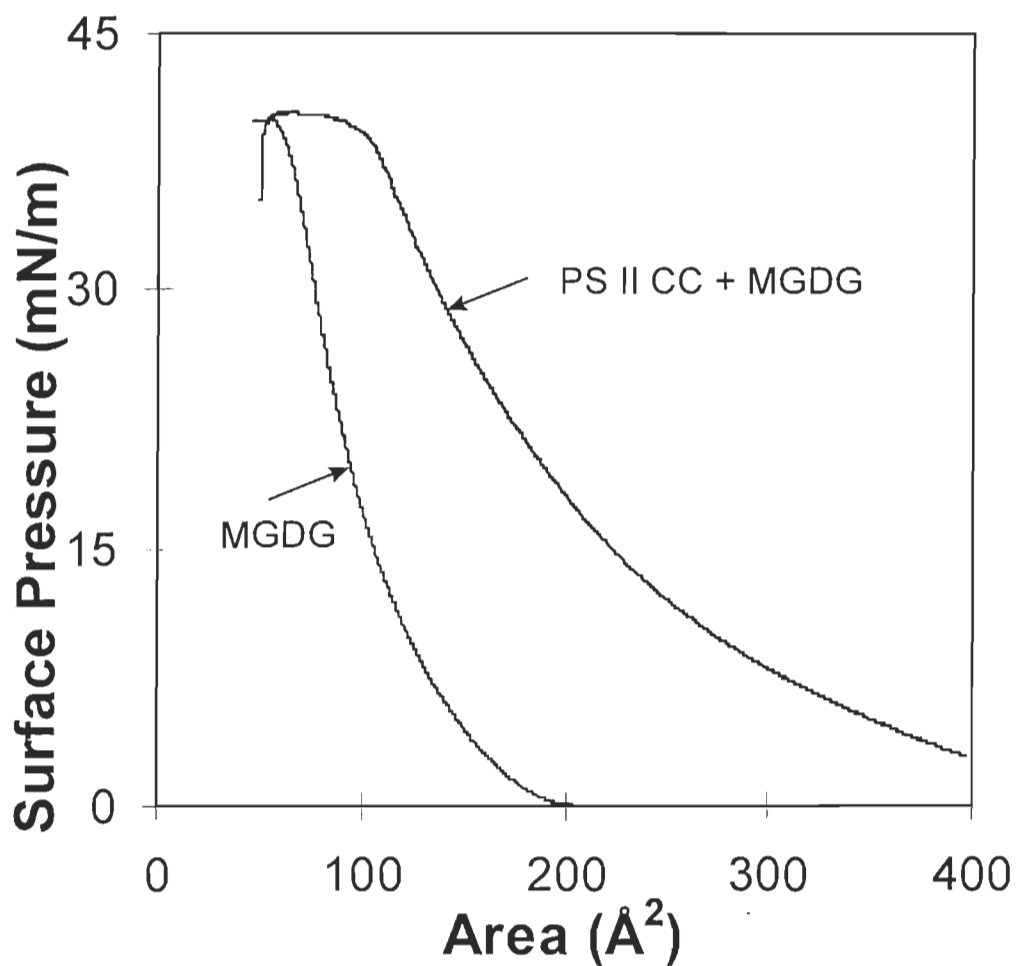
Figure 3.5. The surface pressure-area isotherms of MGDG alone and the mixture of PS II core complex particles and MGDG. In the mixture, the ratio of PS II core complex to MGDG is 76.7 to 23.3 by weight. The experimental conditions are the same as Fig. 3.3.

transition (Albrecht et al., 1981). Even for the mixture of PS II core complex with MGDG, the isotherm has a steeper slope than that of protein sample alone and indicates better quality of the monolayer structure. MGDG lipid functions as a matrix for the protein complex and the resulting mixture forms higher quality films than PS II core complex particle alone.

To understand the interaction between PS II core complex particle and MGDG, we have compared the molecular areas of the mixture calculated through the additivity rule with the experimental molecular areas. For any "ideal" mixed two-components monolayer, the average area per molecule, A_{12}, can be expressed as followed (Birid, 1989):

$$A_{12} = \chi_1 A_1 + \chi_2 A_2 \hspace{3cm} (3.5)$$

where 1 and 2 represent the two constituent components of the monolayer receptively, χ_1 and χ_2 are the mole fractions of the components in the mixed monolayer, and A_1 and A_2 are the molecular areas of the pure components at the same surface pressure. For the mixture used in our experiment (the ratio of PS II core complex particle to MGDG is 76.7 to 23.3 by weight or 1 to 99 mol/mol), the molar fraction of the each component can be calculated as, $\chi_{PS\ II}$ equals to 9.67×10^{-3} and χ_{MGDG} equals to 0.9903, using molecular weight of 275 kDa for PS II core complex particle and 816 g/mol for MGDG, respectively. Table 3 lists the calculated and experimental molecular areas in

the monolayer of the PS II core complex particle and MGDG mixture for various surface pressures.

Figure 3.6 shows the measured average molecular area as well as that calculated using the additivity rule as a function of the surface pressure of the PS II core complex particle and MGDG mixture. The negative deviations of the molecular areas from the additivity rule are observed at all surface pressures for the PS II core complex particle and MGDG mixture. This results indicate that two types of molecules are intermixed with each other and the resulting monolayer is miscible. The negative deviation also suggests that there may have some disorders in the monolayer film of the PS II core complex particle and MGDG mixture. A more plausible explanation is that an attractive interaction exists between PS II core complex particle and MGDG molecules and this attraction interaction exceeds the interaction between pure PS II core complexes and pure MGDG molecules.

Since MGDG sample was dissolved in chloroform and the organic solvent can damage the protein structure, we prepared our mixed monolayer by a method of sequentially adding MGDG and PS II core complex particle onto the air-water interface, as described in experimental section. However, this kind of successive addition procedure may not be the best way to obtain homogeneous mixture in monolayer, although we did not have much choice for the preparation of the monolayer.

Table 3

The calculated and experimental average molecular area in the mixture

monolayer of PS II core complex particles with MGDG.

π (mN/m)	$A_{PS\,II\,CC}$ (Å^2)	A_{MGDG} (Å^2)	A_{Cal} (Å^2)	A_{Exp} (Å^2)
5	30741	146.7	442.6	350.8
10	21709	122.4	331.2	272.8
15	16692	105.7	266.2	222.3
20	13241	93.4	220.6	186.9
25	10603	84.3	186.1	158.7
30	8459	76.5	157.6	136.4
35	6745	69.3	133.8	117.7

$A_{PS\,II\,CC}$ (Å^2): molecular area of PS II core complex particle.

A_{MGDG} (Å^2): molecular area of MGDG.

A_{Cal} (Å^2): calculated molecular area of the mixture of PS II core complex particle with MGDG.

A_{Exp} (Å^2): experimental molecular area of the mixture of PS II core complex with MGDG.
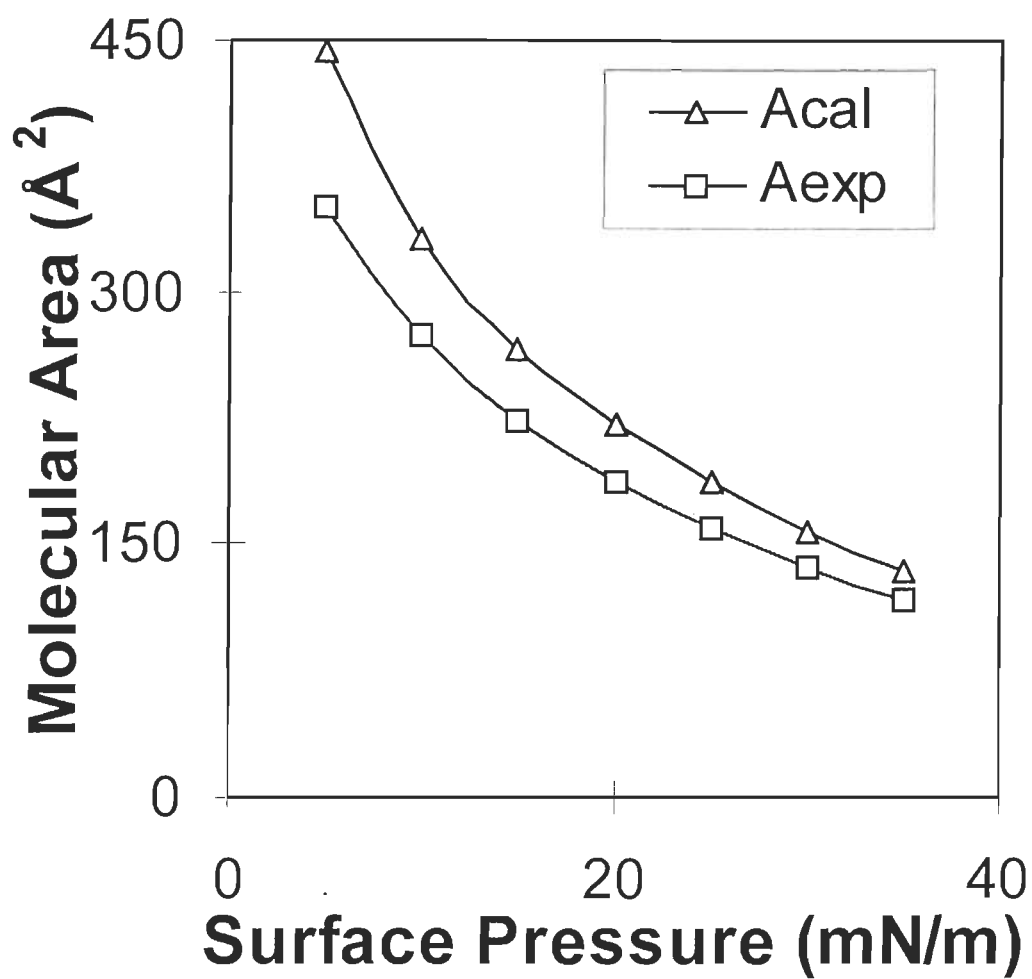
Figure 3.6. The average molecular area versus the surface pressure isotherm of the mixture of PS II core complex particles and MGDG.

<u>Surface potential –area studies</u>

The surface potential as function of particle area (ΔV-A isotherm) is another indicator of the quality of the monolayer structure. The surface potential at the air-water interface changes as the film-forming molecules reorient themselves during compression process. For a closely packed monolayer, the surface potential is directly proportional to the surface dipole moment ($\mu_\perp$) by (Gaines, 1966):

$$\Delta V = 12\,\pi\,\mu_\perp\,/A \qquad\qquad (3.6)$$

where ΔV is the surface potential change in millivolts when a monolayer is spread at the air-water interface. A is the molecular area in Å^2 /molecule, and $\mu_\perp$ is the surface dipole in millidebye (mD).

Figure 3.7 displays the surface pressure-area (π-A) and surface potential-area (ΔV-A) isotherms of PS II membranes. As the surface area is compressed from 400 to 175 nm^2, the surface potential remains at a constant value, whereas the surface pressure increases slightly from 6.5 mN/m to 10 mN/m. Further compression results in a decrease in surface potential and a sharp increase in surface pressure. Both decrease in surface potential and sharp increase in surface pressure after 175 nm^2 clearly indicate the collapse of monolayer structure and the formation of the multilayer at surface pressure larger than 10 mN/m. The formation of multilayered structure may have

partially cancelled out the molecular dipole moment of the PS II membrane protein and results in a decrease in surface potential. The independent AFM studies confirmed that the monolayer structure of PS II membrane protein collapses under high surface pressure (Burnap and Sherman, 1991). From the ΔV-A isotherm of PS II membrane protein, we can calculate a surface dipole moment of about 1.58×10^5 mD.

It should be mentioned that the π-A isotherms of PS II membrane shown in figure 3.7 were taken using a large Langmuir trough (3340 cm^2 in size) whereas the π-A isotherms of figure 3.2 were taken using a mini trough (225 cm^2 in size). The large trough can produce larger compression ratio.

Figure 3.8 shows the surface pressure-area (π-A) and surface potential-area (ΔV-A) isotherms of PS II core complex particles. The ΔV-A isotherm of PS II core complex is rather different from that of PS II membranes. The surface potential of monolayers of PS II core complex particles increases slightly as the molecular area is compressed from 600 to about 150 nm^2, while surface pressure changes from 5 to 35 mN/m. Further compression results in a sharper increase in surface potential. The surface potential starts to decrease only after the surface area being compressed to about 80 nm^2 or surface pressure larger than 40 mN/m. This is consistent with previous discussion that PS II core complex particles form more ordered monolayer structure at relatively high surface potential. At surface area of 320 nm^2, the

dipole moment of PS II core complex particles monolayer can be calculated from corresponding surface potential at about 2.38×10^5 mD.

This work demonstrated that both PS II membranes and PS II core complex particles from higher plants can form monolayer structure at the air-water interface. Surface pressure-area and surface potential-area isotherms indicated that PS II membrane proteins can form stable monolayers directly at the air-water interface, although a fraction of large protein fragments sink into the aqueous subphase. Since PS II core complex particles surrounding by detergent molecules, it is hard to form a monolayer directly at the air-water interface without increasing density of subphase. However, addition of moderate concentration of NaCl (100 mM) into the subphase greatly enhances the film forming ability of PS II core complex particles and quality of the resulting monolayer. We also demonstrated that the addition of the lipid MGDG to PS II core complex particles also greatly enhances film forming ability and the mixture monolayer shows good miscibility at all surface pressures. These results confirm that the lipid MGDG can function as supporting material in the mixture monolayer.
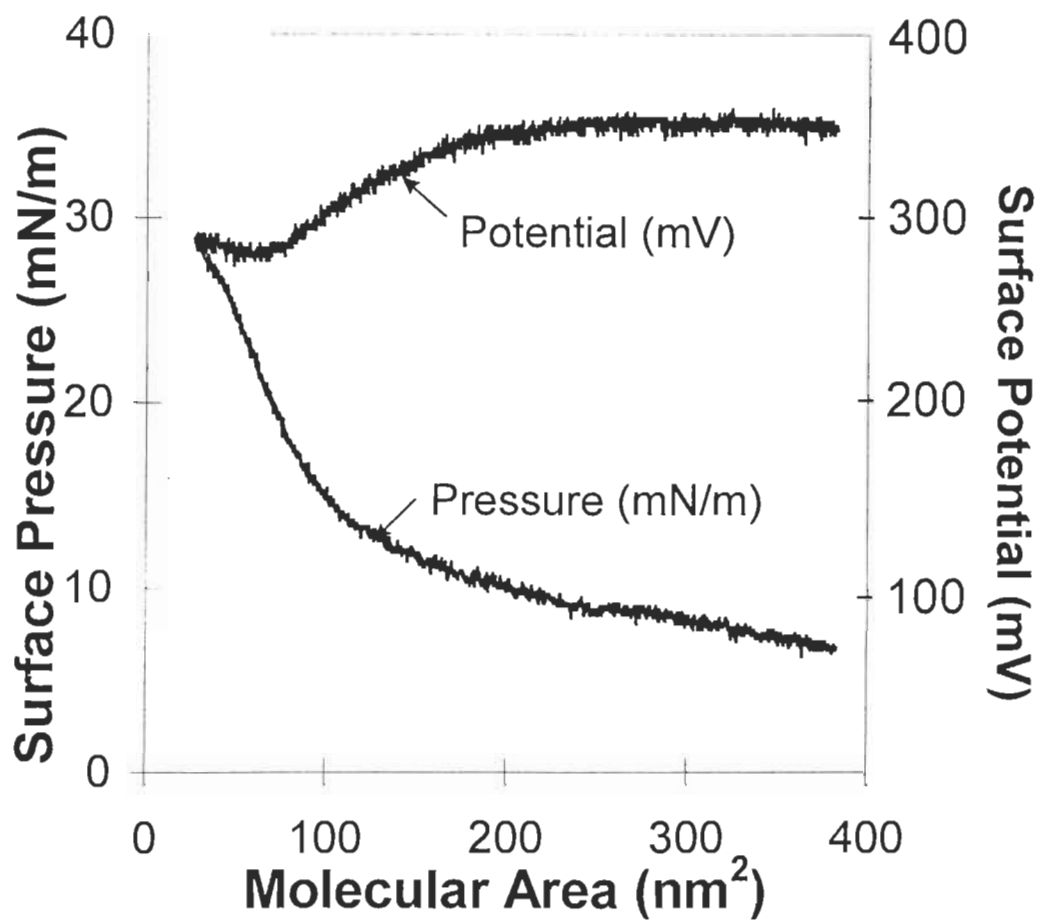
Figure 3.7. The surface pressure-area (π-A) and surface potential-area (ΔV-A) isotherms of PS II membranes. The experimental conditions are the same as Fig. 3.2.
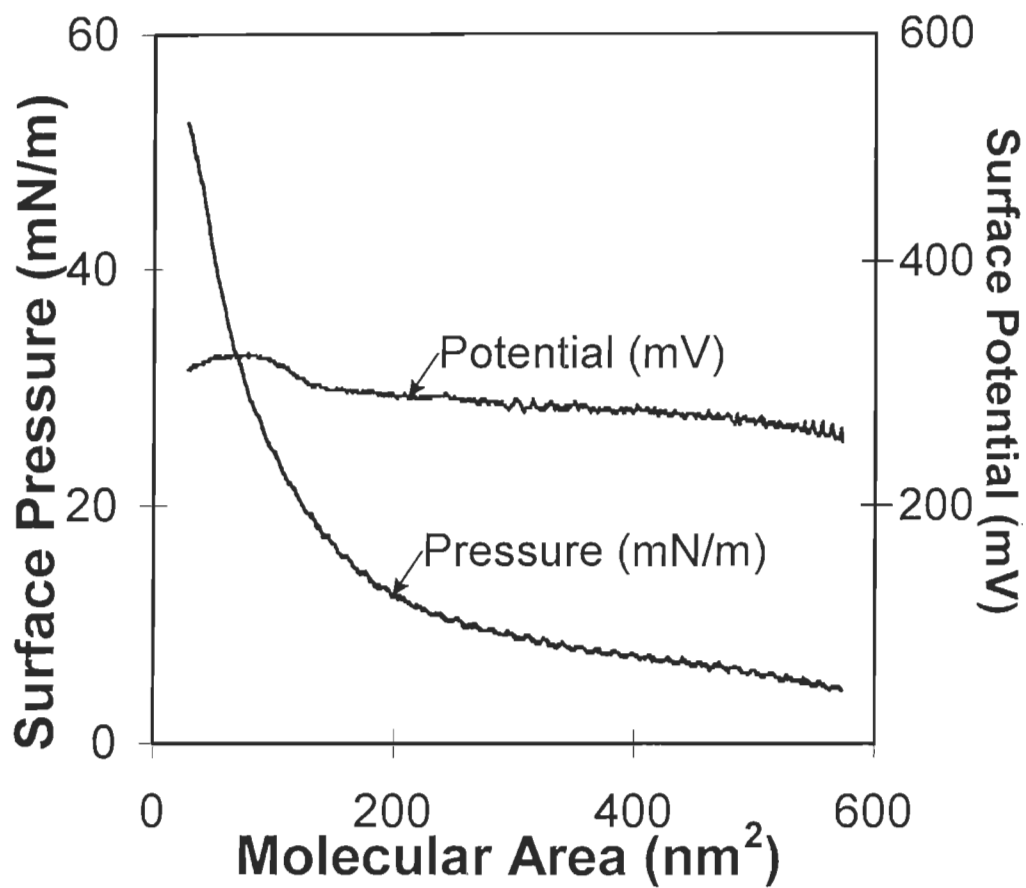
Figure 3.8. The surface pressure-area (π-A) and surface potential-area (ΔV-A) isotherms of PS II core complex particles. The experimental conditions are the same as Fig. 3.4.

CHAPTER IV

SURFACE SPECTROSCOPIC STUDIES OF PHOTOSYSTEM II

PS II utilizes specialized pigment binding proteins to perform its light harvesting, electron transfer, energy transfer and charge separation functions. Every subunit in the PS II contains several pigment molecules. For example, light harvesting complex (LHC II) contains both Chl a and b including carotenoids which has primary function of absorbing solar energy and transferring the excitation energy to the reaction center (RC). The reaction center contains a special pair of Chl a which converts light energy into chemical potential in the form of charge separation across the membrane and function as primary electron donor for the water splitting redox reactions. Pigment molecules are also existing in the internal antenna proteins (CP43 and CP47) where they also function as complementary light harvesting and energy transfer media. These pigment molecules have strong absorption in the visible region and possess characteristic spectroscopic fingerprints that are sensitive to the molecular environment. Although the absorption and emission spectra of PS II are extremely rich in their information contents, detailed assignments are also difficult to obtain due to the complexity of the system. Many specialized techniques such as spectral hole burning (Vacha

et al., 1991; Groot et al., 1996) and low temperature spectroscopy (van Kan, 1990; Otte et al., 1992) studies have been applied to facilitate the spectral assignment by removing inhomogeneous broadening and electron-phonon interactions that broaden and complicate the spectral features. These studies have identified many unique features in the spectra of PS II and paved the way for applying this knowledge to probe the structure and function of PS II complexes. In this thesis, we do not intend to perform sophisticated spectral analysis of PS II, nor do we have the capability to do so. We will, however, monitor the spectral features, which infer the conformational changes of PS II complexes, at different preparation states.

Absorption spectrum of PS II membranes taken from buffer solutions exhibits major absorption bands at 340, 436, and 680 nm (spectrum shown in the following section). These absorption bands mostly arises from chlorophyll a molecules which are abundant in PS II complexes. The 680 nm band is of particular interest because this main peak position strongly depends on the its surrounding environments and the aggregation states of the Chl a molecules. For example, absorption maximum of low concentration Chl monomer dissolved in anhydrous ether peaks at 663 nm whereas if water is present in the solvent, absorption peak shifts to the red (Goedheer, 1966). Moreover, the absorption peak of aggregated Chl a molecules will not only red shift but also broaden (Goedheer, 1966). Chl a molecules are present in PS II antenna protein as aggregates and also exist in PS II reaction center as a "special pair". It has been suggested in literature that the red absorption

band in photosynthesis reaction center will blue shift when the protein complex is denatured (Braun et al., 1990). Therefore, the spectral signature of Chl molecules in photosynthetic protein provides us a "window" for monitoring the structural integrity of PS II complexes. In this study, fluorescence spectroscopy has been extensively utilized because it offers similar spectroscopic signature with higher sensitivity than that can be obtained from absorption technique. Moreover, fluorescence spectroscopy provides us information about pigment molecules packed within the PS II protein particle because pigment molecules can quench the fluorescence of other nearby pigment molecules.

In this chapter, absorption and emission spectra of PS II membranes and PS II core complex particles were taken from their buffer solutions as reference. Protein particles in their buffer solutions are very close to their native biological states as indicated by their oxygen evolution rates. These protein samples were then spread onto the air-water interface using Langmuir technique. Comparison of spectra of PS II particles at the air-water interface with that of solution phase reference revealed structural integrity of PS II particles in monolayer films.

Experiments

Langmuir Films

Monolayers of PS II membranes, PS II core complex particles and the mixture of PS II core complex particles with MGDG were prepared on a commercial KSV spectral mini-trough (KSV Instruments, Finland), at room temperature (23.0 ± 0.5 °C) and relative humidity of 40 ± 5%, as described in chapter 3.

Absorption and Fluorescence spectra of the sample solutions

Absorption spectra of PS II membranes and PS II core complex particles were recorded using a HP 8452A diode array spectrophotometer (Hewlett-Packard, USA) operating over the 350-800 nm range. Fluorescence emission spectra of PS II membranes and PS II core complex particles were obtained using a Spex Fluorolog-2 double monochromator fluorometer (Instruments, S. A., Inc., Edison, NJ, USA). The measurements were conducted with the excitation wavelength set at 440 nm, and the emission range from 600 to 800 nm.

Surface Spectral Measurements

The surface absorption and fluorescence spectra of PS II membranes, PS II core complex particles and the mixture of PS II core complex particles with MGDG monolayers were measured with a home-built measuring station.

Appendix described the details of instrumentation. Briefly, several commercial instruments including a KSV spectral mini trough, Spex fluorometer, and a HP diode array spectrophotometer were modified and assembled together on top of an optical breadboard using home-built holding frames, as shown in Figure 4.1. This instrument allows us to prepare monolayers of various protein particles at the air-water interface using Langmuir technique and measures their surface absorption and emission spectra *in situ*. The absorption spectra were taken by turning the HP spectrophotometer 90° using the home-built holding frames whereas the emission spectra were taken using Spex fluorometer with a custom designed optical fiber holder and attachment arm.
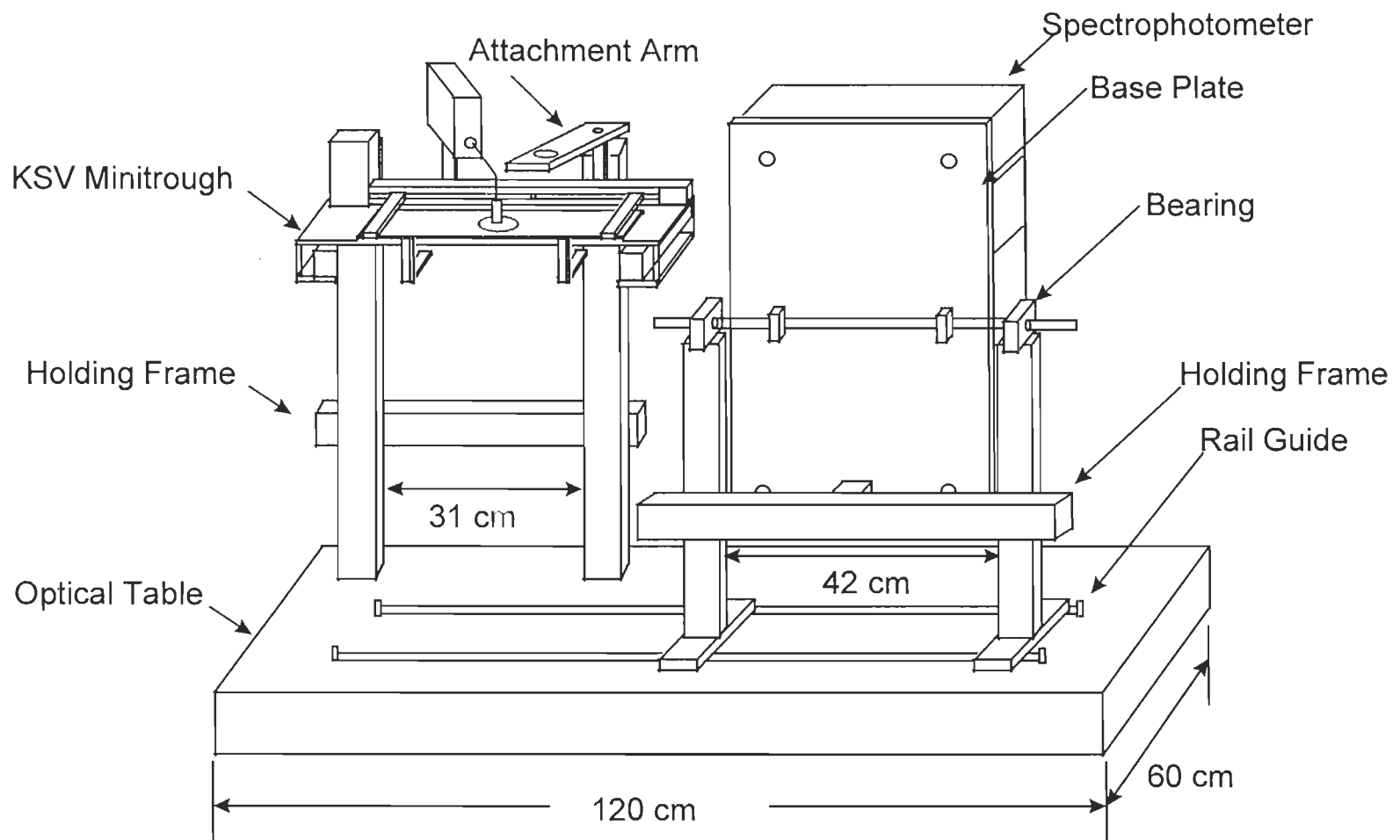
Figure 4.1 The schematic drawing of surface spectroscopy measurement station.

<u>Results and discussion</u>

<u>Absorption and fluorescence spectra of the sample solutions</u>

Figure 4.2a is an absorption spectrum of PS II core complex particles in buffer solution, taken at room temperature. The resolution of the spectrometer is 2 nm. Spectrum shows major absorption peaks at 340, 436, and a broad feature at 672 to 680 nm, in addition to many other small features. It is difficult to deconvolute all the spectral features at room temperature because of the complex nature of pigment molecules and protein matrixes. van Kan and coworkers (1990) have assigned many features of the absorption spectrum of PS II reaction centers taken at 10 K. The analysis indicated that the absorption peak at 680 nm can be attributed to the Chl a "special pair" in the PS II reaction center, whereas the shoulder at 672 nm belongs to the accessory chlorophylls (van Kan et al., 1990). However, spectra of Figure 4.2 are taken using PS II membrane and PS II core complex at room temperature. In cases of PS II membrane and PS II core complex, unlike reaction center studies of van Kan, most of Chls exist in the antenna proteins and thus it is difficult to pin down the exact assignments of the 672-680 nm band. Most of other spectral features can also be attributed to the Chl a pigment molecules.

Figure 4.2b shows absorption spectrum of PS II membranes at room temperature. Spectrum is similar to that of PS II core complex particles as the main features arises from Chl a molecules. However, PS II membrane proteins contain more Chl b and carotenoid pigments that contribute to the
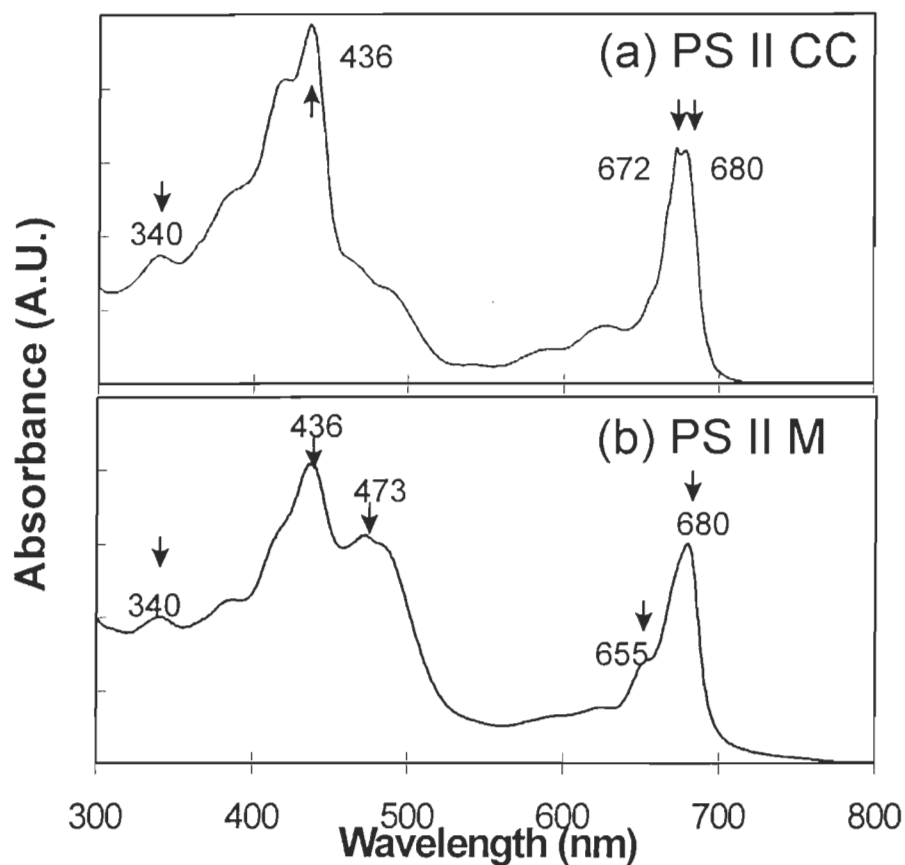
Figure 4.2. The absorption spectra of (a) PS II core complex particles and (b) PS II membranes. PS II membranes were suspended in buffer of 20 mM MES/NaOH, pH 6.5, 15 mM NaCl, 5 mM $MgCl_2$ and 400 mM sucrose. PS II core complex particles were in the buffer of 20 mM Bis-Tris, pH 6.5, 20 mM $MgCl_2$, 5 mM $CaCl_2$, 10 mM $MgSO_4$, 0.03% (w/v) n-dodecyl-β-D-maltoside, and about 32% sucrose. Temperature: 22.0 ± 0.5 °C.

absorption spectrum, as indicated by the spectral features at 655 and 473 nm. Although very small amounts of Chl b and carotenoid also exist in the PS II core complex particles, their contribution is overwhelmed by the Chl a and can not be resolved in our room temperature spectrum. In Figure 4.2, the intensities of the absorption spectra are arbitrary and do not reflect the relative absorbance of the two complexes.

Figure 4.3 shows the fluorescence spectra of PS II membranes and PS II core complex particles. Both of them have a major peak at 684 nm with a shoulder at about 730 nm. Those fluorescence signals arise from Chl a molecules in PS II complexes. Since both PS II membranes and PS II core complex proteins contain Chl a molecules which have different aggregation states and environments, it is not fully understood which Chl a pigment molecules contribute to these fluorescence features. However, these bands are most likely arising from the accessory Chl a in the PS II reaction center and Chl a in the antenna proteins (Barber et al., 1987; Jankowiak et al., 1989). The Chl a "special pair" of primary electron donor may not contribute to the fluorescence emission because their dimeric structure was shown to result in fluorescence quenching (Lavorel, 1957).

Surface absorption and fluorescence spectra of PS II membranes

Figure 4.4 shows the surface absorption spectra of PS II membranes. The measurements were taken at the different surface pressures of the
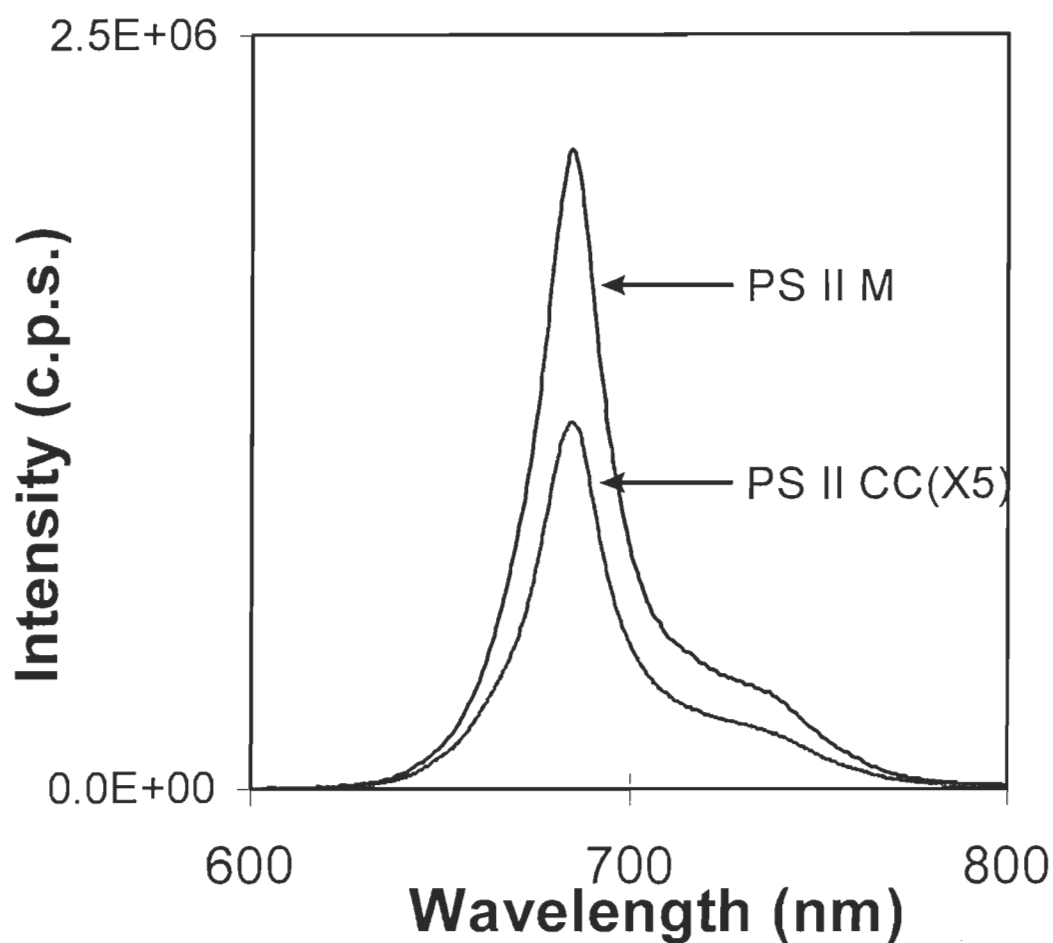
Figure 4.3. The fluorescence spectra of PS II membranes and PS II core complex particles. PS II membranes were suspended in buffer of 20 mM MES/NaOH, pH 6.5, 15 mM NaCl, 5 mM $MgCl_2$ and 400 mM sucrose. PS II core complex particles were in the buffer of 20 mM Bis-Tris, pH 6.5, 20 mM $MgCl_2$, 5 mM $CaCl_2$, 10 mM $MgSO_4$, 0.03% (w/v) n-dodecyl-β-D-maltoside, and about 32% sucrose. Temperature: 22.0 ± 0.5 °C.
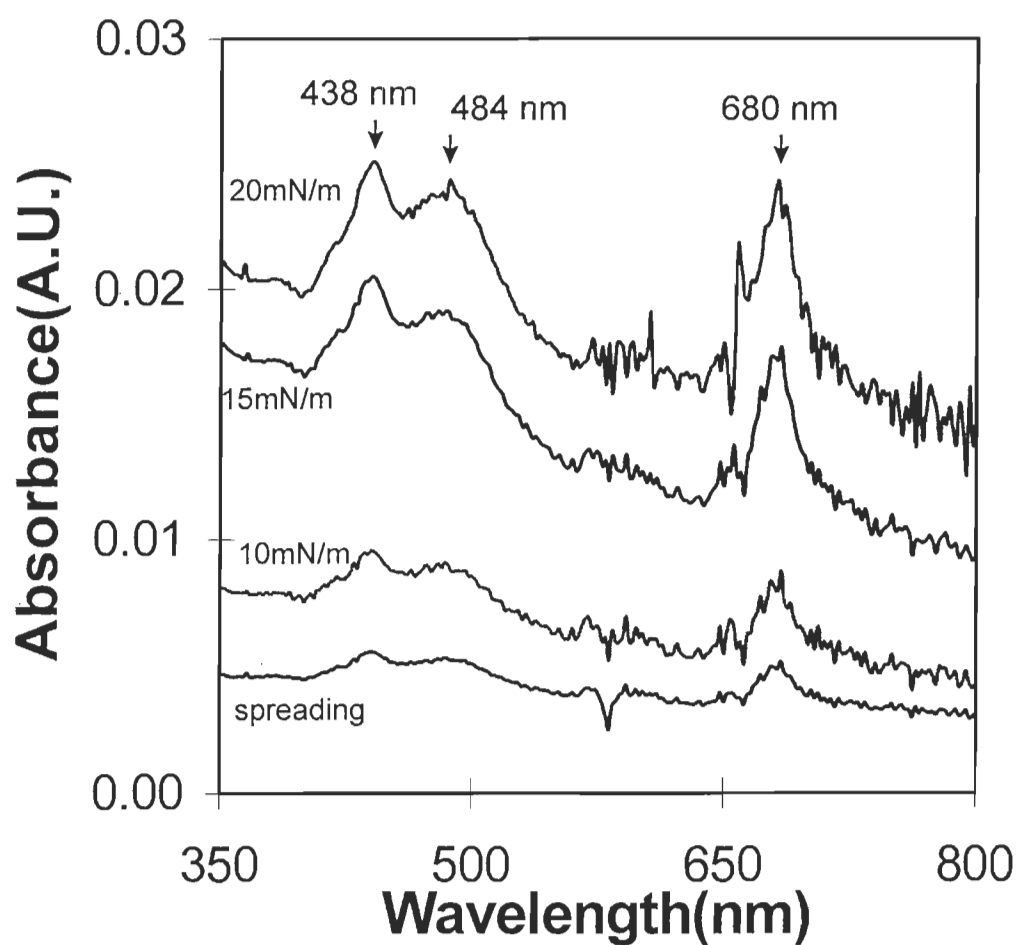
Figure 4.4. The surface absorption spectra of PS II membranes. Monolayer subphase, 2 mM $CdCl_2$, 2 mM ascorbate, and 2 mM MES/NaOH, pH 6.5. Temperature, 23.0 ± 0.5 °C.

initial spreading of ~2, 10, 15 and 20 mN/m. The major surface absorbance

peaks are at 438, 484 and 680 nm, similar to that of solution spectrum. With

increasing surface pressure from spreading to 20 mN/m, the absorbance

increased and the baseline absorption from protein matrixes also increased,

which indicate that the particle density per unit area increased during the

compression. Comparison of surface absorption spectra at different surface

pressures with spectrum of buffer solution shows that absorption peaks

of 680 nm band do not shift as function of different preparations, i. e. solution

compare to monolayer. Previous studies have indicated that absorption

spectra of Chl a will be red shifted as these pigment molecules become more

aggregated (Goedheer, 1966). Our results indicated that the aggregation

state of the Chl a molecules in the PS II membrane do not change at surface

pressures under studied. Since the state of aggregation of Chl a in PS II

membrane is determined by its surrounding protein structures, our results

also suggest that the PS II membrane protein maintains its structural integrity

during the surface compression.

Figure 4.5 shows the surface fluorescence spectra of PS II membranes.

These emission spectra are similar to that in solution. They all have a major

peak at 682±1 nm and a shoulder at about 730 nm. When the surface

pressure is increased from 7.9 to 17.5 mN/m, results show no spectral shifts.

It should be pointed out that the spectral features in the fluorescence

emission arise from light-harvesting Chl a and accessory Chl a,
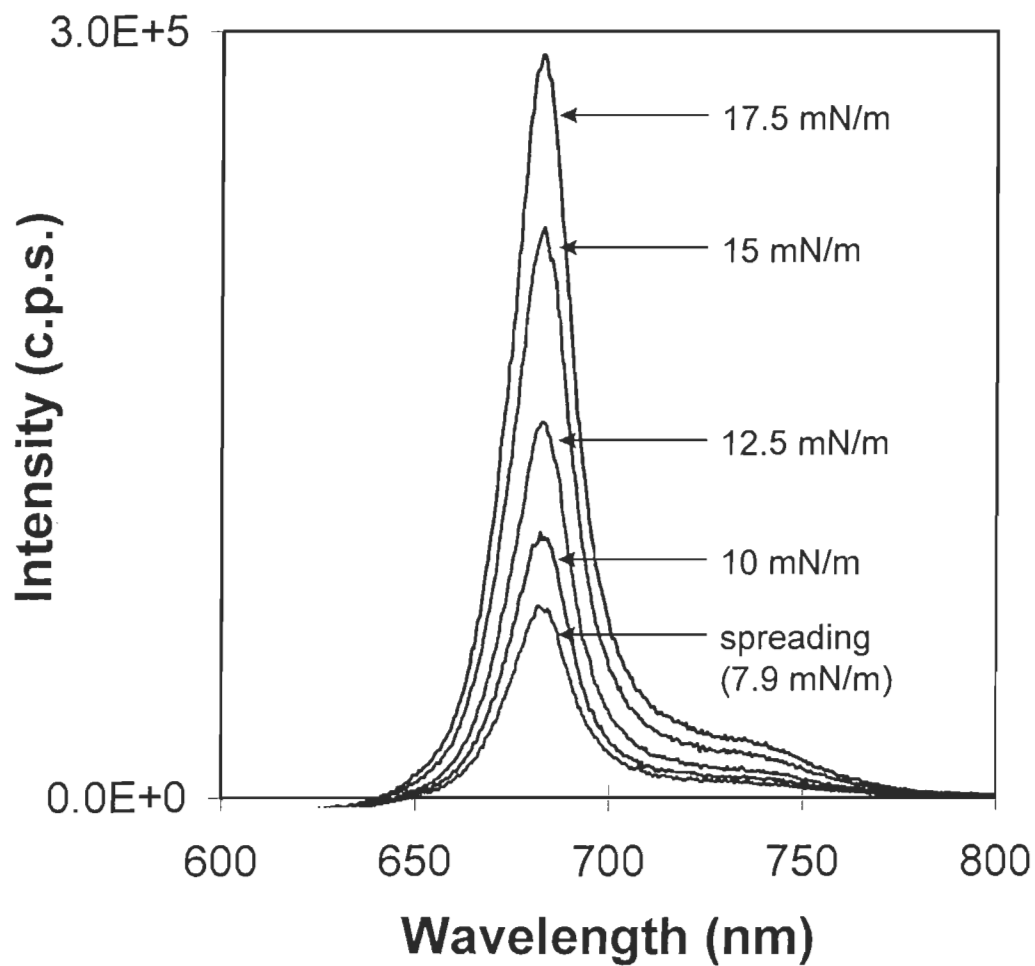
Figure 4.5. The surface fluorescence spectra of PS II membranes.
Experimental conditions are the same as in Fig. 4.4.

because fluorescence from "special pair" Chl a in the reaction center is quenched by each other due to their close proximity. The fluorescence intensity measurements therefore reinforce the absorption results without any ambiguities in spectral assignment. Our results from both absorption and fluorescence measurements support the idea that the lipids surrounding PS II particles in membrane result in a more rigid complex and protect the inner structure of the complex from change with surface pressure.

Surface fluorescence spectra of PS II membranes have also been measured using different excitation wavelengths. Figure 4.6 shows the surface fluorescence spectra of PS II membrane monolayer at the air-water interface with different excitation wavelengths at a surface pressure of 15 mN/m. As expected, the 682 ±1 and 730 nm emission peaks are the same for all excitation wavelengths. The changes of fluorescence intensities using different excitation wavelengths agree with their corresponding oscillator strength in absorption.

Surface absorption and fluorescence spectra of PS II core complex

Figure 4.7 shows the surface absorption spectra of PS II core complex particles. An increase in absorbance and baseline during compression has also been observed similar to that of PS II membranes. When comparing these data to the absorption spectrum of solution, two major absorption peaks at 340 and 436 nm remain same, however, the signature peak around

Figure 4.6. The surface fluorescence spectra of PS II membrane monolayer at the air-water interface with different excitation wavelengths at surface pressure of 15 mN/m. Experimental conditions are the same as in Fig. 4.4.
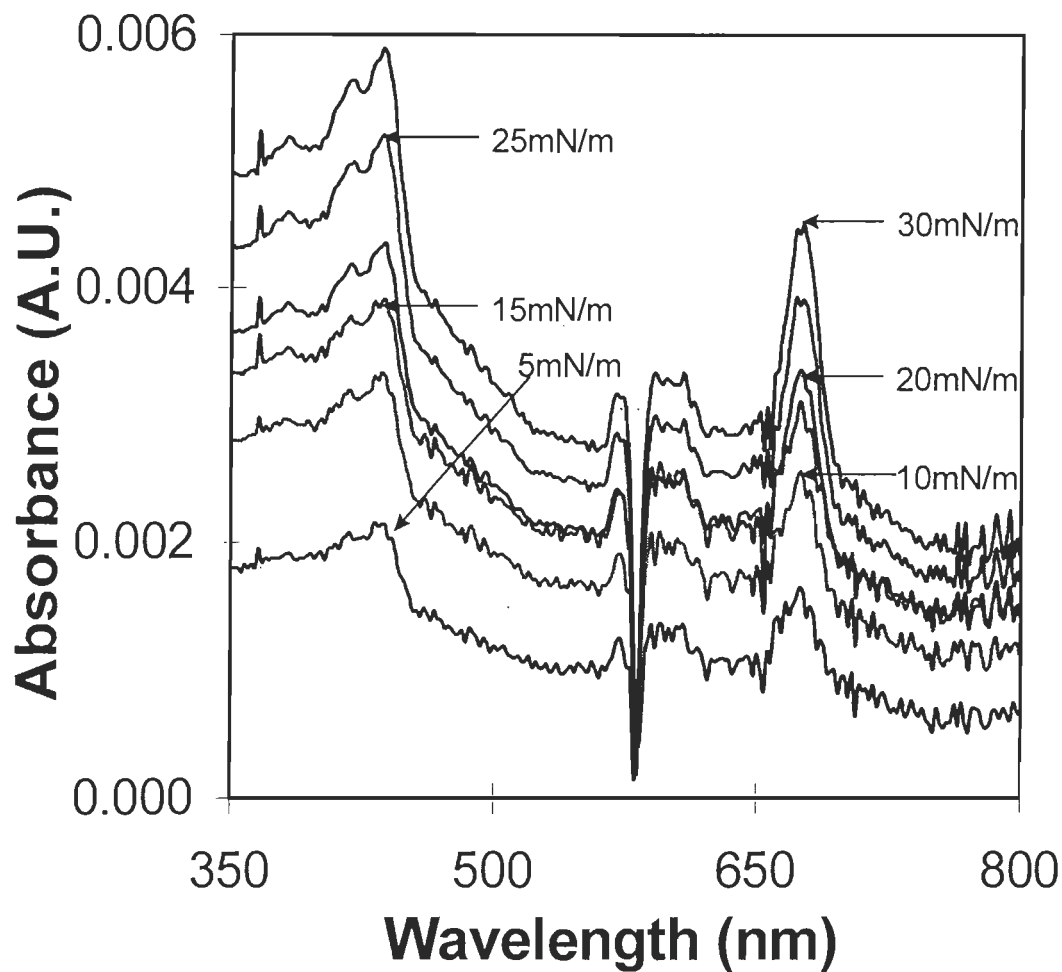
Figure 4.7. The surface absorption spectra for PS II core complex particles.
Monolayer subphase, 10 mM Tris-HCl, pH 8.0, 2 mM sodium ascorbate and
100 mM NaCl. Temperature, 23.0 ± 0.5 °C.

680 nm shifts from 680 in solution spectrum to 674 nm once spreading onto the air-water interface. When external surface pressures of 5 to 30 mN/m are applied to compensate the surface tension, the 674 nm peak shifts to 676 nm, but not completely recovers back to 680 nm as in the solution. Since the signature peak arise from Chl molecules attached to the PS II core complex, these spectral shifts suggest that, in contrast to the case of PS II membranes, the structural integrity of PS II core complex particles changes when the samples are spread at the air-water interface. In addition, these structural changes can not be completely restored by applying external surface pressures to compensate surface tension. The physiological implication of these observations is that PS II core complex particles might be denatured by the surface tension when spread them onto the air-water interface.

It should be noted that a sharp dip at 580 nm appears on every PS II core complex particles surface absorption spectrum. This is an artifact caused by the diode array spectrometer in which baseline substraction is performed incorrectly. The artifact becomes prominent only when the extremely low absorption measurements are performed. We observed this occasionally when measuring surface absorption of PS II membranes as well. Since this artifact occurs in the wavelength region outside of our interest, no particular action was taken to remove it. The presence of this artifact should not affect the outcome of this study.

Figure 4.8 shows the surface fluorescence spectra of PS II core complex particles. They have one major peak with a shoulder at about 730 nm. When spreading the sample at the interface, a major fluorescence peak appeared at 675 ± 1 nm, instead of 684 nm as in the solution. The major peak shifts from 675 to 682 nm when surface pressure increases from 5 to 30 mN/m. These results are consistent with the absorption measurements and both indicate that surface tension at the air-water interface changes the structural integrity of PS II core complex particles. These results are not surprising, however, when considering that unlike PS II membrane proteins, PS II core complex lacks supporting lipid molecules which are crucial for strengthening the inner structure of the protein particles.

It is also interesting to note that the intensity of fluorescence emission decreases as the film is being compressed. Since the density of protein particles and hence the density of fluorescent chromophores increases as the film is being compressed, one can only explain the decrease in emission intensity by fluorescence quenching. When the PS II core complex particles sample were first spread at the surface, there is plenty of space between each particle. During compression, these particles come closer to each other. The fluorescence from light-harvesting Chl a molecules can be partially quenched by the Chl a molecules in the nearby particles. This kind of inter-particle quenching is only possible in PS II core complex particles because the supporting lipid molecules have been removed from protein
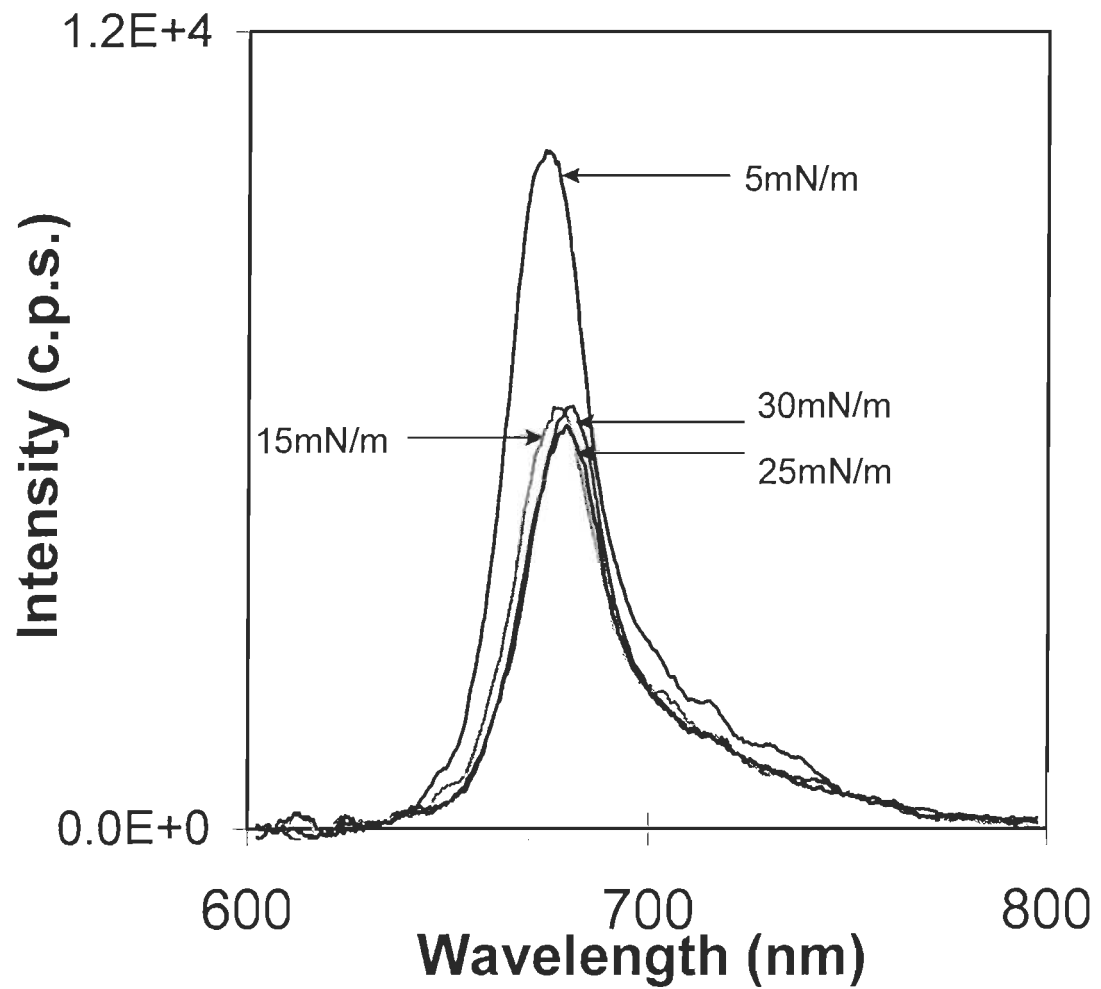
Figure 4.8. The surface fluorescence spectra of PS II core complexes.

Experimental conditions are the same as in Fig. 4.7.

backbone. For example, the fluorescence intensity increases as the monolayer film of PS II membranes is being compressed, as indicated in Figure 4.5.
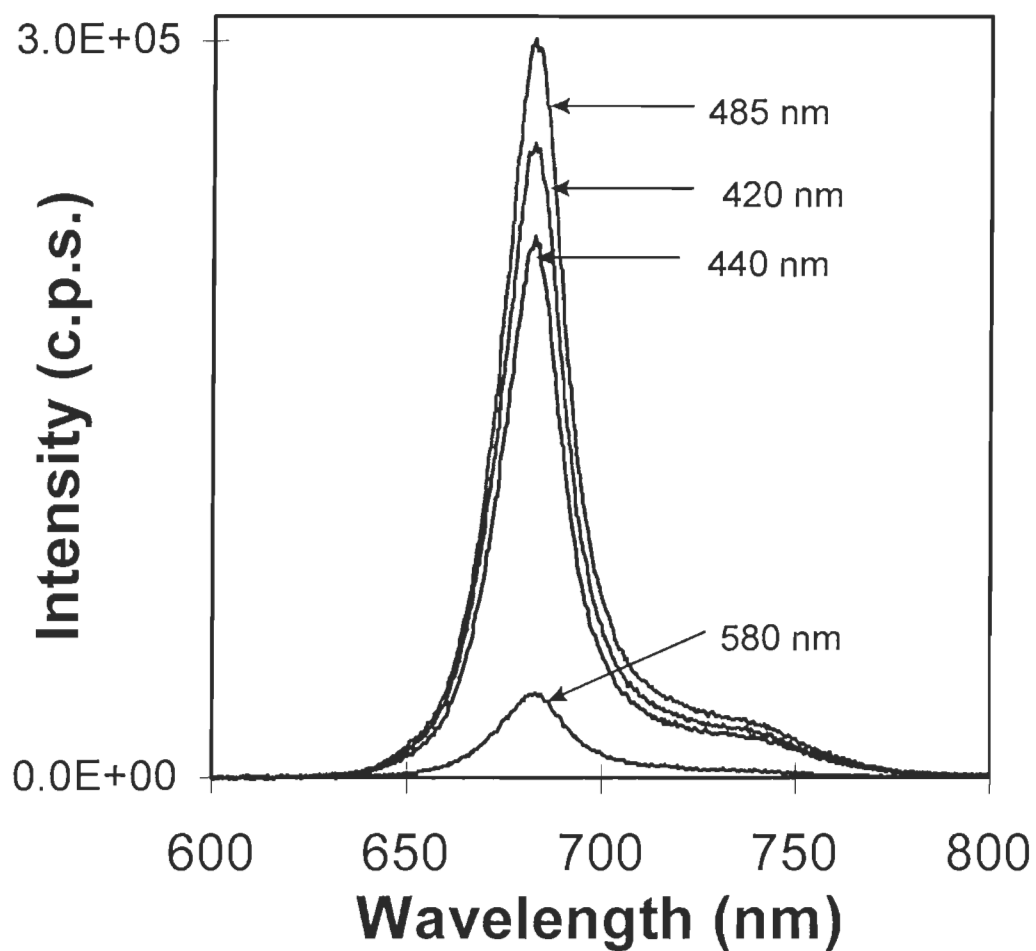
Figure 4.9 gives the surface fluorescence spectra of PS II core complex particles monolayer at the air-water interface with different excitation wavelengths at a surface pressure of 15 mN/m. They all have one major peak at 676 ± 0.5 nm and a shoulder at about 730 nm for all excitation wavelengths. The intensity changes with different excitation wavelengths, which agree with the absorption spectrum.
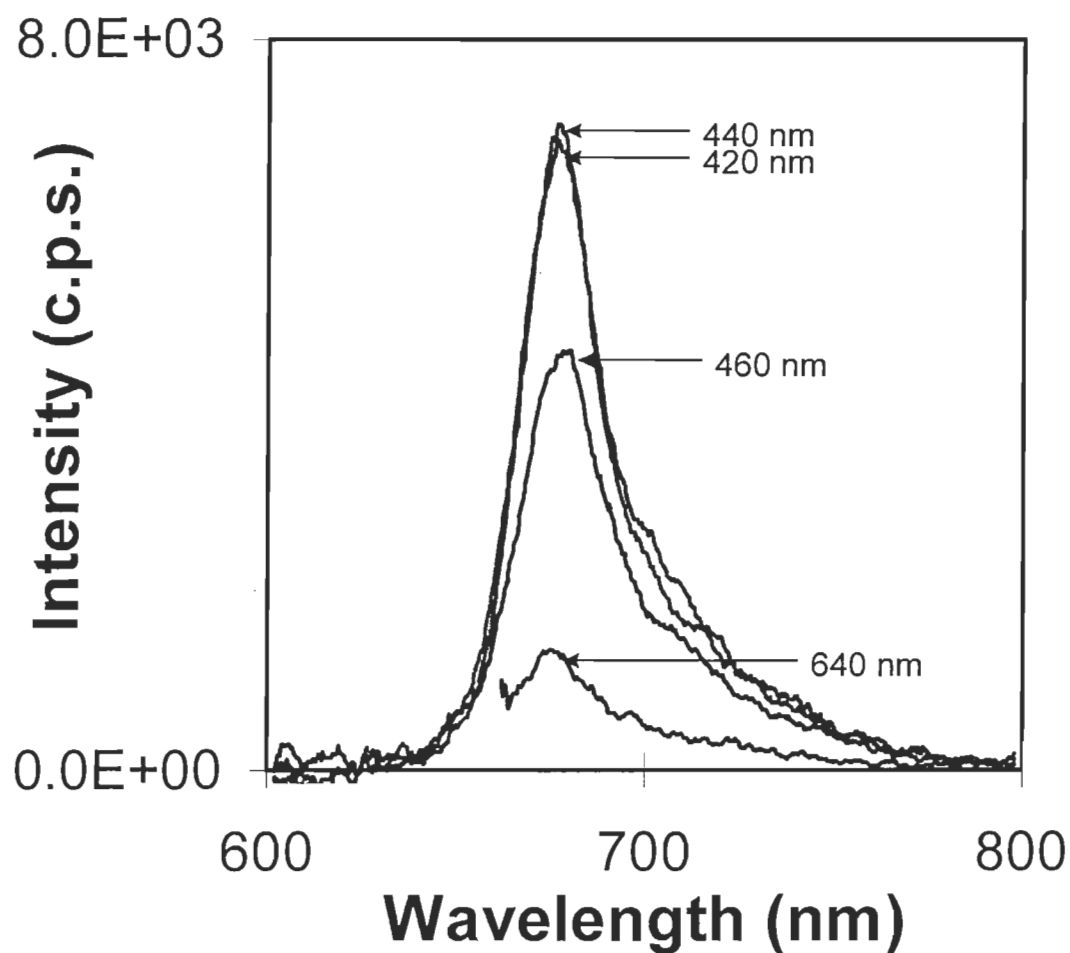
Figure 4.9. The surface fluorescence spectra of PS II core complex particles in monolayer at the air-water interface with different excitation wavelengths at surface pressure of 15 mN/m. Experimental conditions are the same as in Fig. 4.4.

<u>Surface fluorescence spectra of the mixture of PS II core complex</u>
<u>particles with MGDG</u>

Comparison of surface spectroscopy data of PS II membranes and PS II core complex particles indicates that lipid molecules in the protein complexes might play a central role in stabilizing their structures. Instead of removing lipids from natural protein complexes, as in case of preparing PS II core complex particles from PS II membranes, we artificially added MGDG, the main lipid component of biomembranes. The surface spectroscopy study of the mixture of PS II core complex particles and MGDG may offer additional insight into the role of lipids in the protein complexes.

Because of low concentration of PS II core complex in the mixture monolayer, surface absorption spectra of PS II core complex monolayers cannot be obtained using our current instruments. High sensitivity of fluorescence spectroscopy, however, allows us to measure emission spectra of low concentration PS II core complex.

Figure 4.10 shows the surface fluorescence spectra of the mixture of PS II core complex and MGDG in monolayers at the air-water interface. In the mixture, the ratio of PS II core complex particles and MGDG is 76.6 to 23.4 by weight. Those spectra were taken at different surface pressures of the initial spreading of 1.4, 10, 20 and 30 mN/m. As shown in this figure, they all have a major peak at 677 nm with a shoulder at about 730 nm. The main peak at 677 nm shifts from 677 to 680 nm as the surface pressure increases. During the compression, the area per molecules is reduced and the
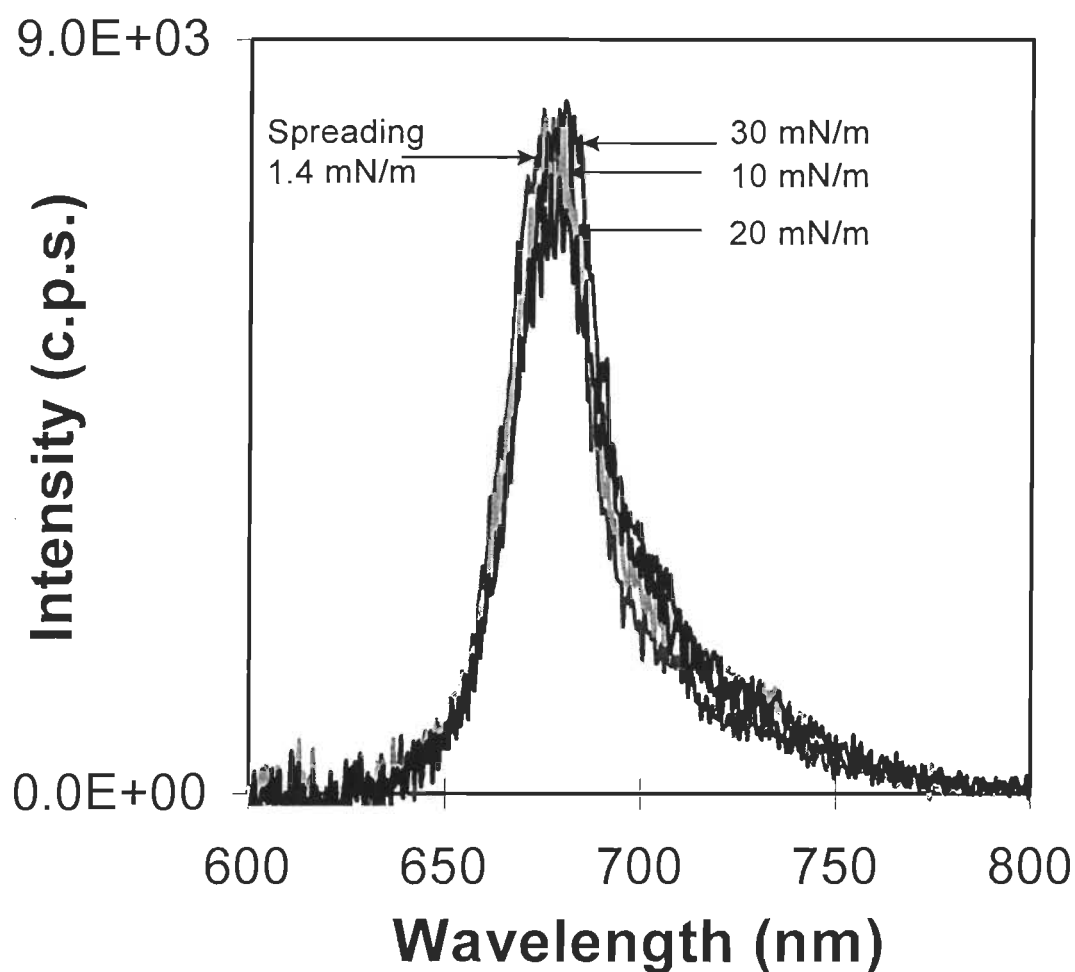
Figure 4.10. The surface fluorescence spectra of the mixture of PS II core complex particles and MGDG monolayer at the air-water interface. In the mixture, the ratio of PS II core complex and MGDG is 76.6 to 23.4 by weight. Monolayer subphase, 10 mM Tris-HCl, pH 8.0, 2 mM sodium ascorbate and 100 mM NaCl. Temperature, 23.0 ± 0.5 °C.

concentration of PS II core complex is increased. One would expect that the fluorescence intensity will increase as surface pressure increases. However, our data show that the fluorescence intensities are virtually unchanged during compression. The molar ratio of PS II core complex is extremely low (1%) in the mixture and the distribution of PS II core complex is uneven at the interface (as indicated by our preliminary AFM data). It is possible that the number of PS II CC particles in the limited illumination area from fiber tip remain unchanged during compression.

Comparing Figure 4.10 with the fluorescence spectra of PS II membranes and PS II core complex particles monolayers, it is clear that the major fluorescence peak is shifted to a lesser extent for the mixed monolayer than for pure PS II core complex particles monolayer. The fluorescence intensity data also indicate that the MGDG lipid molecules indeed fill up space between PS II core complex particles. These results confirmed that the presence of lipid in the mixed monolayer protects PS II core complex structure from external force.

This work demonstrated that both PS II membranes and PS II core complex particles from higher plants form mono-layered structures at the air-water interface. PS II membranes retain their native protein conformation structure upon spreading onto the interface. However, PS II core complex particles may have changed its structure at the interface because of the surface tension. Mixing PS II core complex particles with lipid molecules may offer a remedy for preventing structural changes at the air-water interface.

CHAPTER V

STRUCTURAL STUDIES OF PHOTOSYSTEM II WITH TAPPING MODE ATOMIC FORCE MICROSCOPY

In the seventeenth century, the development of the optical microscopy by van Leeuwenhoek in 1660 allowed the investigation of the micron-sized world after the invention of simple magnifying lenses. Since that time, the optical microscopy has played, and continues to play, an enormous role in the studies of microcosmos. Because optical resolution is limited by the wavelength of light to about 0.2 microns, the submicron world still was out of reach.

The invention of the electron microscope by Ruska and Knoll in the 1930s pushed this resolution limit to atomic dimensions by using high-energy electrons rather than photons as the imaging medium. However, even today, electron image resolution is limited by deficiencies in properly preparing samples rather than by any inherent limitation of the electron microscope (Zasadzinski and Hansma, 1990).

With the advent of scanning force microscopy (SFM), an instrument became available for investigating a variety of insulating organic surfaces, including biological matter such as nucleic acid (Hansma et al.,1988),

proteins (Drake et al., 1989; Egger et al., 1990; Lin et al., 1990), cell

surfaces (Butt et al., 1991; Häberle et al., 1991), biomembranes

(Worcester et al., 1988; Singh and Keller, 1990), and Langmuir-Blodgett

films (Egger et al., 1990; Weisenhorn et al., 1990; Meyer et al., 1991;

Weisenhorn et al., 1991; Hansma et al., 1991; Lea et al., 1992; Garnaes

et al., 1992; Goettgens et al., 1992; Viswanathan et al., 1992; Garnaes et

al., 1992; Meyer et al., 1992; Overney et al., 1992; Weisenhorn et al.,

1992; Bourdieu et al., 1993).

Although AFM is only one decade old, it has been applied to every field

that concerns the structure of matter. For biological applications, the

instrumentation convincingly demonstrated various known structures, such as

DNA (Lyubchenko et al., 1992, 1993; Bustamante et al., 1992; Vesenka et

al., 1992; Hansma et al., 1992 a,b; Yang et al., 1992; Henderson, 1992;

Zenhausern et al., 1992; Rees et al., 1993), supported membranes

(Zasadzinski et al., 1991; Yang et al., 1993 a; Mou et al., 1994 a,b),

membrane proteins (Butt et al., 1990 a; Hoh et al., 1991, 1993; Yang et al.,

1993 a,b), and soluble proteins (Ohnishi et al., 1992; Yang et al., 1994 a,b).

Despite many years of intensive studies (Andersson and Adderson,

1980; Michel, 1982; Deisenhofer et al., 1984; Haag et al., 1990; Peter and

Thornber, 1991; Lyon et al., 1993; Holzenburg et al., 1993, 1996; Santini et

al., 1994; Facci et al., 1994; Yamada et al., 1994; Boekema et al., 1995;

Seibert, 1995; Nakazato et al., 1996), the exact structure of photosystem II is

still not well understood. Much of the structural ambiguity arises from the

preparation of sample and the techniques used for the measurements. Primary tools used in structural determination have been X-ray crystallography (Michel, 1982; Deisenhofer et al., 1984) and electron microscopy (EM) (Hagg et al.,1990; Holzenburg et al., 1993, 1996; Santini et al., 1994; Boekema et al., 1995; Nakazato et al., 1996). X-ray crystallography is a very powerful and extremely versatile tool because it can precisely determine the three dimensional structure of the protein crystals at atomic resolution. However, this technique requires the sample protein to be prepared in a crystal form. This sample preparation is not only difficult and sometimes impossible to implement but also, more importantly, may distort the protein structure from their bioactive states. Electron microscopy has also been widely used to probe protein structure. Application of this technique to biological systems, however, requires the samples to be dye stained or metal coated or cryogenically treated. This kind of sample preparations may also lead to ambiguous results because dye stain may not cover every parts of protein complex and metal coating may distort the complex structure.

Scanning tunneling microscopy (STM) and atomic force microscopy (AFM) have the capability to image biological molecules under conditions close to their native states (Amrein and Marti, 1993). However, since electrons cannot directly tunnel through large insulating molecules such as PS II, platinum replicates or metal coated PS II membranes were used in recent STM studies (Facci et al., 1994; Seibert, 1995). AFM works both for conductive and non-conductive samples and therefore requires no metal

coating of the samples, but the AFM tip can seriously distort and even damage soft biological materials when operated in the contact mode. Furthermore, the large lateral tip force requires the samples be strongly attached to a substrate, which usually results in a large sample-substrate interaction that may distort the natural structure of the sample. AFM has been recently used to image titanium coated PS II crystals (Yamada et al., 1994) and Langmuir-Blodgett (L-B) films of photosynthetic membranes isolated from bacteria *Rhodopseudomonas viridis* deposited on glass substrates (Lyon et al., 1993).

In the present study, we applied a tapping mode AFM (Zhong et al., 1993; Hansma et al., 1993 a) to the studies of untreated PS II membranes from spinach deposited on an atomically flat mica substrate using the Langmuir-Blodgett method. Since the oscillating tip in the tapping mode AFM only briefly touches the sample during each cycle of oscillation, it drastically reduces tip-induced distortion to soft biological materials. The use of atomically flat mica as substrate removes the complication in the image interpretation due to rough features in substrates such as glass.

Experiments

Langmuir-Blodgett films

PS II membranes are extracted and isolated from fresh spinach leaves using methods described in Chapter 3. The bioactivity of these particles was examined for their oxygen evolution rates. PS II membrane monolayers were then deposited by the Langmuir-Blodgett method (Langmuir, 1917; Blodgett and Langmuir, 1934) at constant surface pressures of 10, 12.5 and 15 mN/m, on fresh-cleaved mica substrates using a lab-build Langmuir-Blodgett trough.

In order to prepare the L-B monolayer of PS II, the mica slide was cleaved before the deposition. Since mica can be easily cleaved to obtain a clean and atomically flat surface that does not have intrinsic feature to complicate the AFM image, it has been the favorite material as the AFM substrate (Drake et al., 1989). The fresh-cleaved mica slide was mounted on a home-made dipper with its plane at 90° to the air-water interface. The mica slide was inserted into the aqueous subphase and through the Langmuir film prepared as described above and maintained at constant surface pressure. The PS II membranes were spread at the interface of air and aqueous solution (2 mM $CdCl_2$, 2 mM sodium ascorbate, and 2 mM MES (pH 6.5)), compressed to a desired surface pressure. The dipping speed was kept constant at 10 mm/min.

Surface fluorescence spectra of L-B films

The coverage of the PS II membranes L-B film on each substrate was examined by spectrofluorometry. The surface fluorescence emission spectra of PS II membranes and PS II core complex particles L-B film on mica were obtained using a Spex Fluorolog-2 model 212 double monochromator fluorometer (Instruments, S. A., Inc., Edison, NJ, USA). The measurements were conducted with the excitation wavelengths of 440 nm, and the emission range covers 600 to 800 nm. The peak position and shape of the fluorescence spectrum of the membranes deposited on mica are nearly identical to those obtained in buffer solution. The peak height, as expected, increases as the surface pressure increases.

Tapping mode AFM imaging

The tapping mode AFM study was carried out on a MultiMode Nanoscope system in air at room temperature. Etched Si tips with a resonant frequency of $\approx$ 319 kHz, force constant of $\approx$ 50 nN/nm and nominal radius of curvature of 5 - 10 nm were used. The quality factor, Q which is a measure of the internal mechanical energy loss of the material, of the tip at the resonant frequency was determined to be $\approx$ 500. The tip was driven to oscillate at a slightly lower frequency than the resonant frequency with an amplitude of $\approx$ 30 nm. The images were obtained with various setting points that allow us to obtain information about the elastic properties of the sample.

<u>Results and discussion</u>

Figure 5.1 shows the fluorescence spectra of PS II membrane L-B films on mica. The fluorescence intensity at different surface pressures indicated that the density of PS II membranes on mica increases as the surface pressure increases. From 10 mN/m to 12.5 mN/m, the fluorescence intensity of the LB film increased by about 50%. From 10 mN/m to 15 mN/m, the fluorescence intensity of PS II membranes L-B film increased about 120%. The fluorescence spectra of LB films on mica substrate are identical to these of Langmuir films formed at the air-water interface. In addition, the trend of fluorescence intensity changes as function of surface pressure also agrees with that obtained at air-water interface. These spectroscopic results suggest that the PS II membranes transferred from the Langmuir trough to mica substrates maintain their structural integrity.

Figure 5.2A is a tapping mode AFM image of the PS II membranes prepared at 10 mN/m. The image reveals the PS II particles as blob-like features that appear to be randomly distributed on the surface. The height of the particles above the membrane surface measured from the AFM image varies from 0.5 to 2.5 nm, compared to 3 nm as estimated from transmission electron microscopy (Santini et al., 1994). The dimension of the particles measured from this image is about 25 ± 5 nm, which is somewhat greater than the 17 -19 nm value determined by electron microscopy (Holzenburg et al., 1993). This discrepancy may be at least partially due to the finite radius
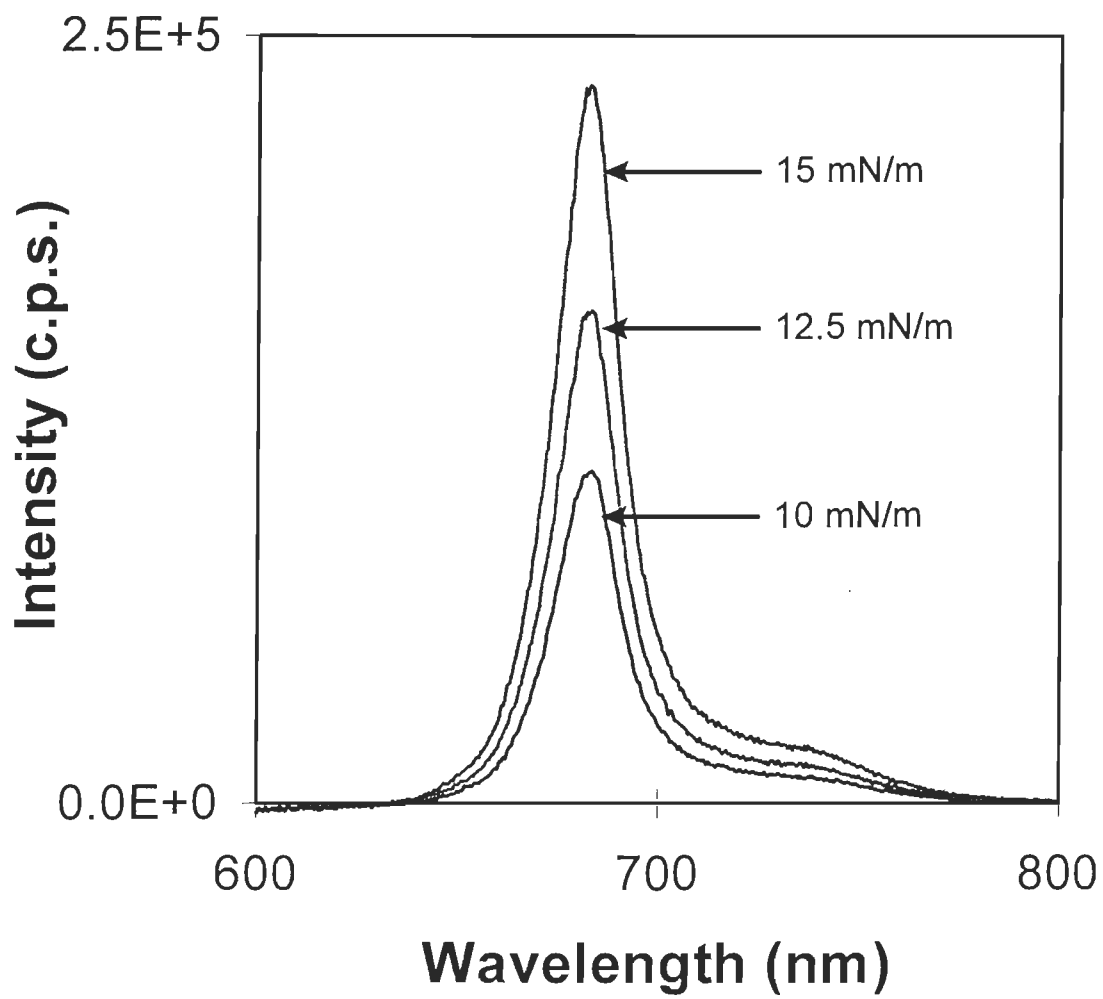
Figure 5.1. Fluorescence spectra of PS II membrane LB films deposited on mica at surface pressures of 10, 12.5 and 15 mN/m.
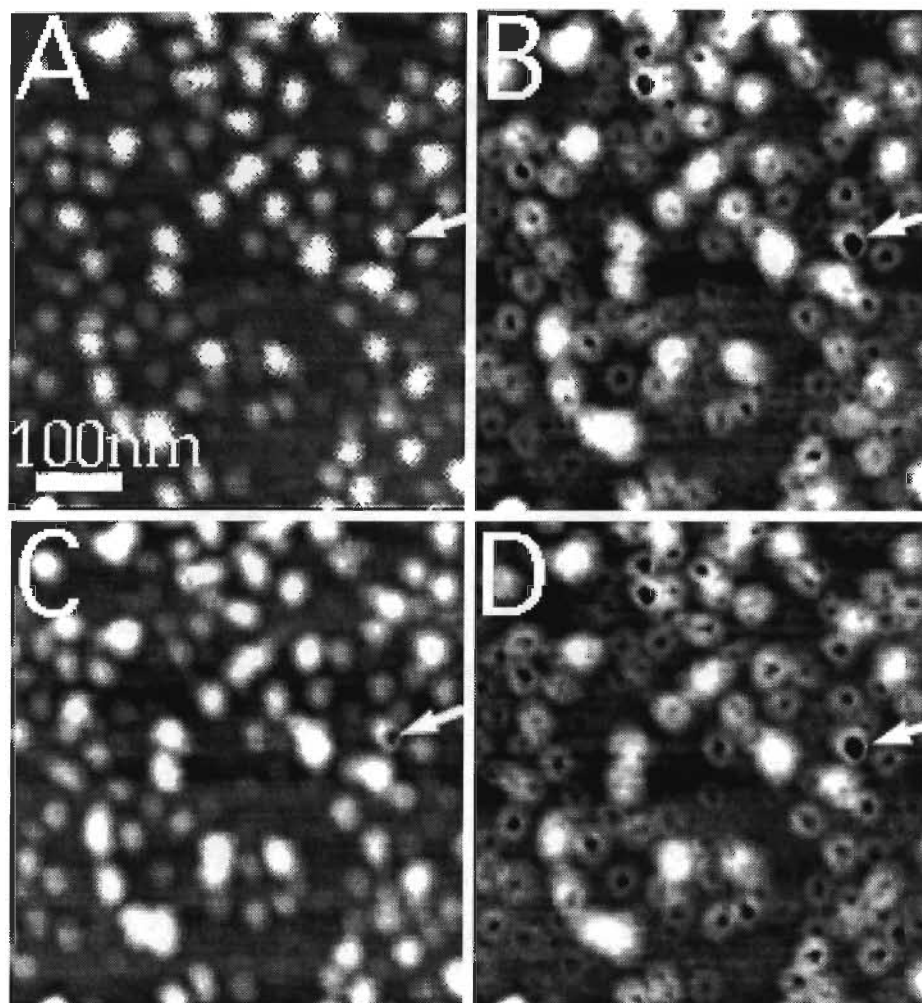
Figure 5.2. AFM images of a PS II membrane L-B film obtained with different

tip forces. A). ~0.3 nN; B). ~5 nN . The sample is almost completely

recoverable by reducing C). ~0.3 nN; and reincreasing D). ~ 5nN the applied

tip force. The film was deposited on mica at 10 mN/m.

of the AFM tip, and can be estimated using simple geometrical deduction. As schematically illustrated in Figure 5.3, if we approximate a PS II particle as a sphere embedded in the membrane with a slight protrusion out of the membrane surface and assume that the tip of the AFM probe is spherical in shape, then the broadening due to the finite tip radius is about

$$B = 2\ Rh/W_0 \qquad\qquad (6.1)$$

where R is the radius of curvature of the tip, h is the extent of protrusion and W_0 is the actual width of the particle. Using R=10 nm, h=2.5 nm and W_0=17 nm, the extent of broadening amount is estimated to be 3 nm. This result is in excellent agreement with that 17 -19 nm value determined by electron microscopy (Holzenburg et al., 1993).

Since AFM can probe tip-sample interactions, it may be used to study microelastic properties of biological material from the tip-induced deformation on the sample (Maivald et al., 1991; Tao et al., 1992). We have used this unique advantage to study elastic properties of the PS II particles by applying various forces on the individual particles via the AFM tip. Figure 5.2A was obtained with the smallest possible force that allowed the tip to follow the sample surface topography. The force, estimated from the amplitude setting point and resonant response of the AFM cantilever, is about 0.3 nN. The image clearly reveals individual PS II particle as blobs. Upon increasing the
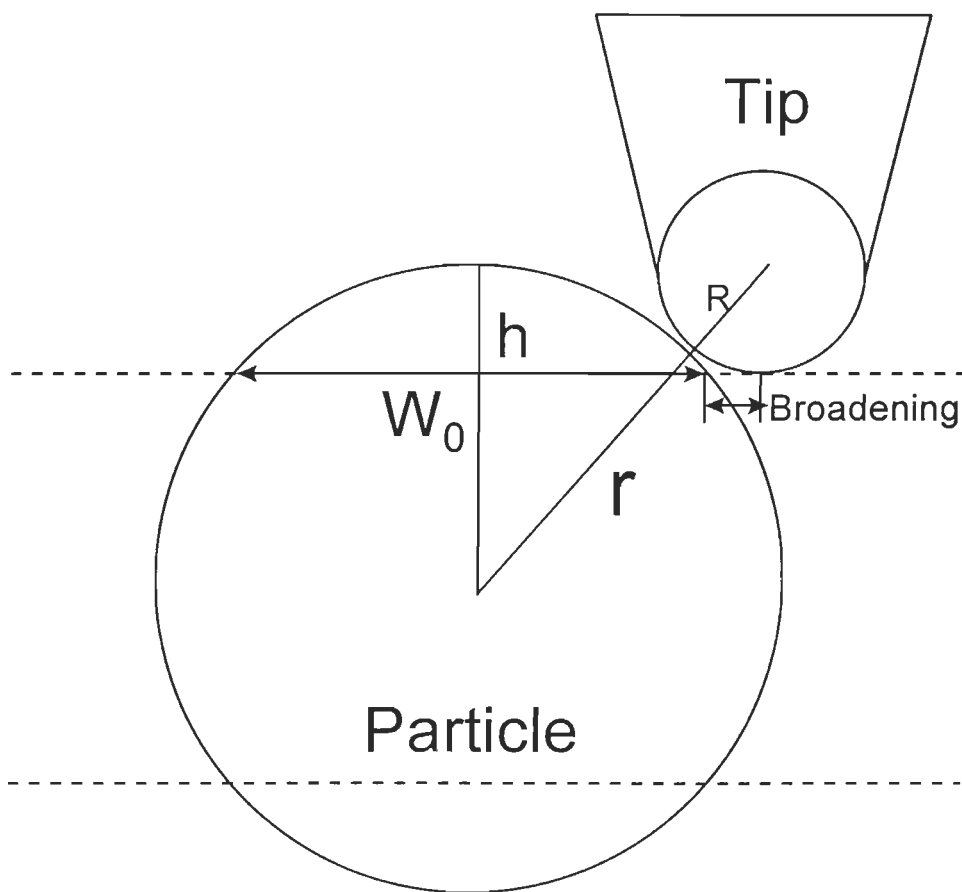
Figure 5.3. Scheme for estimating the broadening of measured particle size due to the finite tip radius of AFM. R is the radius of curvature of the tip, h is the extent of protrusion, r is the actual particle radius and W_0 is the actual width of the particle.

tip force applied on the sample, a circular cavity gradually appears near the center of each PS II particle (Figure 5.2B). The cavities cannot be clearly resolved by the AFM under a small force. This is probably because they are filled up with small molecules such as solvent and salt. Under a larger force, the tip penetrates into the cavity by enlarging the cavity. As expected, we found that the cavity size increases with the increase in force. Decreasing the force back to the lowest level ($\approx$ 0.3 nN), the cavities in almost all the PS II particles disappear completely and the particles return to their original shape (Figure 5.2C). Occasionally we have observed these cavities in some particles (pointed by an arrow) do not disappear, indicating a permanent damage to the particles. By controlling the tip force applied on the sample, we have reproducibly made the cavities to appear (Figure 5.2D) and to disappear in 9 different samples prepared under various conditions. We note that cavities also appear on the 'bright' particles that are not clearly shown in the image because the image contrast was adjusted to show the cavities of most particles. However, we have observed that $\approx$ 3% particles never exhibit cavities even under the largest applied force ($\approx$10 nN). This is possibly due to the placement of PS II membranes with lumenal side face to the mica substrate (inverted position).

It is interesting to compare our AFM results with electron microscopy studies (Holzenburg et al., 1993; Santini et al., 1994; Boekema et al., 1995). The electron microscopic images of negatively stained two-dimensional

crystals PS II complexes revealed that the lumenal side of PS II particles consists of four large domains and eight smaller protrusions surrounding a central cavity. These intramolecular cavities are believed to serve as special intramolecular microenvironment for oxygen evolution (Holzenburg et al., 1994). Due to the limited resolution, AFM images can only reveal the central cavity but cannot resolve the four domain structures that surrounding the central cavity.

We have monitored the deformation of a single PS II particle under various forces (Figure 5.4 A-C) to understand their nature and avoid any erroneous conclusion on PS II dimensions. The height profiles across the center of the particle in the vertical direction of the images are shown in Figure 5.4 D-F. Accompanying the appearance of the cavity, the particle protrusion above the membrane surface is compressed by 1 nm (Figure 5.4 E) by the tip loaded with a force of 5 nN for the PS II monomers in the direction vertical to the membrane surface. The particle lateral dimension has also been expanded by as many as 20 nm which indicates that the oscillating AFM tip is in constant contact with the particle under such a large force. The cavity diameter varies from particle to particle between 5 nm and 30 nm with a typical value of about 20 nm. Using a half-cone angle of 25° for the tip, the 5 nN vertical force corresponding to a lateral force of $\approx$ 2 nN and the 20 nm cavity radius gives a force constant of $\approx$ 0.1 nN/nm for enlarging the cavity. Increasing the tip force to 10 nN (beyond that the image loses contrast and
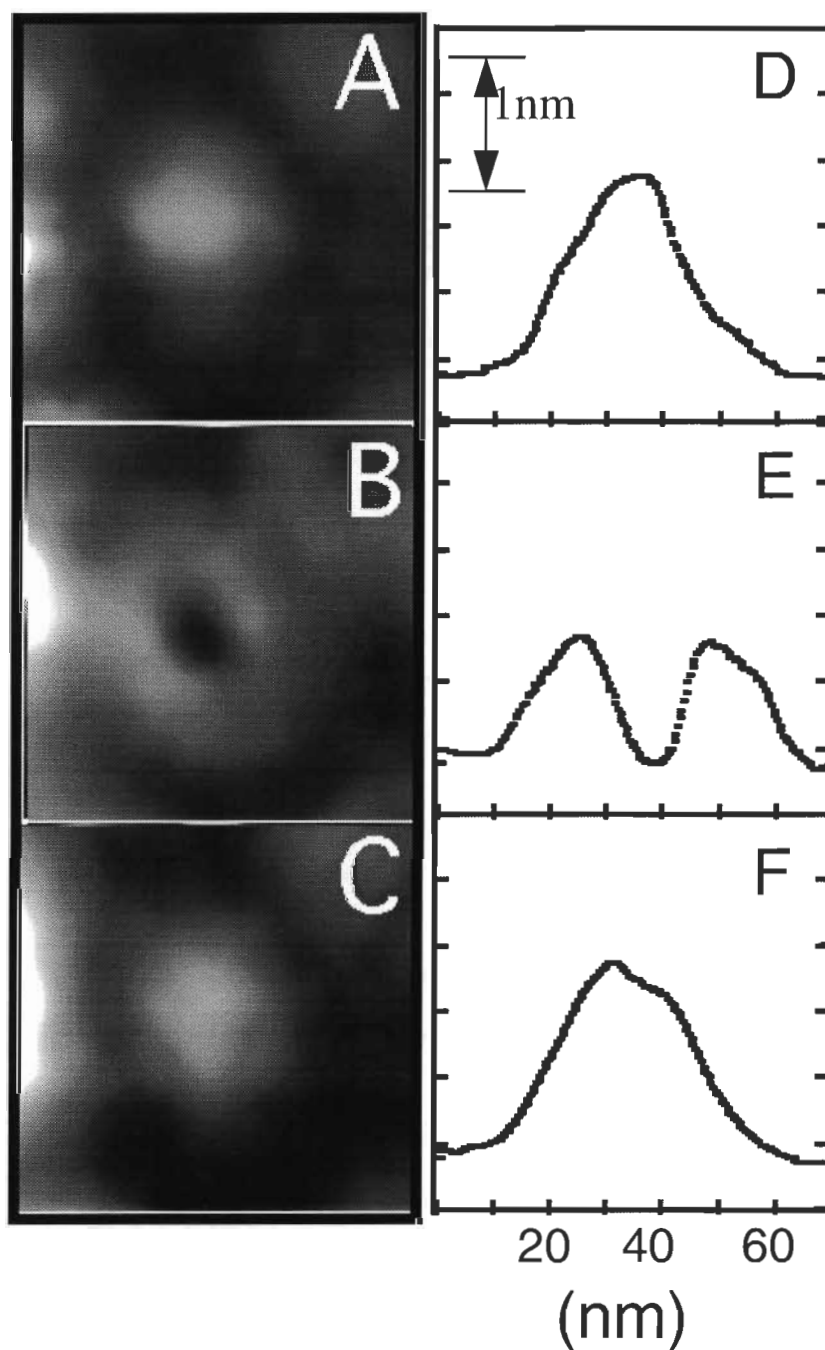
Figure 5.4. AFM tip-induced deformation of a single PS II particle. A-C are images obtained with various tip forces (A and C, the smallest force, 0.3 nN; B, 5 nN) and D-E are the height profile across the center of the particle.

become noisy), the cavity was enlarged to ≈40 nm, wich is even larger than the original particle size, but the original shape still returns immediately after decreasing the force. Using the data, the corresponding energy for binding the four protein domain (Holzenburg et al., 1993) together to form the cavity is estimated to be greater than 104 kcal/mol. Such a large binding energy rules out the possibility that the four domains are held together via the simple van der Waals force or hydrophobic interactions.

We have studied PS II membranes L-B films prepared at different surface pressures of 10, 12.5 and 15 mN/m. The corresponding typical AFM images are shown in Figure 5.5. At 10 mN/m, the particles are shown to be uniformly distributed on the surface. The height difference between bright dots and dark valley in the image is about 2.5 nm. The high magnification image shown in the insert reveals more structures between bright dots. The valley in the high magnification image shows the boundary between PS II particles rather than the surface of the substrate. The AFM image indicates a complete coverage in the monolayer (Figure 5.5A). The coverage of the particles determined from the AFM images is about 1 particle per 1000 nm^2. At 12.5 mN/m, aggregate-like features begin to appear, corresponding to the formation of a second layer on the mica surface (Figure 5.5B). The lighter area in Figure 5.5B is about 10 nm higher than the dark area. The dark area is also covered by the PS II particles rather than mica surface alone, as indicated by the higher magnification image of Figure 5.6 where the closely

packed particle like structures are clearly evident in both layers. Further increasing the deposition surface pressure, the second layer expands and eventually covers the entire surface (Figure 5.5C). Higher resolution images of the second layer clearly resolve individual PS II particles (insets in Figure 5.5 B-C). First glance at the images in Figure 5.5 A and B may give one an impression that the PS II particles are more densely packed in the film deposited at 12.5 mN/m than that at 10 mN/m. However, by carefully counting the particles per unit area, we found that the particle densities at the two surface pressures are about the same. The false impression is due to that the particle height variation in the first layer (10 mN/m) is much greater than that in the second layer (12.5 mN/m). The difference in the particle height variations can be attributed to the fact that the first layer is on the flat and relative rigid mica while the second layer is on the first layer which has many PS II particles protruding out of the surface and is also softer than mica. From the AFM images, the second layer is determined to contribute ≈ 80% and 100% to the total particle coverage in the 12.5 and 15 mN/m films, respectively. This result agrees reasonably well with the fluorescence spectra which show that the fluorescence intensities of the films at 12.5 and 15 mN/m are about 50% and 120% more intense than the film at 10 mN/m.
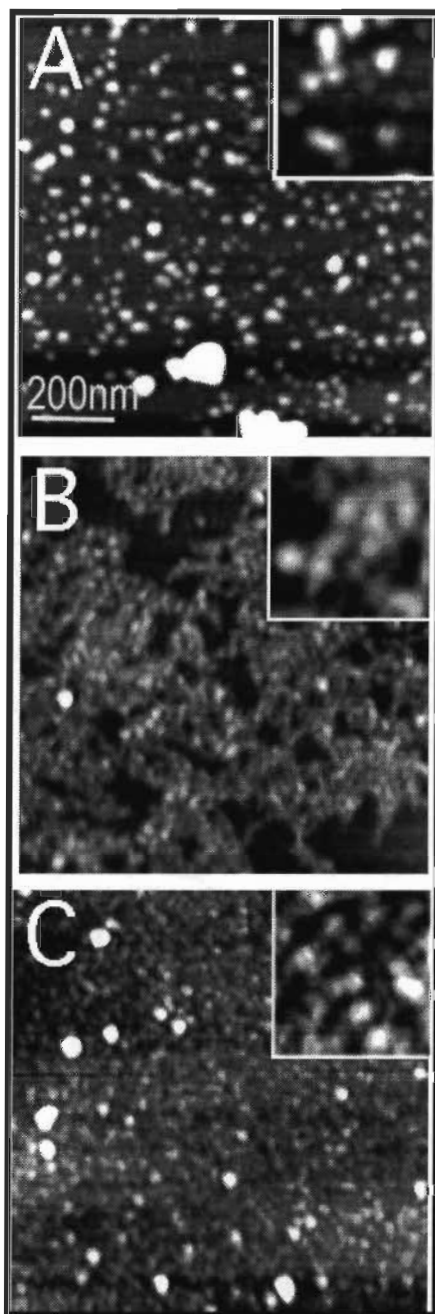
Figure 5.5. AFM images of PS II membrane L-B films deposited at 10 (A), 12.5 (B) and 15 mN/m (C). The inset in each image is a higher magnification image of the corresponding film that shows more clearly the individual PS II particles.
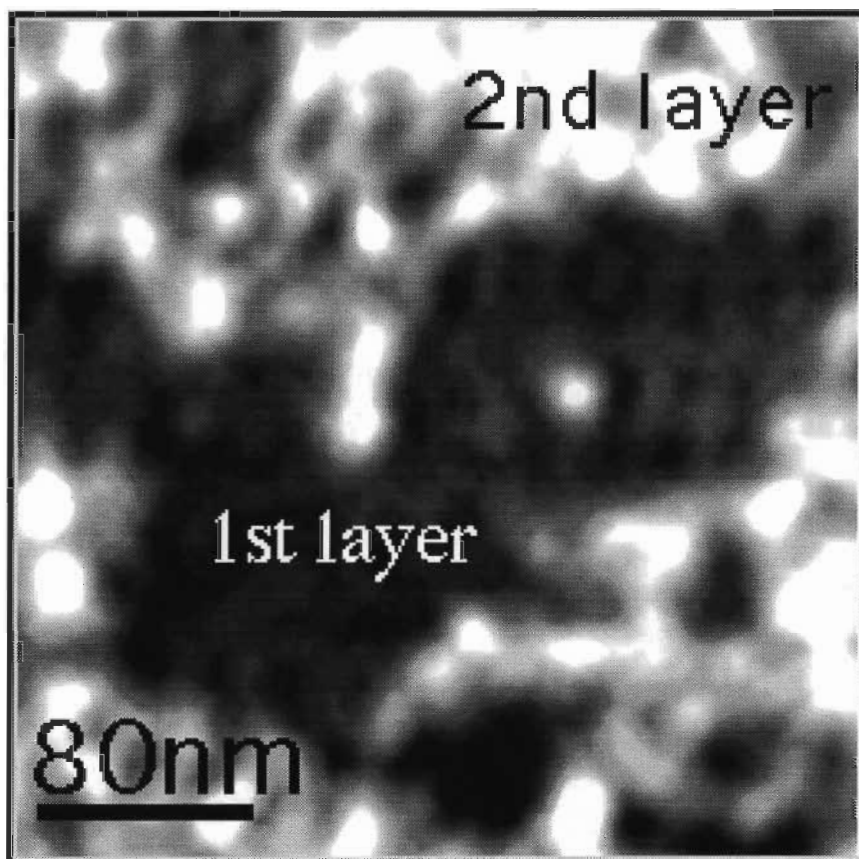
Figure 5.6. AFM image that shows PS II particles in both first and second layers.

We have attributed the formation of second layer and aggregates at higher surface pressures to the collapse of the monolayer film at the air-water interface under these surface pressures and the resulting multilayer films are transferred to the mica surface. Although adsorption of PS II particles from subphase onto mica surface may also results in the formation of aggregates, it is unlikely that adsorption can produce ordered multi-layer structures. Moreover, the fact that the aggregates and multilayer structures occurred only at higher surface pressures suggests that adsorption alone cannot be responsible for these observations because it will occur at any surface pressures.

In summary, we have studied the structural and microelastic properties of PS II membranes prepared with the Langmuir-Blodgett technique by using the tapping mode AFM. The PS II particles are fairly uniformly distributed in the membrane with a density of 10^{-3} particles/nm^2, but they do not pack into an ordered structure in 9 different samples studied and in all the areas surveyed by AFM. The particle coverage in the films prepared at three different surface pressures determined from the AFM images are in good agreement with the fluorescence spectra. In addition to structural studies, we have investigated the microelastic properties of the PS II by utilizing the unique advantage that the AFM tip can apply a local force onto each individual PS II particle. An intramolecular cavity located near the center of each particle is observed when the PS II particles were deposited at different

surface pressures. Under a large AFM tip force, the particle can be compressed in the vertical direction which allows us to determine the elastic constant to be ≈ 5 nN/nm in this direction. The large tip force can also enlarge the intramolecular cavity by penetrating into the cavity which provides information about the binding energy between the four domains that make up each PS II particle. Releasing the tip force, the particle fully recovers its original size and shape even after enlarging the cavity to a diameter twice as large as the original diameter of the entire particle.

CHAPTER VI

CONCLUSION

This work has applied standard protein separation and purification techniques to extract and isolate PS II membranes and PS II core complex protein particles from green plant spinach while maintaining their bioactivity. These isolated particles were tested for their film forming ability using standard Langmuir techniques. Experiments determined that while PS II membrane particles can readily form stable monolayer films at the air-water interface, PS II core complex particles can not form stable monolayer structures at the air-water interface alone without increasing the subphase density. Our data indicated that by adding NaCl into subphase in order to increase its ionic strength and density or by adding MGDG lipid molecules to PS core complex sample can greatly enhance its film forming ability. The conditions for producing monolayers of PS II membranes and PS II core complex protein particles while introducing minimum perturbation to the system have also been determined.

In pursuing the experimental objectives of this thesis, a spectroscopic apparatus was designed and built to measure absorption and fluorescence spectra at the air-water interface. This instrument in combination with

Langmuir-Blodgett surface techniques allowed us to study the spectroscopy of PS II membranes and PS II core complex proteins in a well controlled fashion. Comparison of surface spectroscopy of PS II protein particles with that of solution phase revealed important structural information at different stages of the preparations. Our studies suggested that PS II membranes retain their native protein structure integrity upon spreading onto the interface, while PS II core complex particles may have changed its structure at the interface because of the surface tension. This work also indicates that lipid molecules may play a role in supporting the structural integrity of PS II protein particles in bio-membrane. Our results showed that artificially adding MGDG molecules to PS II core complex particles reduce the spectral shift in surface fluorescence spectra and suggests that MGDG may relief some of structural changes of PS II core complex particles at the air-water interface.

The studies in sample extraction and purification, oxygen evolution test, Langmuir techniques for monolayer film production, and spectroscopic monitoring and probing paved the way for direct observation of PS II complex structures using scanning force microscopy. In this thesis, we demonstrated for the first time the feasibility of using tapping mode atomic force microscopy to probe directly PS II protein complex. We have studied the structural and microelastic properties of PS II particles prepared with the Langmuir-Blodgett technique using the tapping mode AFM. Our results indicated that the PS II particles are fairly uniformly distributed in the membranes with a density of 10^{-3} particles/nm^2, but they do not pack into an ordered structure. The particle

coverage in the films prepared at three different surface pressures determined from the AFM images are in good agreement with the fluorescence spectra. Particle sizes measured directly from AFM images are in agreement with that obtained using electron microscopy. In addition, AFM images revealed an intramolecular cavity located near the center of each particle. By applying a force to AFM tip, we can determine the microelastic force constant that may provide some information about the binding energy between the four domains that make up each PS II particle. These results clearly demonstrated the versatility of AFM technique and advantages of applying this experimental tool into the studies of complex biological systems.

Future prospects

Because of its functional and structural complexities, PS II still offers many technical challenges and excitements for future research. For example, PS II consists of at least 17 functional polypeptide subunits and the functions and structures of many of these subunits remain to be determined. Reduction of complex PS II into smaller subunits offers a powerful scheme for studying function-structure relationship. This motif can certainly be extended beyond the examples studied in this thesis. PS II reaction center, LHC II and extrinsic protein subunits, for example, can be further isolated from rest of PS II core complex and probed using the spectroscopic and scanning force microscopy techniques developed in this work. Langmuir-Blodgett technique is particularly useful in this as it allows researcher to create complicated

biomembrane systems using isolated small subunits in a well controlled fashion. This is not only important in determining structure and function of each individual protein subunits, but also in studying association among various functional units. In combination with tapping mode AFM and other structural monitoring tools, such as cryo-AFM and cryomicroscopy, a complete 3D model of PS II can be constructed, in principle. The methodology and techniques developed in this work can, of course, also be applied to the studies of other complex biological systems, such as all kinds of biological membranes, membrane proteins, cells and organelles.

REFERENCES

Albrecht, O., Gruler, H. and Sackmann, E. (1981) Pressure-composition phase-diagrams of cholesterol-lecithin, cholester-phosphatidic acid, and lecithin-phosphatidic acid mixed monolayers: A Langmuir film balance study. *J. Colloid Interface Sci.*, 79, 319-339.

Albrecht, T. R., Akamine, S.,Carver, T. E. and Quate, C. F. (1990) Microfabrication of cantilever styli for the atomic force microscope. *J. Vac. Sci. Technol.*, A8, 3386-3396.

Alegria, G. and Dutton, P. L. (1991) Langmuir-Blodgett monolayer films of bacteria photosynthetic membranes and isolated reaction centers: Preparation, spectrophotometric and electrochemical characterization. *Biochim. Biophys. Acta*, 1057, 239-257.

Allen, J. P., Feher, G., Yeates, T. O., Rees, D. C. and Deisenhofer, J. (1986) Structural homology of reaction centers from *Rhodopseudomonas sphaeroides* and *Rhodopseudomonas viridis* as

determined by X-ray diffraction. *Proc. Natl. Acad. Sci. USA*, 83, 8589-8593.

Amrein, M. and Marti, O., Editors. (1993). STM and SFM in Biology. Academic Press, London.

Anderson, J. M. (1987) Molecular organization of thylakoid membranes. In New Comprehensive Biochemistry. Vol 15, Photosynthesis (Amesz, J. ed.), pp 273-297, Elsevier, Amsterdam.

Anderson, J. M. and Andersson, B. (1988) The dynamic photosynthetic membrane and regulation of solar energy conversion. *Trends. Biochem. Sci.*, 13, 351-355.

Andersson, B. and Adderson, J. M. (1980) Lateral heterogeneity in the distribution of chlorophyll-protein complexes of the thylakoid membranes of spinach chloroplasts. *Biochim. Biophys. Acta.*, 593, 427-440.

Andersson B. and Akerlund, H-E. (1987) Proteins of the oxygen evolving complex. In Topics in Photosynthesis. Vol 8, The Light Reactions, (Barber, J., Ed.), pp 379-420, Elsevier, Amsterdam.

Andersson, B. and Styring, S. (1991) Photosystem II: Molecular organization, function, and acclimation. In Current Topics in Bioenergetics. Vol. 16, (Lee, C. P., Eds.), pp 1-81, Academic Press, San Diego.

Aoki, K., Ideguchi, T., Kakuno, T. Yamashita, J. and Horio, T. (1986) Intermolecular relations of the photosystem II complex in spinach chloroplasts as detected by immunochemical assay. *J. Biochem.*, 100, 875-882.

Arnon, D. I. (1949) Copper enzymes in isolated chloroplasts. Polyphenoloxidase in *Beta vulgaris. Plant Physiol.*, 24, 1-15.

Babcock, G. T., Barry, B. A., Debus, R. J., Hoganson, C. W., Atamian, M., McIntosh, L., Sithole, I. and Yocum, C. F. (1989) Water oxidation in photosystem. 2. From radical chemistry to multielectron chemistry. *Biochemistry*, 28, 9557-9565.

Barber, J., Chapman, D. J. and Telfer, A. (1987) Characterization of a PS II reaction centre isolated from the chloroplasts of *Pisum sativum. FEBS Lett.*, 220, 67-73.

Barber, J. (1993a) Photosystem II: no longer the black box of photosynthesis. *Biochem. Soc. Trans.*, 22, 313-318.

Barber, J. (1993b) Learning about photosystem II from analogies with purple photosynthetic bacteria. *Biochem. Soc. Trans.*, 21, 981-986.

Bassi, R., Ghiretti-Magaldi, A., Tognon, G., Giacometti, G. M. and Miller, K. (1989) Two-dimensional crystals of the photosystem II reaction center complex from higher plants. *Eur. J. Cell Biol.*, 50, 84-93.

Bennoun P., Spierer-Herz, M., Erickson, J., Girard-Bascow, J., Pierre, Y., Delosme, M. and Rochaix, J. -D. (1986) Characterization of photosystem II mutants of *Chlamydomonas reinhardtii* lacking the *PSAb* gene. *Plant Mol. Biol.*, 6, 151-160.

Berthold, D. A., Babcock, G.T. and Yocum, C. F. (1981). A highly resolved O_2-evolving photosystem II preparation from spinach thylakoid membranes: EPR and electron transport properties. *FEBS Lett.*, 134, 231-234.

Binnig, G., Rohrer, H. (1982) Scanning tunneling microscopy. *Helv. Phys. Acta*, 55, 726-735.

Binnig, G., Quate, C. F.and Gerber, C. (1986) Atomic force microscopy. *Phys. Rev. Lett.*, 56, 930-933.

Birid, K. S. (1989) Lipid and Biopolymer Monolayer at Liquid Interfaces. Plenum Press, New York.

Blodgett, K., and Langmuir, I. (1934) Monomolecular films of fatty acids on glass. *J. Am. Chem. Soc.*, 56, 495-.

Boekema, E. J., Wynn, R. M. and Malkin, R. (1990) The structure of spinach photosystem I studied by electron microscopy. *Biochem. Biophys. Acta*, 1017, 49-56.

Boekema, E. J., B. Hankamer, D. Bald, J. Kruip, J. Nield, A. Boonstra, J. Barber and M. Rögner. (1995). Supramolecular structure of the photosystem II complex from green plants and cyanobacteria. *Proc. Natl. Acad. Sci.* USA. 92,175-179.

Bourdieu, L., Ronsin, O. and Chatenay, D. (1993) Molecular positional order in Langmuir-Blodgett films by atomic force microscopy. *Science*, 259, 798-801.

Bowlby, N. R. and Frasch, W. D. (1986) Isolation of a manganese-containing protein complex from photosystem II preparations of spinach. *Biochemistry*, 25, 1402-1407.

Braun, P., Greenberg, B. M. and Scherz, A. (1990) D1-D2-cytochrome b559 complex from the aquatic plant *Spirodela Oligorrhiza*: correlation between complex integrity, spectroscopic properties, photochemical activity, and pigment composition. *Biochemistry*, 29, 10376-10387.

Bricker, T. M. (1990) The structure and function of CPa-1 and CPa-2 in photosystem II. *Photosynth. Res.*, 24, 1-13.

Burnap, R. L. and Sherman, L. A. (1991) *Biochemistry*, 30, 440-446.

Burns, G. (1985). Solid State Physics, Academic Press, San Francisco, CA.

Bustamante, C., Vesenka, J., Tang, C. L., Rees, W., Guthod, M. and Keller, R. (1992). Circular DNA Molecules Imaged in Air by Scanning Force Microscopy. *Biochemistry*, 31, 22-26.

Butt, H. -J., Downing, K. H. and Hansma, P. K. (1990a) Imaging the Membrane Protein Bacteriorhodopsin with the Atomic Force Microscope. *Biophys. J.*, 58, 1473-1480.

Butt, H. -J., Prater, C. B. and Hansma, P. K. (1991) Imaging purple membranes dry and in water with the atomic force microscope. *J. Vac. Sci. Technol.*, 9B, 1193-1196.

Camm, E. L., Green, B. R., Allred, D. R. and Staehelin, L. A. (1987) Association of the 33 kDa extrinsic polypeptide (water-splitting) with PS II particles: Immunochemical quantification of residual polypeptides after membrane extraction. *Photosynth. Res.*, 13, 69-80.

Chua, N. H., and Gillham, N. W. (1977) Sites of synthesis of principal thylakoid membrane polypeptides in *Chlamydomonas reinhardtii*. *J. Cell Biol.*, 74, 441-452.

Deisenhofer, J., Epp, O., Miki, K., Huber R.and Michel, H. (1984) X-ray structure analysis of a membrane protein complex. *J. Mol. Biol.* 180, 385-398.

Drake, B., Prater, C. B., Weisenhorn, A. L., Gould, S. A. C., Albrecht, T. R., Quate, C. F., Cannell, D, S., Hansma, H. G. and Hansma, P. K. (1989) Imaging crystals, polymers, and processes in water with the atomic force microscope. *Science*, 243, 1586-1589.

Dunahay, T.G., Staehelin, A., Siebert, M., Ogilive, P.D. and Berg, S.P. (1984) Structural, biochemical and biophysical characterization of four oxygen-evolving photosystem II preparations from spinach. *Biochim. Biophys. Acta*, 764, 179-193.

Egger, M., Ohnesorge, F., Weisenhorn, A. L., Heyn, S. P., Drake, B., Prater, C. B., Gould, S. A. C., Hansma, P. K. and Gaub, H. E. (1990) Wet lipid-protein membranes imaged at submolecular resolution by atomic force microscopy. *J. Struct. Biol.*, 103, 89-94.

Enami, I., Miyaoka, T., Mochizuki, Y., Shen, J-R. Satoh, K. and Katoh, S. (1989) Nearest neighbor relationships among constituent proteins of oxygen-evolving potosystem II membranes: Binding and function of the extrinsic 33 kDa protein. *Biochim. Biophys. Acta*, 973, 35-40.

Erickson, J.M. and Rochaix, J-D. (1992) The molecular biology of photosystem II. In: The Photosystems: Structure, Function and Molecular

Biology (Barber, J., Ed.), pp 101-177, Elsevier Science Publishers B.V., New York.

Erokhin, V. and Feigin, L. A. (1991) Deposition and investigation of protein Langmuir-Blodgett films. *Progress in Colloid & Polymer Science*, 85, 47-51.

Evstigneev, V. B., Gavrilova, V. A. and Krasnovskii, A. A. (1950) Effect of oxygen on absorption spectrum and fluorescence of chlorophyll in solutions. *Dokl. Akad. Nauk S.S.S.R.*, 70, 261-.

Facci, P., Erokhin V. and Nicolini C. (1994) Scanning tunneling microscopy of a monolayer of reaction centres. *Thin Solid Films*. 243, 403-406.

Fleming, G. R. and van Grondelle, R. (1994) The primary steps of photosynthesis. *Physics Today*, Feb., 48-55.

Frommer, J. and Meyer, E. (1991) Atomic force microscopy: A tool for surface science. *J. Phys.: Condens. Matter*, 3, S1-S9.

Gabrielli, G., Guarni, G. G. T. and Ferroni, E. (1976) On the mechanism of collapse of arachidic acid films at the water/air interface. *J. Colloid Interface Sci.*, 54, 424-429.

Gaines, G. L. Jr (1966) Insoluble Monolayers at Liquid-gas Interfaces. Wiley Interscience, New York.

Garnaes, J., Schwartz, D. K., Viswanathan, R., Zasadzinski, J. A. N. (1992) Domain boundaries and buckling superstructures in Langmuir-Blodgett films. *Nature*, 357, 54-57.

Ghanotakis, D.F., Demetriou, D.M. and Yocum, C.F. (1987) Isolation and characterization of an oxygen evolving photosystem II reaction center core preparation and a 28 kDa chlorophyll *a*-binding protein. *Biochim. Biophys. Acta*, 891, 15-21.

Goedheer, J. C. (1966) Visible absorption and fluorescence of chlorophyll and its aggreates in solution. In The Chlorophylls. (Vermon, L. P. and Seely, G. R., Eds), pp 147-184, Academic Press, New York.

Goettgens, B. M., Tillmann, R. W., Radmacher, M. and Gaub, H. E. (1992) Molecular order in polymerizable Langmuir-Blodgett films probed by microfluorescence and scanning force microscopy. *Langmuir*, 8, 1768-1774.

Gounaris, K., Barber, J. and Harwood, J. L. (1986) The thylakoid membranes of higher plant chloroplasts. *Biochem. J.*, 237, 313-326.

Gouterman, M. (1961) Spectra of porphyrins. *J. Mol. Spectrosc.*, 6, 138-.

Green, B. R. and Camm, E. L. (1982) The nature of light-harvesting complex as defined by sodium dodecyl sulfate polyacrylamide gel electrophoresis. *Biochim. Biophys. Acta*, 681, 256-262.

Green, B. R. (1988) The chlorophyll-protein complexes of higher plant photosynthetic membranes, or just what green band is that? *Photosynth. Res.*, 15, 3-32.

Greene, B. A., Allred, D. R., Morishige, D. and Staehelin, L. A. (1988) Hierarchical response of light-harvesting chlorophyll proteins in a light-sensitive chlorophyll *b* deficient mutant of maize. *Plant Physiol.*, 87, 357-364.

Green, B. R. and Durnford, D. G. (1996) The chlorophyll-carotenoid proteins of oxygenic photosynthesis. *Annu. Rev. Plant Physoil. Plant Mol. Biol.*, 47, 685-714.

Häberle, W., Hörber, J. K. H. and Binnig, G. (1991) Force microscopy on living cells. *J. Vac. Sci. Technol.*, 9B, 1210-1213.

Haag, E., Irrgang, K. D., Boekema, E. J. and Renger, G. (1990) Functional and structural analysis of Photosystem II core complexes from spinach with high oxygen evolution capacity. *Eur. J. Biochem.* 189, 47-53.

Hann, R. A. (1990) In Langmuir-Blodgett Films. (Roberts, G. G., Ed.), pp. 17-92, Plenum Press, New York.

Hansma, P. K. and Tersoff, J., J. (1987) Scanning tunneling microscopy. *Appl. Phys.*, 61, R1-R23.

Hansma, P. K., Elings, V. B., Marti, O. and Bracker, C. E. (1988) Scanning tunneling microscopy and atomic force microscopy: Application to biology and technology. *Science*, 242, 209-216.

Hansma, H. G., Gould, S. A. C., Hansma, P. K., Gaub, H. E., Longo, M. L. and Zasadzinski, J. A. N. (1991) Imaging nanometer scale defects in Langmuir-Blodgett films with the atomic force microscope. *Langmuir*, 7, 1051-1054.

Hansma, H. G., Sinsheimer, R. L., Li, M.-Q. and Hansma, P. K., (1992a) Atomic Force Microscopy of Single- and Double-stranded DNA. *Nncl. Acids Res.*, 20, 3585-3590.

Hansma, H. G., Vesenka, J., Siegerist, C., Kelderman, G., Morrett, H., Sinsheimer, P. L., Elings, V., Bustamante, C. and Hansma, P. K. (1992b) Reproducible Imaging and Dissection of Plasmid DNA under Liquid with Atomic Force Microscopy. *Science*, 256, 1180-1184.

Hansma, H. G., Bezanilla, H., Zenhausern, F., Adrian, M., and Sinsheimer, R. L., (1993a) Atomic Force Microscopy of DNA in Aqueous Solutions. *Nucl. Acids Res.*, 21, 505-512.

Hansma, H. G., Sinsheimer, R. L., Groppe, J., Bruice, T. C., Elings, V., Gurley, G., Bezanilla, M., Mastrangelo, I. A., Hough, P. V. C. and Hansma, P. K. (1993b) Recent advances in atomic-force microscopy of DNA. *Scanning*, 15, 296-299.

Hansma, P. K., Cleveland, J. P., Radmacher, M., Walters, D. A., Hillner, P. E., Bezanilla, M., Fritz, M., Vie, D., Mansma, H. G., Prater, C. B., Massie, J., Fukunaga, L., Gurley, J., and Elings, V. (1994) Tapping Mode Atomic Force Microscopy in Liquids. *Appl. Phys. Lett.*, 64, 1738-1740.

Hansson, O. and Wydrzynski, T. (1990) Current perceptions of Photosystem II. *Photosynth. Res.*, 23, 131-162.

Henderson, E. (1992) Imaging and Nanodissection of Individual Supercoiled Plasmid by Atomic Force Microscopy. *Nucl. Acids Res.*, 20, 445-447.

Hoh, J. H., Lal, R., John, S. A., Revel, J. -P. and Arnsdorf, M. F. (1991) Atomic Force Microscopy and Dissection of Gap Junctions. *Science*, 253, 1405-1408.

Hoh, J. H., Sosinsky, G. E., Revel, J. -P. and Hansma, P. K. (1993) Structure of the Extracellular Surface of the Gap Junction by Atomic Force Microscopy. *Biophys. J.*, 65, 149-163.

Holzenburg, A., Bewley, M. C., Wilson, F. H., Nicholson, W. V. and Ford, R. C. (1993) Three-dimensional structure of photosystem II. *Nature*, 363, 470-474.

Holzenburg, A., Shephard, F. H. and Ford, R. C. (1994) Localization of the oxygen-evolving complex of photosystem II by Fourier difference analysis. *Micron.* , 25, 447-451.

Holzenburg, A., Flint, T.D., Shephard, F. H., Ford, R. C. (1996) Photosystem II: Mapping the locations of the oxygen evolution-enhancing subunits by electron microscopy. *Micron.*, 27, 121-127.

Ikeuchi, M. and Inoue, Y. (1986) Characterization of O_2-evolution by a wheat photosystem II reaction center complex isolated by a simplified method: Disjunction of secondary acceptor quinone and enhanced Ca^{2+} demand. *Arch. Biochim. Biophys.*, 247, 97-107.

Ikeuchi, M. (1992) Subunit proteins of Photosystem II. *Bot. Mag. Tokyo*, 105, 327-373.

Isoagai, Y. Yamamoto, Y. and Nishimura, M. (1985) Association of the 33-kDa polypeptide with the 43-kDa component in photosystem II particles. *FEBS Lett.*, 187, 240-244.

Ivey, S. and Berg, S. P. (1985) The use of polyclonal antibodies to identify peptides exposed on the stroma side of the spinach thylakoid. *Photosynth. Res.*, 6, 193-199.

Jankowiak, R., Tang, D., Small, G. J., and Seibert, M. (1989) Transient and persistent hole burning of the reaction center of PS II. *J. Phys. Chem.*, 93, 1649-1654.

Jankowiak, R. and Small, G. J. (1993) Spectral hole burning: A window on excited state electronic structure, heterogeneity, electron-phonon coupling, and transport dynamics of photosynthetic units. In The Photosynthetic Reaction Center, Vol II, (Deisenhofer, J and Norris, J. R. Eds.), pp 133-178. Academic Press, New York.

Jansson, S. (1994) The light-harvesting chlorophyll a/b-binding proteins. *Biochim. Biophys. Acta*, 1184, 1-19.

Kobayashi, M., Maeda, H., Watanabe, T., Nakane, H. and Satoh, K. (1990) Chlorophyll-α- and β-carotene content in the D1/D2/cytochrome b559 reaction center complex from spinach. *FEBS Lett.*, 260, 138-140.

Kühlbrandt, W., Wang, D. N. and Fujiyoshi, Y. (1994) Atomic model of plant light-harvesting complex by electron crystallography. *Nature*, 367, 614-621.

Laemmli, U. K. (1970) Cleavage of the structural proteins during the assembly of the head of bacteriophage T4. *Nature*, 227, 680-685.

Langmuir, I. (1917) Constitution and fundamental properties of solids and liquids. II. Liquid. *J. Am. Chem. Soc.*, 39, 1848-1906.

Lavorel, J. (1957) Effect of energy migration on fluorescence in dye solutions. *J. Phys. Chem.*, 61, 864-869.

Lea, A. S., Pungor, A., Hlady, V., Andrade, J. D., Herron, J. N. and Voss, E. W. Jr. (1992) Manipulation of proteins on mica by atomic force microscopy. *Langmuir*, 8, 68-73.

Lin, J. N., Drake, B., Lea, A. S., Hansma, P. K. and Andrade, J. D. (1990) Direct observation of immunoglobulin adsorption dynamics using the atomic force microscope. *Langmuir*, 6, 509-511.

Livingston, R., Watson, W. F. and McArdle, J. (1949) Activation of the fluorescence of chlorophyll solutions. *J. Am. Chem. Soc.*, 71, 1542-.

Ljungberg, U., Akerlund, H-E., Larsson, C. and Andersson, B. (1984) Identification of polypeptides associated with the 23 kDa and 33 kDa proteins of photosynthetic oxygen evolution. *Biochim. Biophys. Acta*, 767, 145-152.

Lowry, O. H. et al., (1951) *J. Biol. Chem.*, 193, 265-.

Lvov, Yu., Erokhin, V. and Zaitsev, S. (1991) Protein Langmuir-Blodgett films. *Biol. Membr.*, 4, 1477-1513.

Lyon, M. K., Marr, K. M. and Furcinitti, P. S. (1993) Formation and characterization of two-dimensional crystals of photosystem II. *J. Struct. Biol.*, 110, 133-140.

Lyubchenko, Y. L., Jacobs, B. L. and Lindsay, S. M. (1992) Atomic Force Microscopy of *Reovirus* dsRNA: a Routine Technique for Length Measurements. *Nucl. Acids Res.*, 20, 3983-3986.

Lyubchenko, Y. L., Oden, P. I., Lampner, D., Lindsay, S. M., and Dunker, K. A. (1993) Atomic Force Microscopy of DNA and Bacteriophage in Air, Water and Propanol: the Role of Adhesion Forces. *Nucl. Acids Res.*, 21, 1117-1123.

Machold, O. (1986) Relationship between the 43 kDa chlorophyll-protein of PS II and the rapidly metabolized 32 kDa Q_B protein. *FEBS Lett.*, 204, 363-367.

Maivald, P., Butt H. J., Gould S. A. C., Prater C. B., Drake B., Gurley J. A., Elings V. B. and Hansma P. K. (1991) Using force-modulation to image surface elasticities in the atomic force microscope. *Nanotechnology*, 2, 103-106.

Marr, K. M., Mastronarde, D. N. and Lyon, M. K. (1996) Two-dimensional crystals of photosystem II: Biochemical characterization, cryoelectron microscopy and localization of the D1 and cytochrome b599 polypeptides. *J. Cell Biol.*, 132, 823-833.

Masojidek, J., Droppa, M. and Horvath, G. (1987) Analysis of the polypeptide composition of grana and stroma thylakoids by two-dimensional gel electrophoresis. *Eur. J. Biochem.*, 169, 283-288.

Mazonski, T., Gasztych, D. and Zielinski, W. (1963) Hydroxylation of allyl alcohol to glycerol by using hydrogen peroxide in the prescence of phosphotungstic acid. *Zeszyty. Nauk. Politech. Slask. Chem.*, 13, 63-.

Meyer, E. and Amer, N. M. (1988) Novel optical approach to atomic force microscopy. *Appl. Phys. Lett.*, 53, 1045-1047.

Meyer, E., Howald, L., Overney, R. M., Einzelmann, H.; Frommer, J., Üntherodt, H. -J., Wegner, T., Schier, H. and Roth, S. (1991) Molecular-resolution images of Langmuir-Blodgett films using atomic force microscopy. *Nature*, 349, 398-400.

Meyer, E., Overney, R. M., Brodbeck, D., Howald, L., Lüthi, R., Frommer, J. and Güntherodt, H. -J. (1992) Friction and wear of Langmuir-Blodgett films observed by friction force microscopy. *Phys. Rev. Lett.*, 69, 1777-1780.

Michel, H. (1982) Three-dimensional crystals of a membrane protein complex. *J. Mol. Biol.*, 158, 567-572.

Michel, H. and Deisenhofer, J. (1988) Relevance of the photosynthetic reaction center from purple bacteria to the structure of photosystem II. *Biochemistry*, 27, 1-7.

Millner, P. A., Gogel, G. and Barber, J. (1987) Investigation of the spatial relationships between photosystem II polypeptides by reversible crosslinking and diagonal electrophoresis. *Photosyn. Res.*, 13, 185-198.

Mou, J., Yang, J. and Shao, Z., (1994a) Tris(hydroxymethyl)aminomethane ($C_4H_{11}NO_3$) Induced Ripple Phase in Supported Unilamellar Phospholipid Bilayers. *Biochemistry*, 33, 4439-4443.

Mou, J., Yang, J., Huang, C. and Shao, Z. (1994b) Alcohol Induces Interdigitated Gel Phase in Phosphatidylcholine Bilayers. *Biochemistry*, 33, 9981-9985.

Murata, N., Miyao, M., Omata, T., Matsunami, H. and Kuwabara, T. (1984) Stoichiometry of components in the photosynthetic oxygen evolution system of photosystem II particles prepared with triton X-100 from spinach chloroplasts. *Biochim. Biophys. Acta.*, 765, 363-369.

Murphy, D. J. (1986) The molecular organization of the photosynthetic membranes of higher plants. *Biochim. Biophys. Acta*, 864, 33-94.

Nakatani, H. Y., Ke, B., Dolan, E. and Arntzen, C. J. (1984) Identity of the photosystem II reaction center polypeptide. *Biochim. Biophys. Acta*, 765, 347-352.

Nakazato, K., Toyoshima C., Enami I. and Inoue Y. (1996) Two-dimensional crystallization and cryo-electron microscopy of photosystem II. *J. Mol. Biol.*, 257, 225-232.

Nanba, O. and Satoh, K. (1987) Isolation of a photosystem II reaction center consisting of D1 and D2 polypeptides and cytochrome b559. *Proc. Natl. Acad. Sci. USA*, 84, 109-112.

Oakley, B. R., Kirsch, D. R., and Morris, N. R. (1980) A simplified ultrasensitive silver stain for detecting proteins in polyacrylamide gels. *Anal. Biochem.*, 105, 361-363.

Ohnishi, S., Hara, M., Furuno, T. and Sasabe, H., (1992) Imaging the Ordered Array of Water-soluble Protein Ferritin with the Atomic Force Microscope. *Biophys. J.*, 63, 1425-1431.

Overney, R. M., Meyer, E., Frommer, J., Brodbeck, D., Lüthi, R., Howald, L., Güntherodt, H. -J., Fujihira, M., Takano, H. and Gotoh, Y. (1992) Friction measurements on phase separated thin films with a modified atomic force microscope. *Nature*, 359, 133-135.

Paulsen, H. (1995) Chlorophyll a/b-binding proteins. *Photochem. Photobiol.*, 62, 367-382.

Peter, G. F. and Thornber, J. P. (1991) Biochemical evidence that the higher plant photosystem II core complex is organized as a dimer. *Plant Cell Physiol.*, 32, 1237-1250.

Pearlstein, R. M. (1987) Structure and exciton effects in photosynthesis. In New Comprehensive Biochemistry. Vol 15, Photosynthesis. (Amesz, J., Ed.), pp 299-317. Elsevier, Amsterdam.

Rees, W. A., Keller, R. W., Vesenka, J. P., Yang, G. and Bustamante, C. (1993) Evidence of DNA Bending in Transcription Complexes Imaged by Scanning Force Microscopy. *Science*, 260, 1646-1649.

Renger, G. (1992) In The Photosystems: Structure, Function and Molecular Biology. (Barber, J., Ed.) pp 45-99. Elsevier, Amsterdam.

Roger, M., Dekker, J. P., Boekema, E. J. and Witt, H. T. (1987) Size, shape and mass of the oxygen-evolving photosystem II complex from the thermophilic cyanobacterium *Synechococcus sp.*. *FEBS Lett.*, 219, 207-211.

Rutherford, A. W. (1989) Photosystem II. The water-splitting enzyme. *Trends Biochem. Sci.*, 14, 227-232.

Santini, C., Tidu V., Tognon G., Magaldi A. G. and Bassi R. (1994) Three-dimensional structure of the higher-plant photosystem II reaction centre and evidence for its dimeric organization *in vivo*. *Eur. J. Biochem.*, 227, 307-315.

Sarid, D. (1991) Scanning Force Microscopy. Oxford University Press, New York.

Seibert, M. (1995) Reflections on the nature and function of the photosystem II reaction centre. *Aust. J. Plant Physiol.*, 22, 161-166.

Shao, L., Tao, N-J. and Leblanc, R. M. (1997) Probing the microelastic properties of nanobiological particles with tapping mode atomic force microscopy. *Chem. Phys. Lett.*, 273, 37-41.

Shinozaki, K, Hayashida, N. and Sugiura, M. (1989) *Nicotinana* chloroplast genes for components of the photosynthetic apparatus. *Photosynth. Res.*, 18, 7-31.

Simpson, D. J. and Wettstein, D. V. (1989) The structure and function of the thylakoid membrane. *Carlsberg Res. Commun.* , 54, 55-65.

Singh, S. and Keller, D. J., (1990) Atomic Force Microscopy of Supported Planar Membrane Bilayers. *Biophys. J.*, 60, 1401-1410.

Skoog, D. A., West, D. M. and Holler, F. J. (1988) In Fundamentals of Analytical Chemistry. pp 457-553. Saunder College Publishing, New York.

Smith, P. K., Krohn R. I., Hermanson G. T., Mallia, A. K., Gartner, F. H., Provenzano M. D., Fujimoto E. K., Goeke N. M., Olson B. J. and Klenk, D. C. (1985) Measurement of protein using bicinchoninic acid. *Anal. Biochem.*, 150, 76-85.

Sonnenfeld, R. and Hansma, P. K. (1986) Atomic-resolution microscopy in water. *Science*, 232, 211-213.

Staehelin, L.A. (1986) Chloroplast structure and supramolecular organization of photosynthetic membranes. In Encyclopaedia of Plant Physiology, New series, vol. 19, Photosynthesis III. (Staehelin, L.A. and Arntzen, C.J., Eds.), pp 1-84. Springer Verlag, New York.

Svensson, B., Vass, I., Cedergren, E. and Styring, S. (1990) *EMBO J.*, 9, 2051-2059.

Tao, N. J., Lindsay S. M. and Lees S. (1992) Measuring the microelastic properties of biological materials. *Biophys. J.*, 63, 1165-1169.

Thornber, J.P. (1986) Biochemical characterization and structure of pigment-proteins of photosynthetic organism. In Encyclopaedia of plant Physiology. New Series, vol. 19, (Staehelin, L.A. and Arntzen, C.J., Eds.), pp 98-115. Springer Verlag, New York.

Thornber, J.P., Peter. G.F., Chitris, P.R., Nechushtai, R. and Vainstein, A. (1988) The light-harvesting complex of photosystem II of higher plants. In Light Transduction in Photosynthesis: Higher Plant and Bacterial Models. (Stevens, Jr. S.E. and Bryant, D.A., Eds.), The American Society of Plant Physiologists.

Tiede, D. M. (1985) Incorporation of membrane proteins into interfacial films: model membranes for electrical and structural characterization. *Biochim. Biophys. Acta.*, 811, 357-379.

Tikhonov, N. V., and Mustafin, I. S. (1965) *Zh. Anal. Khim.*, 20, 390-.

Trurnit, H. J. (1960) The spreading of protein monolayers. *J. Colloid Interface Sci.*, 15, 1-13.

Tsiotis, G., Walz, T., Spyridaki, A., Lustig, A., Engel, A. and Ghanotakis, D. (1996) Tubular crystals of a photosystem II core complex. *J. Mol. Biol.*, 259, 241-248.

Ulman, A. (1990) in Ultrathin Organic Films, Academic Press, New York.

van Grondelle, R. (1985) Excitation energy transfer, trapping and annihilation in photosynthetic systems. *Biochim. Biophys. Acta*, 811, 147-195.

van Kan, P. J. M., Otte, S. C. M., Kleinherenbrink, F. A. M., Nieveen, M., C., Aartsma, T. J. and van Gorkom, H. J. (1990) Time-resolved spectroscopy at 10 K of the Photosystem II reaction center: Deconvolution of the red absorption band. *Biochim. Biophys. Acta*, 1020, 146-152.

van Leeuwen, P. J., Nieveen, M. C., van de Meent, E. J., Dekker, J. P. and van Gorkom, H. J. (1991) Rapid and simple isolation of pure Photosystem II core and reaction center particles from spinach. *Photosynth. Res.*, 28, 149-153.

Veeranjaneyulu, K. and Leblanc, R. M. (1994) Action spectra of photosystems I and II in state 1 and state 2 in intact sugar maple leaves. *Plant Physiol.*, 104, 1209-1214.

Vermaas, W. (1993) Molecular-biological appreaches to analyze photosystem II structure and function. *Annu. Rev. Plant Physiol. Plant Mol. Biol.*, 44, 457-481.

Vesenka, J., Guthold, M., Tang, C. L., Keller, D., Delaine, E. and Bustamante, C. (1992) Substrate Preparation for Reliable Imaging of DNA Molecules with the Scanning Force Microscope. *Ultramicroscopy*, 42, 1243-1249.

Virgin, I., Styring, S. and Andersson, B. (1988) Photosystem II Disorganization and Manganese Release after Photoinhibition of Isolated Spinach Thylakoid Membranes. *FEBS Lett.*, 233, 408-412.

Viswanathan, R., Schwartz, D. K., Garnaes, J. and Zasadzinski, J. A. N. (1992) Atomic force microscopy imaging of substrate and pH effects on Langmuir-Blodgett monolayers. *Langmuir*, 8, 1603-1067.

Volker, M. , Ono, T. , Inoue, Y. and Renger, G. (1985) Effect of trypsin on PS II particles: Correlation between Hill activity, Mn abundance and peptide pattern. *Biochim. Biophys. Acta*, 806, 25-34.

Weisenhorn, A. L., Gaub, H. E., Hansma, H. G., Sinsheimer, R. L., Kelderman, G. L. and Hansma, P. K. (1990) Imaging single-stranded DNA, antigen-antibody reaction and polymerized Langmuir-Blodgett films with an atomic force microscope. *Scanning Microsc.*, 4, 511-516.

Weisenhorn, A. L., Egger, M., Ohnesorge, F., Gould, S. A. C., Heyn, S. -P., Hansma, H. G., Sinsheimer, R. L., Gaub, H. E. and Hansma, P. K. (1991) Molecular-resolution images of Langmuir-Blodgett films and DNA by atomic force microscopy. *Langmuir*, 7, 8-12.

Weisenhorn, A. L., Schmitt, F. -J., Knoll, W. and Hansma, P. K. (1992) Streptavidin binding observed with an atomic force microscope. *Ultramicroscopy*, 42-44, 1125-1132.

Wickramasinghe, H. K. (1989) Scanned-probe microscopes. *Sci. Am.*, 260, 98-105.

Williams, W. P. and Allen, J. F. (1987) State 1/state 2 changes in higher plants. *Photosynth. Res.*, 13, 19-45.

Worcester, D. L., Miller, R. G. and Bryant, P. J., (1988) Atomic Force Microscopy of Purple Membranes. *J. Microsc.*, 152, 817-821.

Yamada, H., Hirata Y., Hara M. and Miyake J. (1994) Atomic force microscopy studies of photosynthetic protein membrane Langmuir-Blodgett films. *Thin Solid Films*. 243, 455-458.

Yang, J., Takeyasu, K. and Shao, Z., (1992) Atomic Force Microscopy of DNA molecules. *FEBS Lett.*, 301, 173-176.

Yang, J., Tamm, L. K., Somlyo, A. P. and Shao, Z. (1993a) Promises and Problems of Biological Atomic Force Microscopy. *J. Microsc.*, 171, 183-198.

Yang, J., Tamm, L. K., Tillack, T. W., and Shao, Z. (1993b) New Approach for Atomic Force Microscopy of Membrane Proteins: The Imaging of Cholera Toxin. *J. Molec. Biol.*, 229, 286-290.

Yang, J., Mou, J. and Shao, Z. (1994a) Molecular Resolution Atomic Force Microscopy of Soluble Proteins in Solution. *Biochim. Biophys. Acta*, 1199, 105-114.

Yang, J., Mou, J., and Shao, Z. (1994b) Structure and Stability of Pertussis Toxin Studies by in site Atomic Force Microscopy. *FEBS Lett.*, 338, 89-92.

Yang, J. and Shao, Z. (1995) Recent advances in biological atomic force microscopy. *Micron*, 26, 35-49.

Yasuda, Y., Hirata, Y., Sugino, H., Kumei, M., Hara, M., Miyake, J. and Fujihira, M. (1992) Langmuir-Blodgett films of reaction centers of *Rhodopseudomonas viridis*: photoelectric characteristics. *Thin Solid Films*, 210/211, 733-735.

Zaitsev, S. Y., Kalabina, N. A., Zubov, V. P., Lukashev, E. P., Kononenko, A. A. and Uphaus, R. A. (1992) Monolayers of photosynthetic reaction centers of green and purple bacteria. *Thin Solid Films*, 210/211, 723-725.

Zasadzinski, J. A. N. and Hansma, P. K. (1990) Scanning tunneling microscopy and atomic force microscopy of biological surfaces. *Annal. New York Acad. Sci.*, 589, 476-491.

Zasadzinski, J. A. N., Helm, C. A., Longo, M. L., Weisenhorn, A. L., Gould, S. A. C. and Hansma, P. K. (1991) Atomic Force Microscopy of Hydrated Phosphatidylethanolamine. *Biophys. J.*, 59, 755-760.

Zenhausern, F., Adriah, M., Heggeler-Bordier, B. T., Emch, R., Jobin, M., Taborelli, M. and Descouts, P. (1992) Imaging of DNA by Scanning Force Microscopy. *J. Struct. Biol.*, 108, 69-73.

Zenhausern, F., Adrian, M., Bordier, B. T. H., Eng, L. M. and Descouts, P. (1992) DNA and RNA polymerase/DNA complex imaged by scanning force microscopy: Influence of molecular-scale friction. *Scanning*, 14, 212-217.

Zhong, Q., Inniss, D., Kjoller K. and Elings, V. B. (1993) Fractured polymer/silica fiber surface studied by tipping mode atomic force microscopy. *Surf. Sci. Lett.*, 290, L688-L692.

Zinth, W. and Kaiser, W. (1993) Time-resolved spectroscopy of the primary electron transfer in reaction centers of *Rhodobacter sphaeroides* and *Rhodopseudomonas viridis*. In The Photosynthetic Reaction Center. Vol II,

(Deisenhofer, J. and Norris, J. R., Eds.), pp 71-104. Academic Press, New York.

APPENDIX

SURFACE SPECTROSCOPY INSTRUMENTATION

To measure the absorption and fluorescence spectra directly from the monolayer at the air-water interface, we built a measuring station by integrating and modifying several commercial instruments. Several factors were taken into the consideration while designing the measuring station: 1. We must make the maximum utilization of our existing instruments with minimum modification. 2. The station can be quickly disassembled and reassembled reliably with reproducible results. These will ensure that instruments can be used either together as a whole unit or standing alone individually.

Figure A.1 schematically shows the basic concept of the measuring station. The central part of the station is a commercial KSV spectral mini-trough (KSV Instruments Ltd., Helsinki, Finland) which is used to prepare Langmuir monolayers at the air-water interface. Fluorescence measurements were taken using a Spex Fluorolog-2 double monochromator fluorometer (Instruments, S. A., Inc., Edison, NJ, USA) with a home built probe holder and an attachment arm. A modified HP 8452A diode array spectrophotometer (Hewlett-Packard, USA) is used to measure optical absorption. I will discuss the detailed modification of these commercial

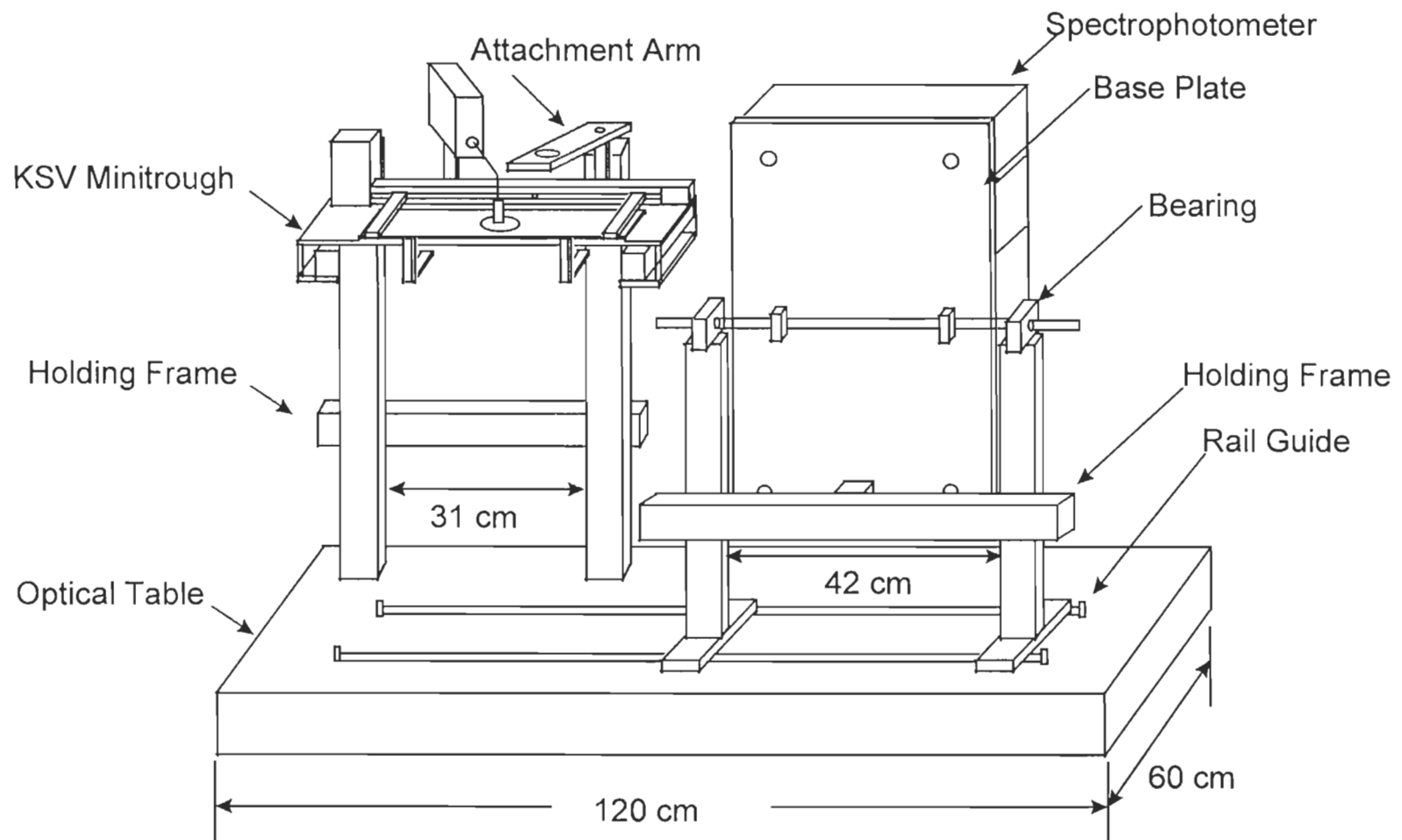instruments and the construction of measuring station in the following sections.

Figure A.1 The schematic drawing of surface spectroscopy measurement station.

Construction of Spectroscopic Measuring Station

As shown in Figure A.1, the measuring station is based on top of a 0.6 × 1.2 m optical breadboard (No. 54-2043, Ealing Electro-optics, Inc., Holliston, MA, USA). Two holding frames are constructed using the 45 mm^2 aluminum Profile Beams and associated angle brackets and couplings (Ealing Electro-optics, Inc., Holliston, MA, USA). The first frame is about 31 cm wide and is directly attached to the optical breadboard. There are two horizontal arms attached to the frame through angle brackets. The minitrough rests on the horizontal arms of the frame and the relative height of the minitrough can be adjusted by changing the position of two horizontal arms. The second frame is about 42 cm wide and is sitting on the top of a set of precision rail guides (Thomas Industries, Inc., Port Washington, NY, USA) that were permanently attached to the optical table. A Hewlett-Packard spectrophotometer is attached to the frame through a base plate and a set of bearings and turning axis assemblies. This arrangement allows us to rotate the spectrometer 90 degree to the vertical position and slide it in and out so that the optical path of the spectrometer intersects the measuring window on the minitrough. Figure A.2 provides the side view of the measuring station. To prevent accidental derail, we built a set of stoppers which can be attached to the ends of rail. As indicated in the mechanical drawing of Figure A.3, the stopper is basically a 0.4 inch thick aluminum ring with inner radius of 0.38 inch and outer radius of 0.68 inch. The ring has a 0.4 inch opening to accommodate the base of the rail guide. The stopper is also drilled
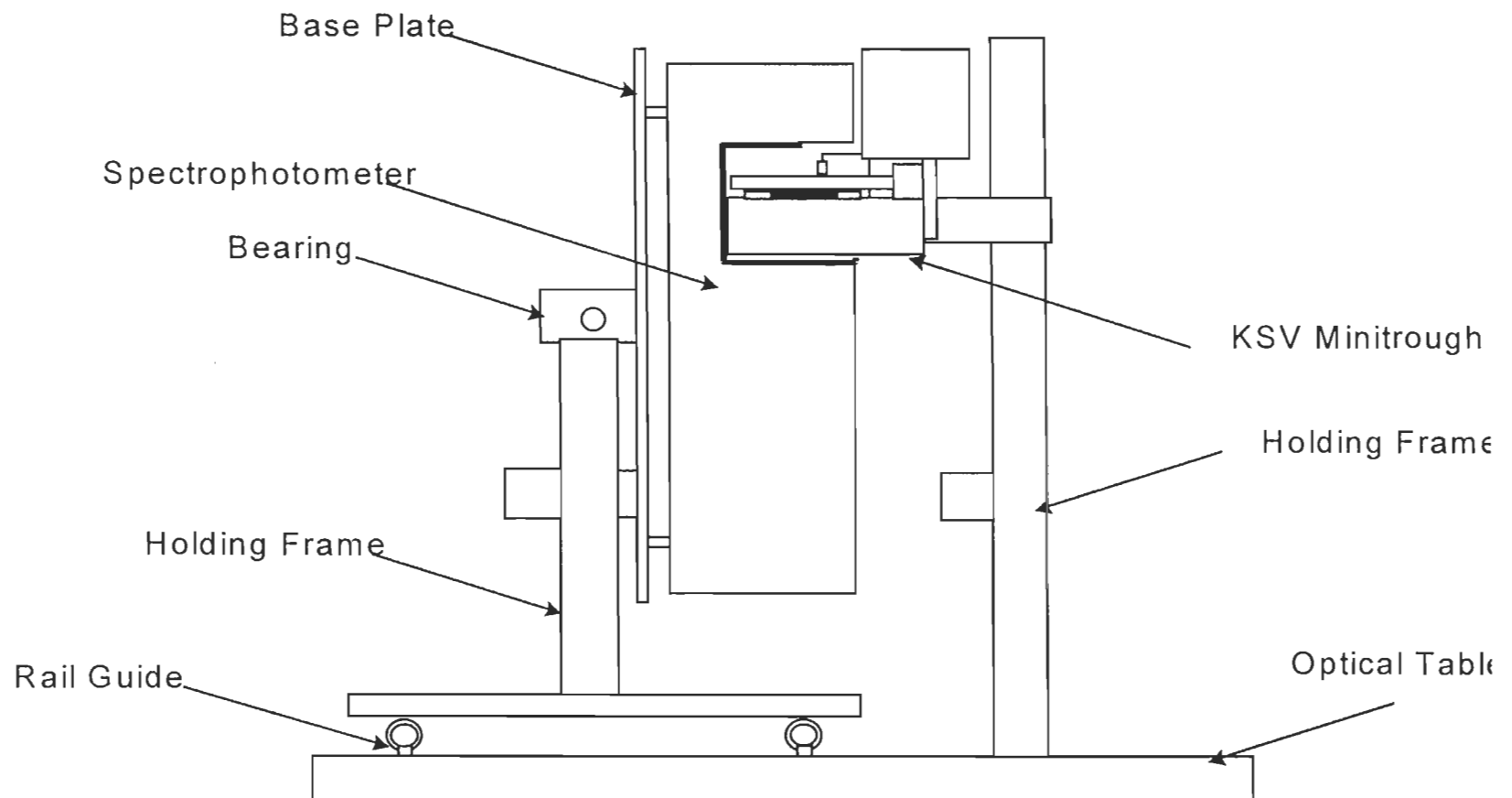
Base Plate

Spectrophotometer

Bearing

KSV Minitrough

Holding Frame

Holding Frame

Rail Guide

Optical Table

Figure A.2 The side view of the spectroscopic measuring station.

Set screw (6-32)

0.38"
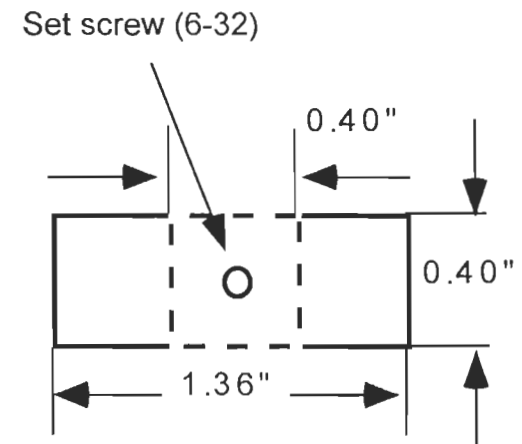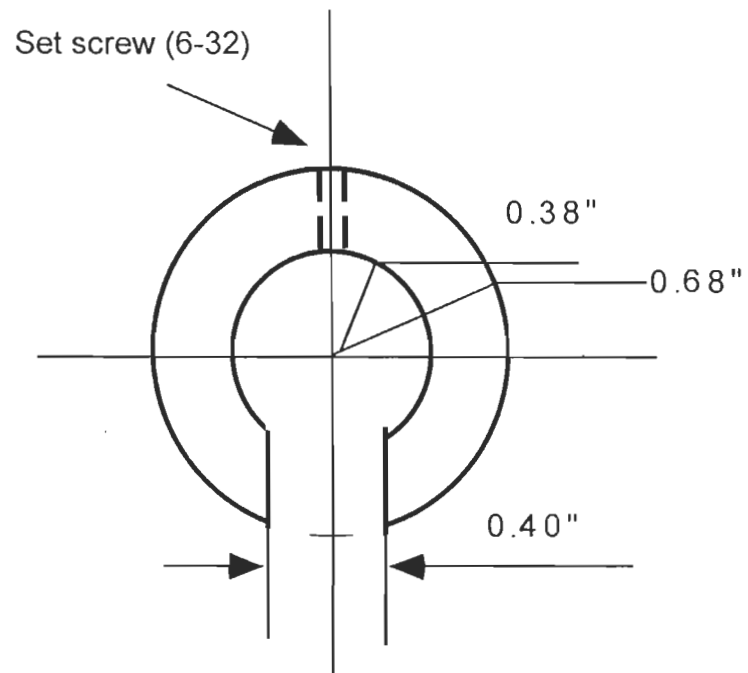
0.68"

0.40"

Set screw (6-32)

0.40"

0.40"

1.36"

Figure A.3 The mechanical diagram of rail stopper.

and tapped for 6-32 set screws. The set screw locks stopper to the rail guide.

Fluorescence measurement

We measure the surface fluorescence spectra using a spectrofluorometer from Spex. The spectrofluorometer is equipped with an optical fiber probe that can simultaneously deliver excitation light and collect the fluorescence. To introduce the fiber probe onto the air-water interface, we build a special holder assembly which allow us to precisely adjust the distance between the fiber probe and the surface.

Figure A.4 schematically shows the KSV mini-spectral trough with the holder attached. The fiber holder is attached to the back of the trough through an attachment arm. As shown in the mechanical drawing of Figure A.5, the attachment arm is made from a piece of half inch thick stainless steel plate (4.35 × 1.25 inch). At one end of the plate a 0.155 inch wide slot is opened to allow the attachment arm to be bolted down to the holding rod on the KSV minitrough. At another end of the attachment arm, a 3/4 inch tapped hole (3/4 - 32 UNC) is made to accommodate the fiber probe holder. A 6 - 32 Nylon set screw can further secure the fiber holder to the attachment arm. The attachment arm is bolted above the mini-trough at a fixed distance.

Figure A.6 shows the mechanical drawing of the fiber probe holder. The probe holder is made from a solid one inch stainless steel rod. The total length of the holder is 4.53 inch long. As indicated in the drawing of Figure 3.6, the holder is center bored for most of the length (0.501 inch diameter). An opening of 0.378 inch diameter at one end of the holder allows the tip of
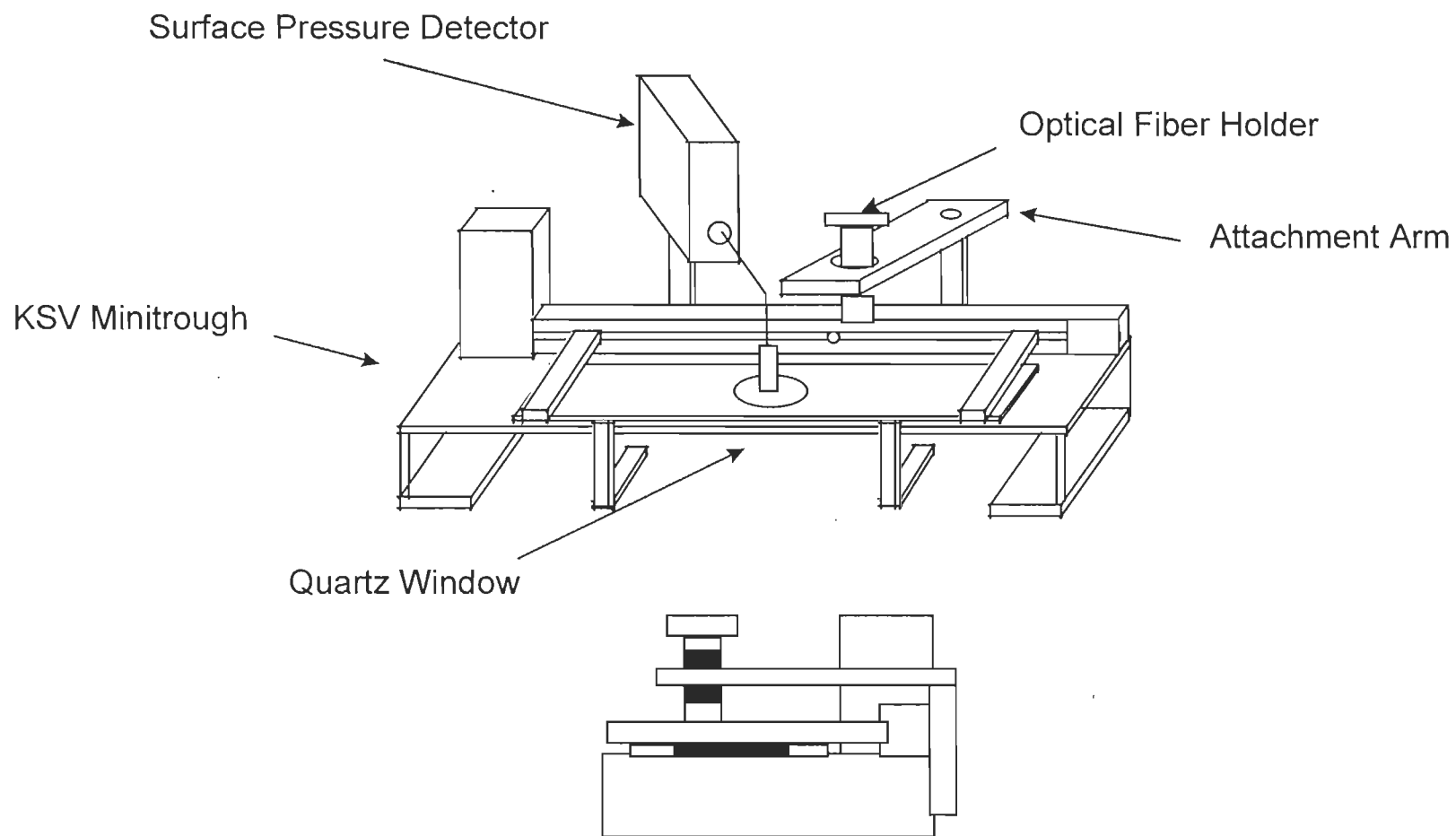
Figure A.4 The schematic drawing of the KSV mini-spectral trough with the holder attached.
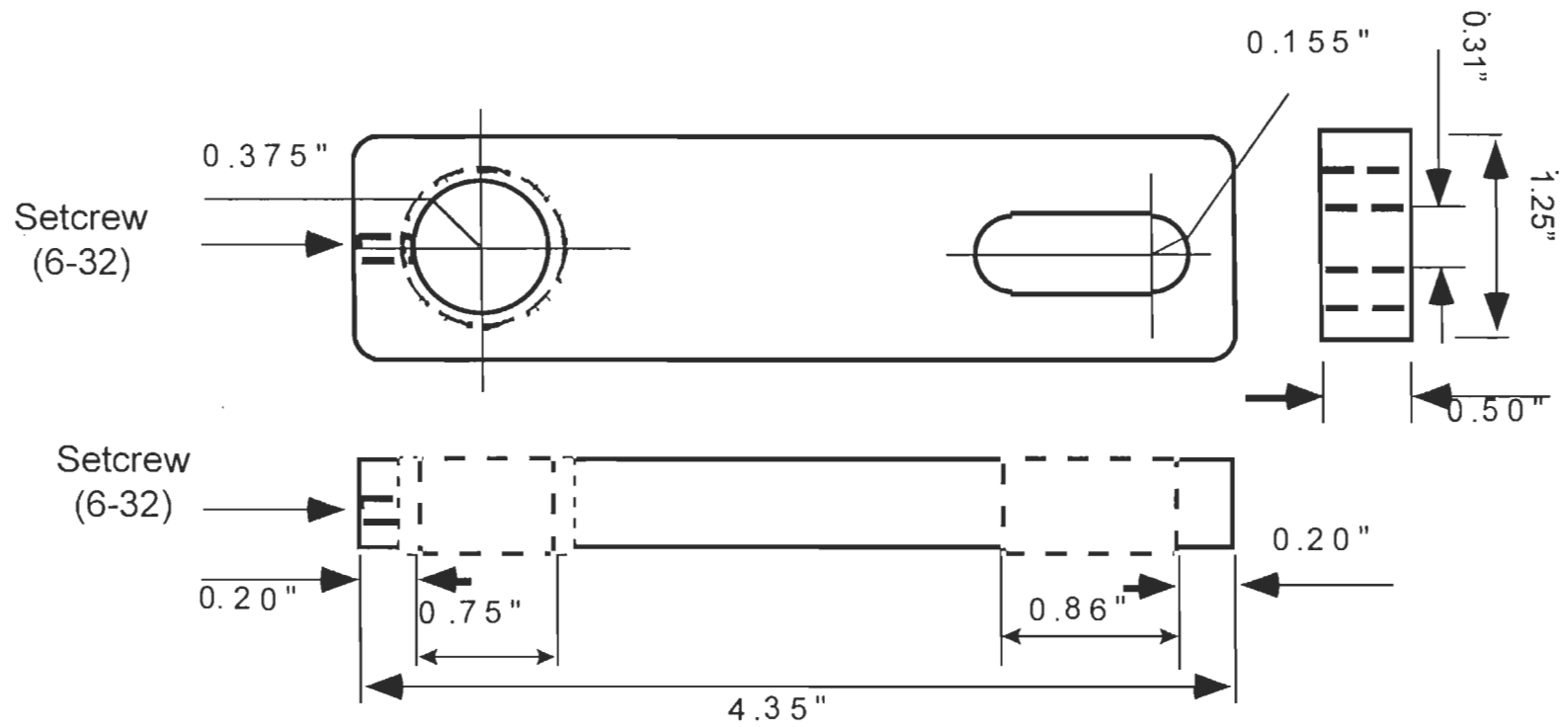
Figure A.5 The mechanical drawing of the optical fiber probe holder attachment arm.
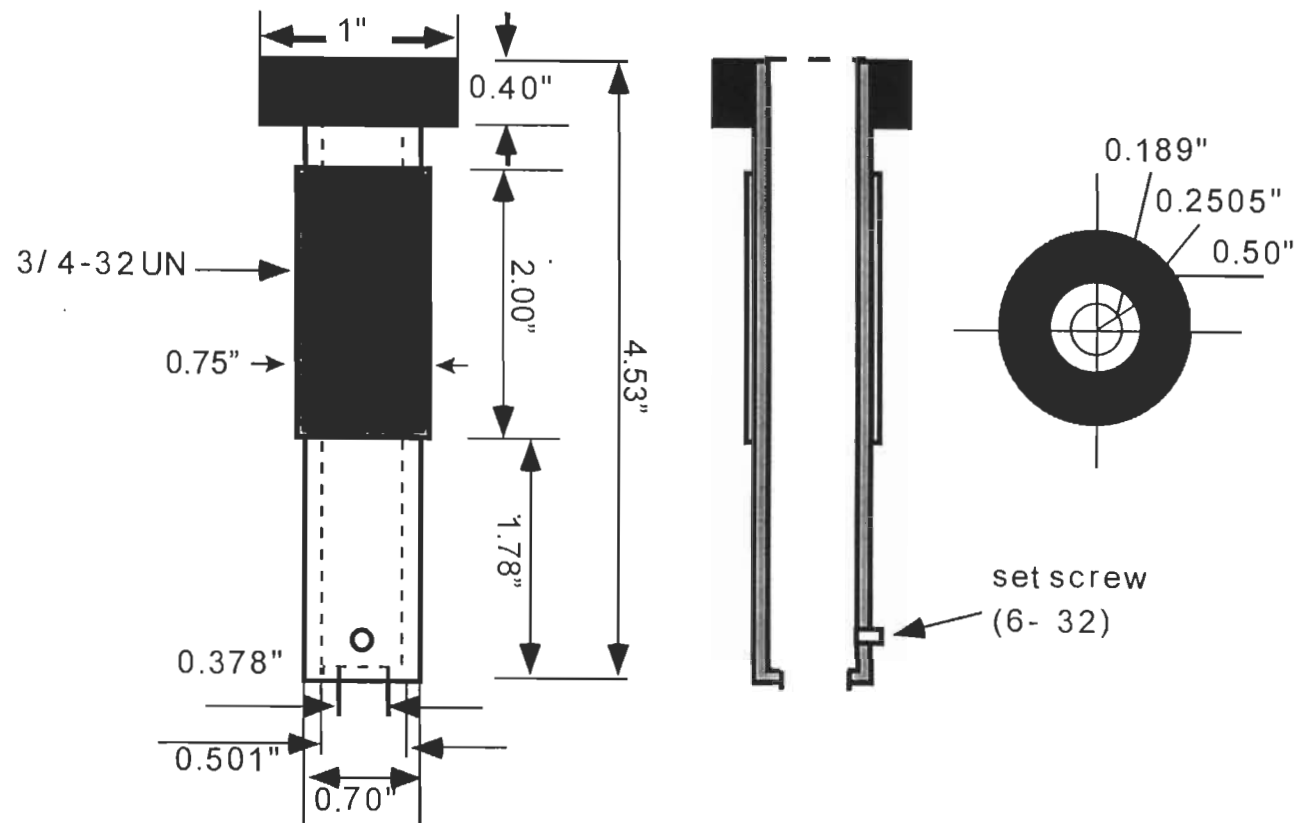
Figure A.6 The mechanical drawing of the optical fiber probe holder.

the optical fiber light guide to extend. A 6 - 32 Nylon set screw holds the optical fiber to the holder. The center portion of the holder is threaded on the outside about 2 inch long (3/4 - 32 UNC) so that it can be attached to the attachment arm through the threading. Moreover, the threading allows us to adjust the relative position of the fiber holder to the attachment arm, and therefore, to adjust the distance between the fiber probe and the liquid surface on the KSV minitrough. Figure A.6 provides the detailed dimensions of the probe holder.

Absorption measurements

The HP 8452A diode array spectrophotometer was designed to take absorption measurements of solution samples. It usually sits on the top of a bench and its optical path is parallel to the table top on the horizontal direction. The sample cell is then inserted into the optical path and is perpendicular to the optical path. However, the Langmuir film on top of the water can only be prepared horizontally because of gravity. In order to take an absorption spectrum of thin films at the air-water interface, the optical path must be perpendicular to the surface, i.e. in the vertical direction. Without substantially modifying the optical layout of the spectrophotometer, a simple solution is to turn the whole spectrometer 90 degrees so that its optical path is perpendicular to the horizontal plane. In this arrangement, the source light from the lamp of the spectrophotometer shines from the top, and then pass through monolayer at the air-water interface, subphase, quartz window of the minitrough, and the dispersion optics to reach the diode array detector of the spectrophotometer. Every optics in the spectrometer can thus be used as originally installed without any realignment.

To accomplish the task, we first attach the spectrometer to a base plate. Figure A.7 shows the mechanical drawing of the base plate. The base plate is made from 5 mm thick and 60×40.5 cm^2 regular steel plate. A set of four 6 mm diameter through holes (3 mm and 6.5 mm from sides, respectively, see Figure A.7 for details) were drilled in four corners so that the
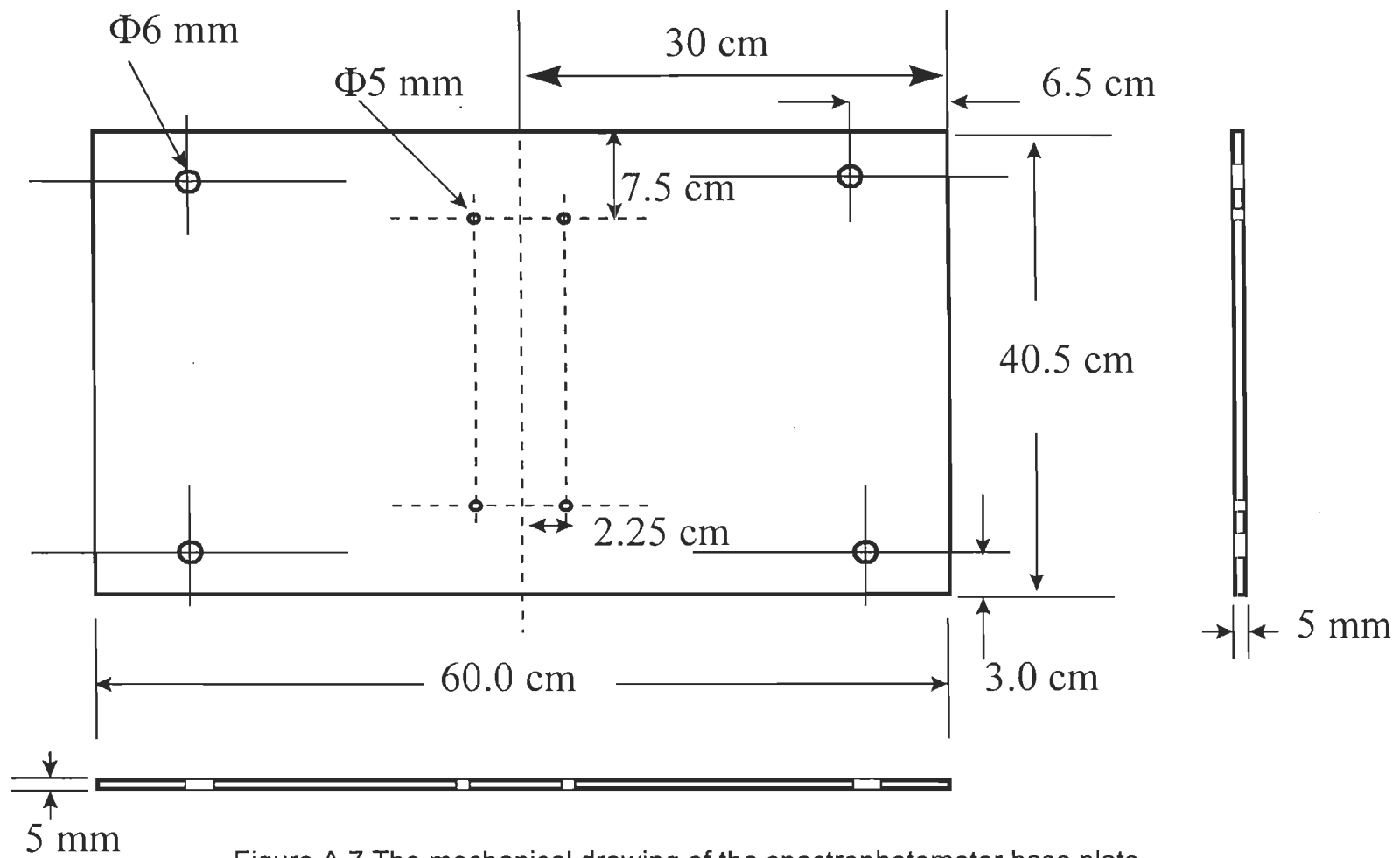
Figure A.7 The mechanical drawing of the spectrophotometer base plate.

spectrophotometer can be attached. Another set of 5 mm through holes were drilled in the middle (see Figure A.7 for exact location) allowed us to attach two ball bearings (Thomson Industries, Inc., Port Washington, NY, USA) on the other side of the plate. An one inch diameter stainless steel rod is installed into these bearings to serve as axis of rotation. Figure A.8 schematically shows the spectrophotometer, base plate, bearings, and rotation axis assembly. The whole assembly of spectrometer, base plate, bearing and rotation axis is then installed through another set of bearings on top of the second holding frame in the measuring station. As indicated in Figures A.1 and A.2, the frame elevated the spectrophotometer and allowed it to rotate in the vertical direction so that the optical path of the spectrophotometer can be either parallel to the bench top for the normal solution measurements or perpendicular to the bench for surface measurements. The rail guide beneath the spectrometer holder allows us to move the whole spectrometer assembly in and out of the measuring region. This arrangement gives us flexibility in both horizontal and vertical directions.

In addition to elevate and rotate the spectrophotometer, we also need to modify its cover. The original space in the sample region is too small to allow the KSV minitrough to fit into it. One could in principle make the measurement without the cover, if willing to take the risk of exposing the electronics of spectrophotometer to the air and water solutions. We decided to modify the Plexiglas cover by cutting out a portion of it, and then reseal it with silicon RTV.
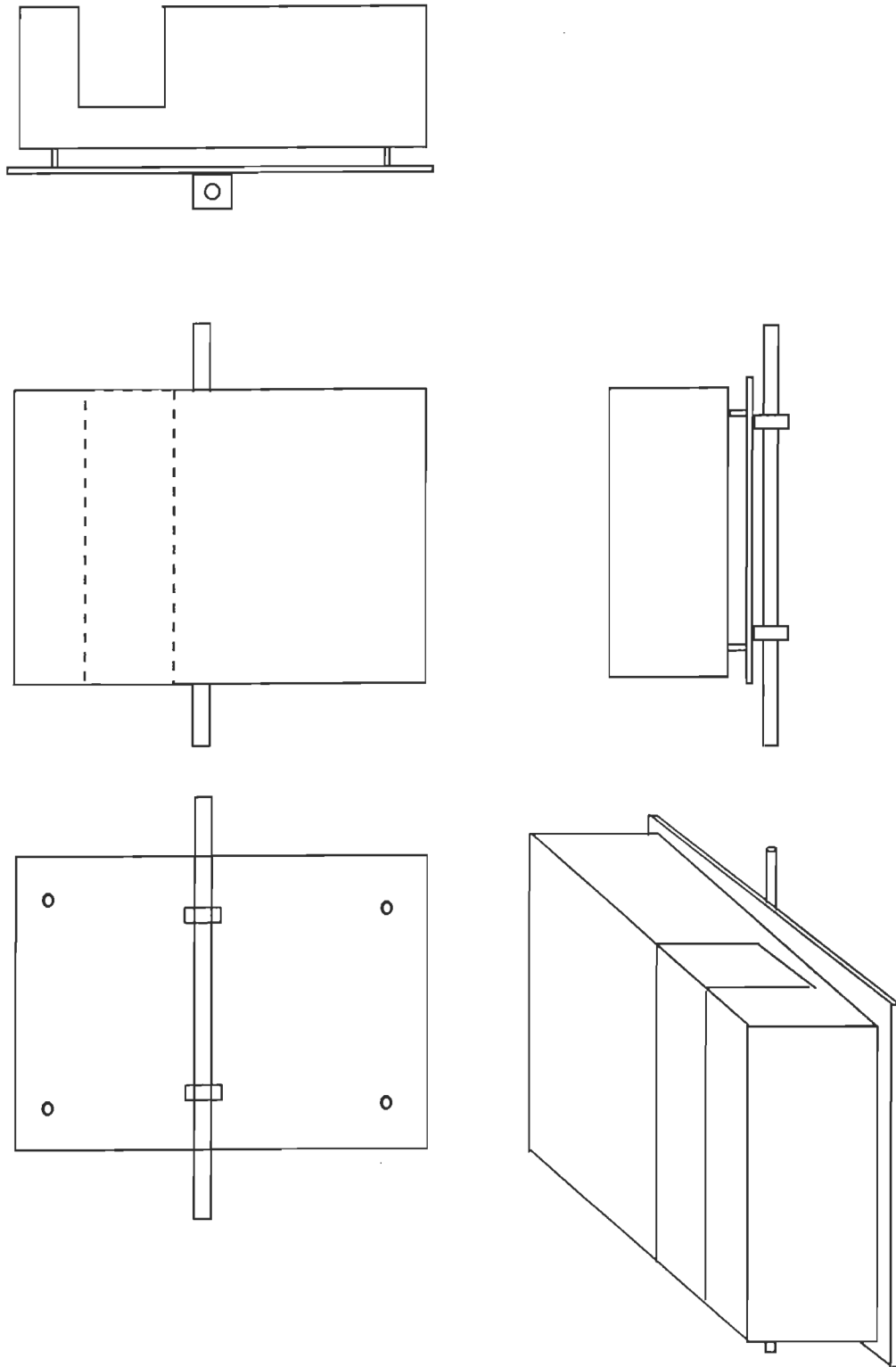
Figure A.8 HP spectrometer, base plate, bearings, and rotation axis assembly.